DOTTORATO DI RICERCA IN
AREA DEL FARMACO E TRATTAMENTI INNOVATIVI

CICLO XXXIV

COORDINATORE Prof.ssa Ghelardini Carla

PROGETTAZIONE, SINTESI E VALUTAZIONE BIOLOGICA DI PEPTIDI BIOATTIVI: MODULATORI DEL TURNOVER DEL COLLAGENE PER USO COSMECEUTICO E ANTIGENI DEL VIRUS SARS-COV-2 PER USO DIAGNOSTICO E VACCINALE.

DESIGN, SYNTHESIS, AND BIOLOGICAL EVALUATION OF BIOACTIVE PEPTIDES: COLLAGEN TURNOVER MODULATORS FOR COSMECEUTICAL USE AND SARS-COV-2 VIRUS ANTIGENS FOR DIAGNOSTIC AND VACCINAL USES.

Settore Scientifico Disciplinare CHIM/08

Dottorando
Dott.ssa Errante Fosca

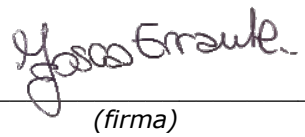

(firma)

Tutore
Prof. Rovero Paolo

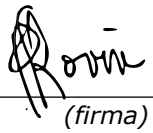

(firma)

Coordinatore
Prof.ssa Ghelardini Carla

(firma)

Anni 2018/2021

A tutte le cose belle della vita.
To all the beautiful things in life.

INDEX

ABSTRACT

Project 1: Collagen turnover modulators for cosmeceutical use

Type I collagen is the most abundant form of collagen in the connective tissue. A proper modulation of collagen turnover is extremely important to prevent pathological conditions and skin alterations, such as skin-aging or unhealed wounds. The cosmetic market, which includes skincare, hair care, make-up, perfumes, toiletries and deodorants, and oral products, in the last decades is hoarding a large portion of the continuously growing global wellness commerce (*Global Wellness Institute*, 2019). In this scenario a new type of products, the "cosmeceuticals", was drawn down as a blend of cosmetics and pharmaceuticals, as they are developed with biologically active ingredients to enhance skin properties, e.g., to prevent chrono- and photo-aging signs [I] [II]. In this context, many peptides have been developed with anti-aging properties.

The present PhD project aimed to develop new cosmeceutical peptides, using a pharmaceutical approach to define their mechanism of action and to increase their pharmacokinetic properties. In particular, we focused on serpin A1, an inhibitor of serine proteases. Previous investigation showed that a 10 residues C-terminal portion of this protein, named SA1-III, was able to decrease collagen fragments formation *in vitro* [III]. An overlapping approach was used to design four shorter tetrapeptides that where then synthetized by solid phase peptide synthesis (SPPS) using a Fmoc/tBu strategy. Their collagen turnover modulation activity was evaluated by treating neonatal normal human dermal fibroblasts (neo-NHDFs), leading to the selection of a promising peptide that was further modified and tested *in vitro* in order to obtain an analogue showing increased stability against dermal proteases. The new bioactive peptide, named AAT11RI, is a partial *retro-inverso* analogue of the lead compound and, due to its unexpected increased potency, it was patented [IV].

We subsequently developed a new methodology to evaluate peptide stability to dermal proteases, based on incubation in human skin homogenate and tandem mass spectrometry (MS/MS) analysis [V]. Thanks to this method, we also evaluated peptide chemical stability to oxidation, to determinate if peptide SA1-III methionine residue in position 1 is oxidized during this *ex-vivo* experiments. The dermal stability against proteases showed by peptide SA1-III classified it as a good candidate for a one-daily dosage cream. Despite this promising data, subsequent skin permeability experiments, performed using Franz cells, showed that peptide SA1-III is unable to permeate the skin. Consequently, to enhance its permeation, the peptide was conjugated with a fatty acid, a modification that is largely used in the field of cosmeceutical peptides, obtaining the peptide pamSA1-III. The collagen turnover modulation activity of this second-

generation compound was also studied, after incorporation in liposomes as a vehicle for the solubilization in the cell culture medium used, and it was showed that the N-terminal conjugation did not affect peptide activity. The mechanism of action of peptides AAT11RI and SA1-III was studied using fibroblasts invasion assays performed in Boyden chambers and it was shown that both peptides inhibit the activity of collagen degrading enzymes. At last, considering the mutual activation of proteases' activity and the release of inflammatory cytokines in skin aging, we evaluate the possible anti-inflammatory property of peptide SA1-III. Preliminary results indicate that the peptide also shows this characteristic, according to the fact that it derives from serpin A1, which is the most potent human neutrophil elastase inhibitor. This peptide feature will be of great interest not only from a cosmeceutical point of view, but also for pharmaceutical applications in pathological dermal problems, e.g., chronic wound unhealing.

In conclusion, the scenario of short peptides endowed with collagen turnover modulation activity that we investigated, suggests that much more can be done to evaluate and then enhance important cosmeceutical peptides characteristics, such as their bioavailability in the skin, and certainly a pharmaceutical approach is the trump card to valorize their attractive potential for the cosmetic market.

Project 2: SARS-CoV-2 virus antigens for diagnostic and vaccinal uses

COVID-19 pandemic emergency, surged in late December 2019 and since that moment spread all over the world, poses a heavy burden to the global health system. The β-coronavirus, to which SARS-CoV-2 belongs, are composed of several membrane proteins, among which spike protein (S) mediates human ACE2 receptor binding and membrane fusion, becoming crucial for the virus-host infection. For this reason, the CoV spike protein represents a key target for diagnostic, therapeutics, and vaccines. In particular, the receptor binding domain (RBD) of the S protein, that maintain a high homology to the previous SARS-CoV S protein, was shown to be a potent immunodominant region.

The second part of the present PhD was run in the framework of an international collaborative research effort started in April 2020, during the lockdown restriction due to the COVID-19 emergency, for the design, synthesis, purification, and optimization of peptide epitopes derived from SARS-CoV-2 S protein RBD, with the final goal to use them for diagnostics and vaccine. We synthesized, purified, and characterized a pool of peptides from the receptor binding motif (RBM) included in the RBD of SARS-CoV-2 S protein. One among them, peptide BIP $^{[VI],[VII]}$, composed of 72 residues, was our major synthetic challenge, due to its length and to the presence of an intramolecular disulfide bridge that we decided to maintain, in order to induce the native conformational constraint present in the parent protein. In fact, circular dichroism measurements

suggest that peptide BIP partially preserved its native beta-conformation. COVID-19 patients sera reactivity to this peptide, obtained by measuring IgG levels in ELISA assays, showed that it is recognized by 35 % of the patient sera (considering the 97th percentile). Interestingly, these patients showed a polyclonal response; in fact, IgA (10 %) and IgM (11.6 %) were also found. Moreover, we also performed ELISA assays with a series of overlapping peptides designed to cover the whole peptide BIP sequence and the results showed an interesting preference for the peptides that represents the N-terminal region of the RBM, suggesting that the immune response is triggered mainly by this region of the RBM. In addition, preliminary results on the immunizing ability of peptide BIP when injected in mice, showed that, despite the global response was lower than the ones observed in mice immunized with the recombinant Spike or RBD proteins, it induces a high immune response that could be an interesting starting point for the development of new peptide-based vaccines.

[I] F. Errante, P. Ledwoń, R. Latajka, P. Rovero, and A. M. Papini, 'Cosmeceutical Peptides in the Framework of Sustainable Wellness Economy', Front. Chem., vol. 8, p. 572923, Oct. 2020, doi: 10.3389/fchem.2020.572923.

[II] P. Ledwoń, F. Errante, A. M. Papini, P. Rovero, and R. Latajka, 'Peptides as Active Ingredients: A Challenge for Cosmeceutical Industry', Chem. Biodivers., vol. 18, no. 2, Feb. 2021, doi: 10.1002/cbdv.202000833.

[III] C. Cipriani et al., 'Serpin A1 and the modulation of type I collagen turnover: Effect of the C-terminal peptide 409-418 (SA1-III) in human dermal fibroblasts: Serpin-A1 C-terminal modulates collagen levels', Cell Biol. Int., vol. 42, no. 10, pp. 1340–1348, Sep. 2018, doi: 10.1002/cbin.11018.

[IV] International patent application WO 2020/245772 A1 (PCT/IB2020/055291) F. Errante, L. Giovannelli, A.M. Papini, P. Rovero.Bioactive peptides and compositions comprising them / Peptidi bioattivi e composizioni che li contengono. Priority:07/06/2019 Italian patent 102019000008364 Applicants: Espikem Srl, Università di Firenze

[V] F. Errante et al., 'Susceptibility of cosmeceutical peptides to proteases activity: Development of dermal stability test by LC-MS/MS analysis', J. Pharm. Biomed. Anal., vol. 194, p. 113775, Feb. 2021, doi: 10.1016/j.jpba.2020.113775.

[VI] A. Traoré et al., 'Seroreactivity of the Severe Acute Respiratory Syndrome Coronavirus 2 Recombinant S Protein, Receptor-Binding Domain, and Its Receptor-Binding Motif in COVID-19 Patients and Their Cross-Reactivity With Pre-COVID-19 Samples From Malaria-Endemic Areas', Front. Immunol., vol. 13, p. 856033, Apr. 2022, doi: 10.3389/fimmu.2022.856033.

[VII] F. Pratesi et al., 'A SARS-CoV-2 Spike Receptor Binding Motif peptide induces anti-spike antibodies in mice and is recognized by COVID-19 patients', Front. Immunol., doi: 10.3389/fimmu.2022.879946.

PEPTIDES AS COLLAGEN TURNOVER MODULATORS FOR COSMECEUTICAL USES

1. INTRODUCTION

1.1 COLLAGEN AND HUMAN SKIN

Covering a surface area of about 1–2 m^2, skin is the largest human body's organ. It permits the sense of touch, contributes to body temperature regulation, and provides a barrier against external threats cooperating with the immune system in organism defense [1], [2]. Skin is composed primarily of two layers, epidermis and dermis, both playing crucial roles in the human body, as reported briefly in Table 1 and Figure 1.

Table 1 Brief information on skin layer

Skin layer	***Most abundant cells***	***Most important roles***
Epidermis	keratinocytes, corneocytes, and melanocytes	protect against external trauma, making a hydrophobic barrier
Dermis	fibroblasts	provide strength and flexibility to the skin

These two layers are placed above a subcutaneous tissue, composed of connective tissue, blood vessels, and fat cells, once considered part of the skin. The outermost layer is the epidermis, a waterproof barrier to the external environment. Epidermis can be further divided into five tissues from the most superficial to the deeper layer, respectively: *Stratum corneum*, *Stratum lucidum*, *Stratum granulosum*, *Stratum spinosum*, and *Stratum basale*. Epidermis most abundant cells are keratinocytes, which are responsible for the production of skin keratin, a protein conferring skin strength and protecting from microorganism penetration and mechanical/chemical damage. These cells proliferate in the *Stratum basale* and rise up along skin layers, changing their shape and composition. Another important kind of cell we can find in epidermis, are corneocytes. They are present in the *Stratum corneum* (named after these peculiar cells) with the crucial role to protect skin against physical harm.

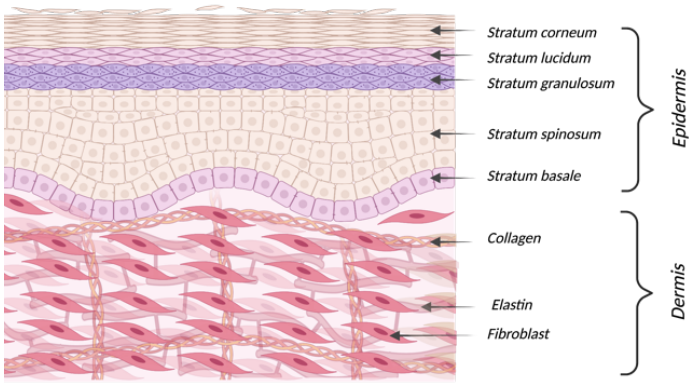

Figure 1 Schematic representation of epidermis and dermis organization.

These cells are also surrounded by lipids that help repel water as well, making skin a lipophilic layer, thus complicating the entry to hydrophilic external agents. The dermis is located just below epidermis and includes connective tissue, hair follicles, sweat glands, and fibroblasts. These cells produce and release collagen and elastin in the extracellular matrix (ECM), thus inducing skin strength and robustness.

Collagens are the most abundant protein family in the human body, composed by nearly 30 different members, numbered with roman numbers, and principally distributed in the mammalian connective tissue (25 % of total protein mass [3]), providing tensile strength and flexibility to bones, dermis, tendons, ligaments, and structural integrity to internal organs [4], [5]. Among this protein family, type I collagen is the fibrillar collagen archetype and the most common one, covering over 90 % of human total collagens.

1.1.1 COLLAGEN TRIPLE HELIX

Collagens have a common tertiary structure, shown in Figure 2 and consisting of a triple helical skeleton, composed by three polypeptide chains, called α chains, with a repetition of a triplet Gly-X_{aa}-Y_{aa}, in which the amino acid residues X and Y close to the glycine are frequently proline (Pro) and hydroxyproline (Hyp), respectively [6].

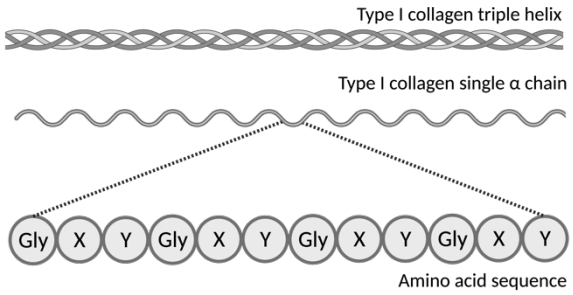

Figure 2 Type I collagen triple helix, single α chain and amino acid composition.

Each type I collagen polypeptide strand is composed by a left-handed polyproline-II-type helix, which is assembled with other two α chains to give rise to a right-handed superhelix, called tropocollagen. This resulting tertiary structure, with a combination of interchain interactions, is strongly connected to collagen stability, thus it is extremely important to understand the basal mechanisms of the triple helical structure to understand the consequent properties.

The high glycine content is important for collagen helix stabilization as this amino acid Cα side chain is represented only by a single hydrogen atom, which allows collagen fibers to combine, facilitating hydrogen bridges and cross-link formation. In fact, glycine residues point at the interior (axis) of the helix, where there is no space for bigger side chains (e.g., Pro and Hyp side chains); therefore, all the other amino acids in sequence are externally presented thus resunting relatively free for binding interactions with the other components

of the ECM [6], [7]. In addition, collagen triple-helix is stabilized by the presence of interchain hydrogen bonds and electrostatic interactions involving lysine and aspartate residues [8], [9].

Moreover, depending on the triple helix nature, collagens can be divided in homo- or heterotrimeric; in particular, homotrimeric forms are those where α chains have the same nature (e.g., type II collagen that has three α_1 chains) while heterotrimeric collagens are composed of chains with different nature (e.g., type I collagen that has two α_1 chain and one α_2 chain)[10].

1.1.2 Collagen Biosynthesis and Maturation

Collagen biosynthesis involves several steps, graphically summarized in Figure 3.

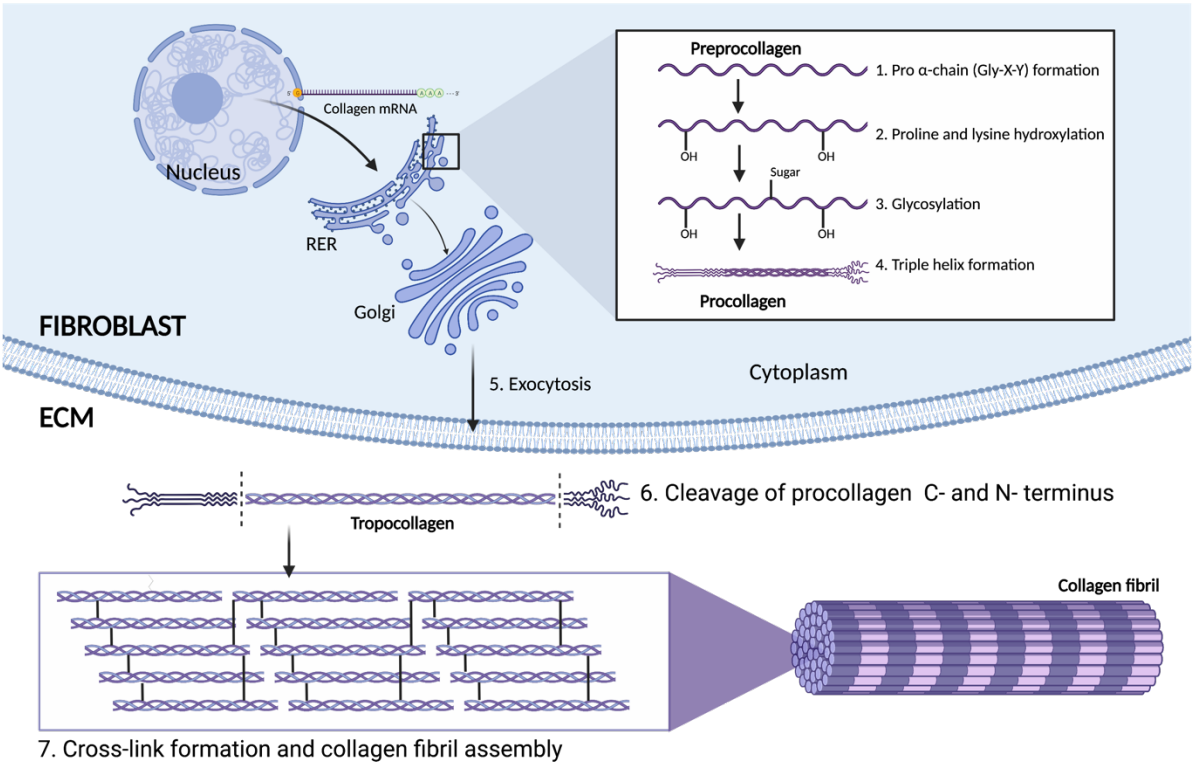

Figure 3 Graphical representation of collagen biosynthesis and maturation pathway.

Briefly, it starts in the fibroblast nucleus when RNA polymerase transcripts the mRNA; this messenger arrives to the rough endoplasmic reticulum (RER), where the synthesis of the very first form of collagen, known as preprocollagen (or preproα chain), occurs. In particular, the codifying genes for type I collagen chains are COL1A1 and COL1A2, for α_1- and α_2- prepro-chains respectively [11].

The formed preproα chains comprise several portions, which must be further processed (in the RER) giving rise to procollagen (shown in Figure 4). In fact, they consist of:

- a signal peptide portion (20 amino acids),
- an N-terminal non-collagenous (NC) domain named propeptide, which contains a proteolytical site to be cleaved by specifical proteases,
- a majority region of triple helix characterized by the Gly-X_{aa}-Y_{aa} motif,
- two 28-mer portions named telopeptides,
- a C-terminal NC domain composed by 220 amino acid residues containing disulfide bonds, which lead to a globular structure.

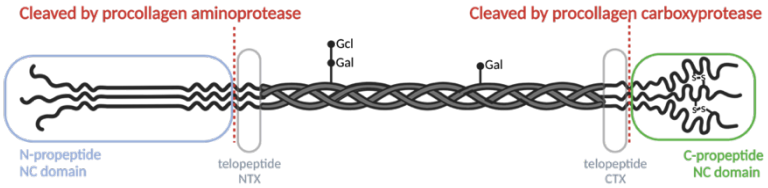

Figure 4 Schematic representation of the most important portions of type I procollagen triple helix, derived from the association between three preprocollagen α chains.

Noteworthy, the C-terminal telopeptide (CTX) is crucial as diagnostic marker in some collagen-related bones pathologies such as postmenopausal osteoporosis [12], [13], while the propeptides in the NC domains direct the triple helix formation in a zip-like manner from C- to N- terminus and their removal represents a crucial step, triggering spontaneous assembly into fibrils that range in diameter from 10 to 300 nm [14], [15].

As anticipated, to obtain the triple helix procollagen form, post-translational modifications including N-terminal signal sequence removal, hydroxylation of lysine and proline residues by prolyl hydroxylase and lysyl hydroxylases, and glycosylation of lysine residues occur.

At that point, unlike other collagen superfamily members, fibrillar collagens require the proteolytic processing by specific collagenases to cleave procollagen extensions and achieve the mature and functional collagen form.

These collagen type-specific metalloproteinase enzymes remove the amino- and carboxy-propeptides forming tropocollagen, the functional unit of collagen. Units of tropocollagen are then associated each other by lysyl oxidase, that packs together five tropocollagen chains, giving rise to microfibers, well-structured tertiary organizations, with variable degrees of tensile strength [16]. Short microfibrils merge into mature fibrils through longitudinal and axial growth. To form mature fibers, lysyl oxidase catalyses the formation of intramolecular and intermolecular covalent crosslinks between collagen molecules. Fibers are bundled together within connective tissue and stabilized via interactions with fibril-associated collagens with interrupted triple helices (FACIT) collagens and small leucine-rich repeat proteoglycans (SLRPs) into linear structures capable of transmitting tensile forces. Finally, multiple tertiary bundles are enclosed by connective tissue, which contains the vascular, lymphatic and nervous components [17].

1.1.3 ECM AND COLLAGEN TURNOVER

The extracellular matrix is a highly dynamic entity composed of several structural proteins, including collagens and elastin, and it continuously undergoes tissue turnover, balancing protein degradation and formation. This turnover is modulated by a complex hormone-regulated feedback system, which also interferes with inflammatory and growth factors including transforming growth factor TGF-β1, epidermal growth factor receptor EGFR and

tumor necrosis factor-α TNF-α [18], [19]. The ECM tissue turnover activity can be also described as the sum of two processes that consist in *tissue modeling*, that occur during tissue generation and growth, and *tissue remodeling*, where functional tissue is maintained by replacing old and damaged proteins and cells with new ones [20], [21]; for this reason a precise orchestration is crucial to the maintenance of physiological conditions and function [22], [23]. In fact, collagen altered metabolism can lead to the onset of serious physiological and pathological conditions. A defect in collagen fibers content in tissues may be related to the hyper-activity of certain proteases responsible for its degradation, or alterations in collagen biosynthesis pathway, partially compromising the outcome of physiological processes, such as wound repair [24].

Skin catabolism is mediated principally by the secretion of fibroblast matrix metalloproteinases (MMPs) which belong to the superfamily of zinc-dependent endopeptidases [25], and compensated by the production of tissue inhibitors of metalloproteinases (TIMPs). These proteins are implicated in physiological processes, such as repair of tissue damage and inflammatory response, but also in pathological processes, such as genesis of tumors and metastases [6]. MMPs main task is to degrade the ECM in specific points so that cells can pass through it, and this process is at the basis of inflammatory phenomena, in which leukocytes spread through the matrix to activate defense mechanisms. For this reason MMPs are usually produced by the organism as non-active precursors, called zymogenes, to reduce their action in the protein biosynthesis site [26]. The importance of MMPs in the regulation of ECM homeostasis in humans has been demonstrated, among others, by the discovery that mutations in the MMP-2 gene induce a disorder involving characteristic facial features, lytic bone lesions, arthritis, and subcutaneous nodules [27]. Moreover, animal model suggest the importance of MMP in tissue remodeling, e.g. a transgenic mouse carrying a mutated COL1A1 gene, coding for a form resistant to collagenase digestion, has been useful in characterizing MMPs in development and wound healing [28]–[30].

MMPs can be grouped based on their reported substrate specificities [e.g., collagenases, gelatinases, stromelysins, (Table 2)] and structures (e.g., membrane-type MMPs). Collagenases (MMP-1, MMP-8, MMP-13) can specifically degrade native fibrillar collagens (types I, II, III, VII, and X) in their stereotypical triple helix domain, as well as denatured collagen (gelatin) [31].

Table 2 Classification of main MMPs responsible for collagen degradation.

MMP	*Category*	*Enzyme*
MMP-1	Collagenases	Collagenase 1 (Interstitial or fibroblast collagenase)
MMP-8		Collagenase 2 (Neutrophil collagenase)
MMP-13		Collagenase 3
MMP-2	Gelatinases	Gelatinase A
MMP-9		Gelatinase B

Type I collagen, together with types II and III has a specific cleavage sequence located at 3/4 of N-terminal and crucial for collagen degradation: Gln-Gly#Ile-Ala in α_1 chains and Leu-Gly#Leu-Pro in α_2 chains, where # indicates the cleavage site [32], [33].
After collagenases have attacked collagen triple helix, the denatured collagen, called gelatin, can be further degraded by gelatinases (as shown in Figure 5).

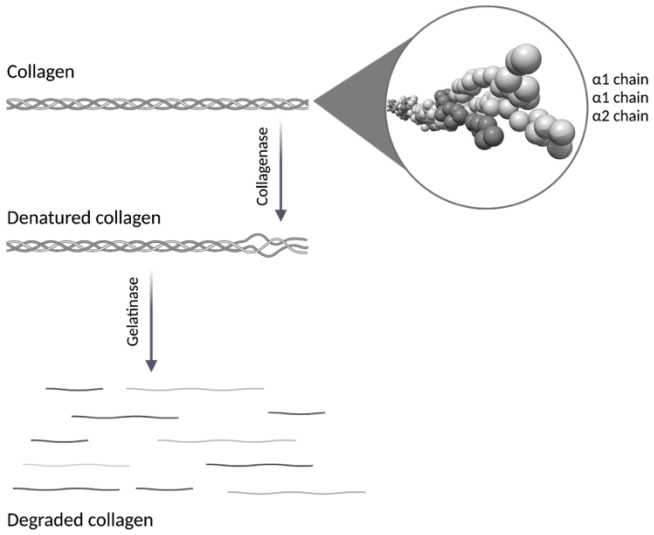

Figure 5 MMPs collagenases and gelatinases cleaving type I collagen (PDB code: 3hqv).

The activity of MMPs is closely connected to the activity of a second enzymes superfamily: Serine Proteinases (SPs).
Serine proteinases are involved in so many biological processes that they are used as model enzymes for studying catalytic processes. In humans or mammals, SPs co-ordinate various physiological functions, especially in food digestion, immune response, blood coagulation, and the complement system, playing also a crucial role in the ECM components turnover. In fact, serine proteases urokinase-type plasminogen activator (u-PA) and neutrophil elastase are released by neutrophils in conditions of tissue damage, and in particular the former is thought to be involved in tissue remodeling and cell migration processes while the latter has a broad substrate specificity and is responsible for the digestion of ECM components, such as elastin, collagen and fibronectin, allowing pro-inflammatory cytokines and leucocytes infiltration through the lesion area [34]. Other SPs are involved in pathological conditions, including carcinogenicity, in particular of colo-rectal tumors [35], [36].
A common structure among SPs is known and consists of a serine, a histidine and an aspartate residue in the substrate-binding pocket that induce a catalytical hydrolysis of peptide bonds. This “classical” triad hypothesis has been substituted during the years by novel triads or dyads based on a serin residue complemented by lysine, histidine or glutamic acid residues [37], [38]. Depending on their substrate specificity, these enzymes are

classified as: trypsin-like, chymotrypsin-like, thrombin-like, elastase-like, kallikrein, cathepsin, and subtilisin-like proteases [39].

The tissue remodulation regulated by serin proteases is crucial, among others, for proper collagen turnover, and in fact an altered functionality of SPs can lead to serious problems including a general collapse of the organism. To prevent excessive SP activation, a class of inhibitors which can be described as “antiproteases shield”, regulates SPs activity limiting their effect within the area interested by the injury and hampering the inflammation spread in adjacent undamaged regions. SPs inhibitors are ubiquitously present in organisms as the SPs themselves, and examples include α1-antitrypsin, α2-macroglobulin, α1-antichymotrypsin and plasminogen activator inhibitor (PAI-1). Evidence suggests that their role in both plasma and interstitial fluids can be overwhelming in chronic wounds and more generally in case of recruitment of large numbers of inflammatory cells, implying the subsequent release of proteases within the involved tissues [34]. SPs can be stopped by an active site competitive inhibition, an exo-site binding competitive inhibition and irreversible inhibition [40]. With regard to the latter mechanism, SERPINs are a class of serin protease inhibitors performing various regulatory functions (as reported in Figure 6; [41]) some of which include suicide substrate inhibition leading to extracellular matrix remodeling. In Figure 6 the structure [B] of serpin A1 (or α1-antitrypsin or α1-AT), the archetype of SERPINs, is shown along with the mechanism of action [C,D,E] of its activity. It is known that SERPINs have a conserved structure, that includes 7–9 α helices, 3 β-sheets, and a RCL (reactive center loop) region containing an enzyme cleavage site, located near the C-terminus of the whole protein. This region seems to be essential for the activity as it captures proteases which are then bound to the inhibitor with a non-covalent Michealis-Menten complex [C]. Following the cleavage at P1-P1’ active site, a conformational modification occurs, and SERPINs spontaneously refold in a more stable form with the RCL cleaved N-terminal portion hidden among β-sheets, so that the resulted covalent binding with the protease leads to its inactivation [D]. Sometimes this covalent binding does not take place, resulting in an active protease that disassociates from the SERPIN [E]. SERPINs and inactivated protease are physiologically swept away by cells used to control defective proteins.

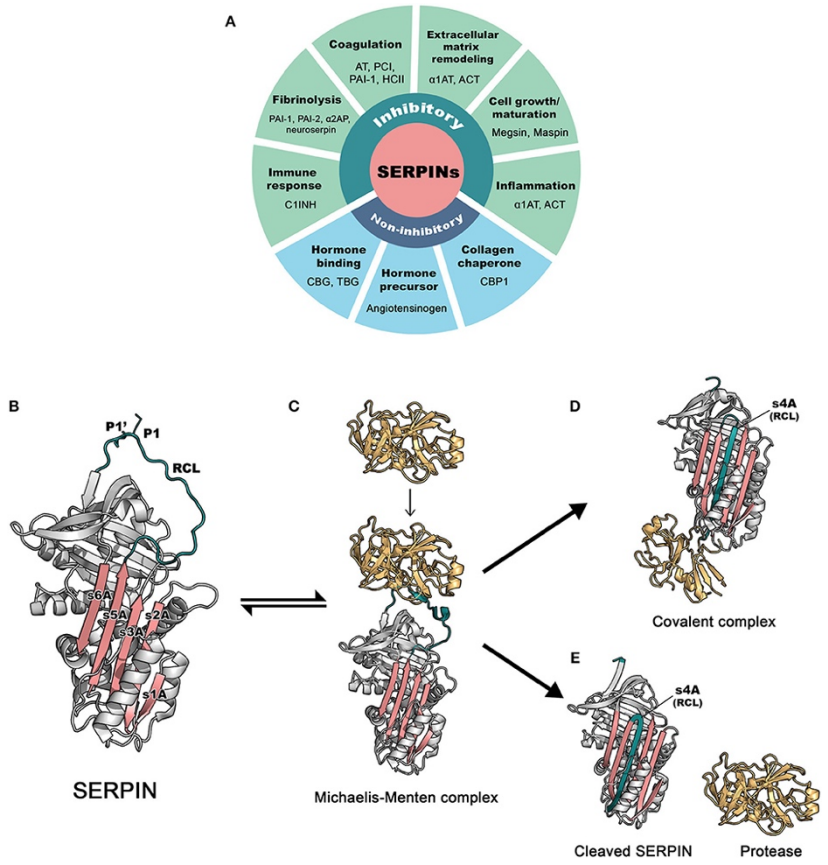

Figure 6 SERPINs family: regulatory functions [A], structure [B] and mechanism of inhibition [C,D,E]. AT: anti-thrombin; PCI, protein C inhibitor; PAI-1, plasminogen activator inhibitor 1; PAI-2, plasminogen activator inhibitor 2; HCII, heparin cofactor II; a1AT, α1-antitrypsin; ACT, anti-chymotrypsin; a2AP, α2-antiplasmin; C1INH, C1 esterase inhibitor; CBG, Corticosteroid-binding globulin; TBG, Thyroxine-binding globulin; CBP1, collagen-binding protein 1 [41].

Given its ubiquitous occurrence, clinical findings of pathologies involving type I collagen are considered as showcases that lead to understand ECM biology. Pathologies related to type I collagen alterations, with reference to its turnover or supramolecular organization, include for example Ehlers-Danlos syndrome, osteoporosis, osteoarthritis, and osteogenesis imperfecta. Moreover, some autoimmune diseases, such as psoriasis or rheumatic pathologies, are correlated with the up-regulation of the hydrolyzing activities of proteases [42]. Not least, it has been observed that the proteolytic activity of serine proteases initiates the final stage of skin desquamation [43] and influences the chronic inflammation state associated with atopic dermatitis [44]. Based on all these observations, the balance between collagen synthesis and degradation can affect the physiological condition of the skin: in particular skin aging has been demonstrated to be associated with collagen alterations.

1.2 SKIN AGING

Skin aging is characterized by wrinkles, loss of elasticity, laxity, and rough-textured appearance as consequences of structural and physiological alterations that spread progressively deeper in each skin layer. In 2005 Christopher Paul Wild, a molecular epidemiologist, invented the term "exposome" to describe all exposures to which an individual is subjected from conception to death, dividing them into three main classes: internal, general external and specifical external [45], [46]. In this scheme, skin aging exposome consists of both external and internal factors (genetics, cellular metabolism, hormone, and metabolic processes), whose interaction can influence the body's response leading to biological and clinical signs. Skin aging can be further divided into two kinds of process: chrono-aging and photo-aging. The former refers to the inevitable and general morphological change that the skin undergoes with time and can be generically considered the results of the internal factors combination. The latter, indeed, is the product of external factors such as solar radiation (ultraviolet radiation, visible light, and infrared radiation), environment pollution, tobacco smoke, nutrition, and the use of inappropriate cosmetic products resulting in skin appearance modification, especially in sun-exposed skin areas. Moreover, clinical appearance of naturally aged skin and photo-aged skin differs substantially: in chrono-aging skin is smooth, pale, and finely wrinkled, the protection barrier is usually not compromised, yet alterations in fibers alignment are observed with unraveled collagen bundles and reduced space between fibers [47]; on the contrary, photo-aged skin is coarsely wrinkled and associated with dyspigmentation and telangiectasia, due to drastic modification of the dermis architecture especially after acute or chronic exposure of UVB-radiation [48].

As a matter of fact, both intrinsic and photo-induced skin aging are conditions in which fibrillar collagens III and I are still functional but their amount *per* cell is remarkably reduced, causing wrinkle formation and elasticity loss [24], [47], [49], [50]. In Figure 7 a schematic representation of the UV-B induced photo-aging pathway comprising both intracellular and extracellular processes is shown.

Briefly, the cascade of events begins with the photochemical generation of reactive oxygen species (ROS) after exposure to UV-B. ROS modify and often degrade cell components such as lipids, proteins, or DNA. Among these highly reactive species are superoxide anions, peroxide, and singlet oxygen. Several studies have shown that the production of ROS induce an inflammatory response through the activation of protein kinases and the inactivation of phosphorylases, implicated in the control of cell growth signaling pathways; however, the mechanism by which this happens is not yet completely clear [51], [52].

The inflammation state induces an increase in gene expression of some ECM components including MMPs, which degrade type I collagen, and cyclooxygenase-2 (COX-2), releasing

pro-inflammatory prostanoids. Furthermore, a parallel cascade of event brings to the down-regulation of gene expression for type I and type III procollagen [53].

Another important aspect in skin aging is the accumulation of growth-arrested senescent cells expressing a senescence-associated secretory phenotype (SASP), wherein these cells secrete high levels of inflammatory cytokines, immune modulators, growth factors, and proteases [54]–[56]. Lastly, when normal tissue repair and regenerative mechanisms no longer function properly, the degradation processes have a cumulative effect, so that subsequent UV exposures worsen tissue damage and could lead to cell apoptosis.

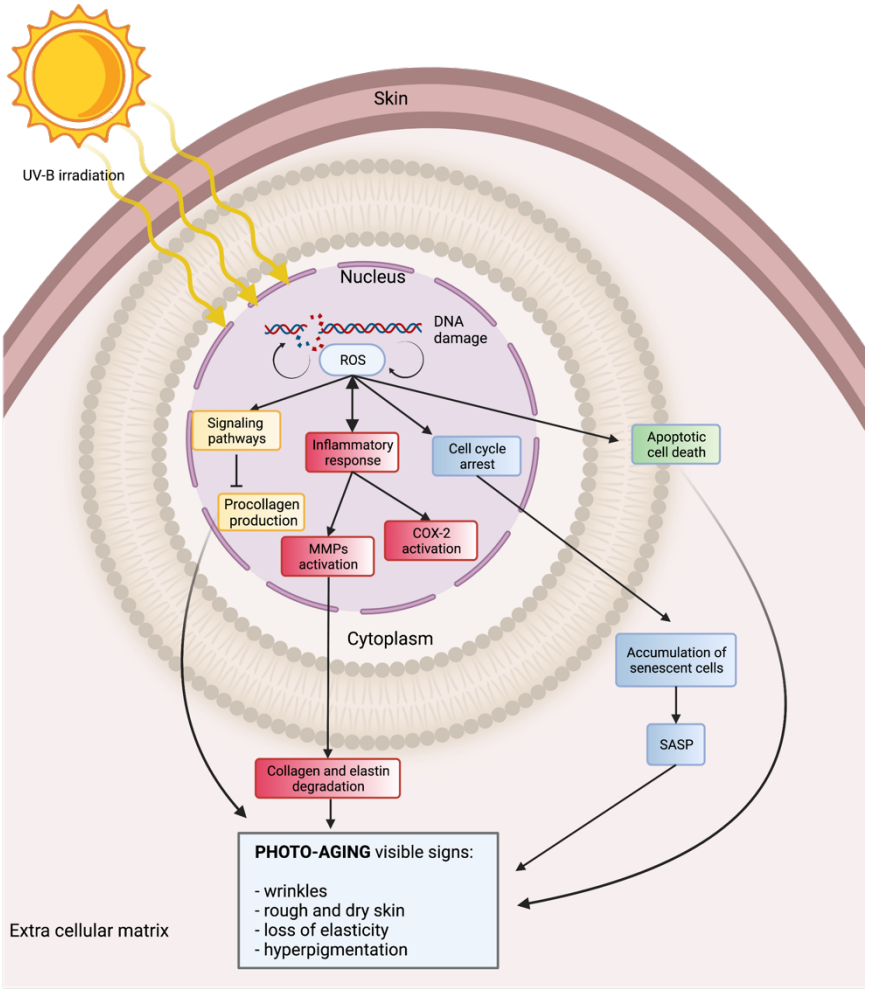

Figure 7 Schematic representation of the key aspects of photo-aging induced by UV exposure.

1.3 COSMECEUTICS

In 2015 the United Nation defined 17 Sustainable Development Goals (SDG) that can contribute to change the world for the better. The third of these goals is to establish “good health and wellbeing”, thus indicating that health and wellness are strictly linked. Among the many aspects that contribute to the wellness of each individual, a healthy and younger-looking skin plays a relevant role, as clearly shown by the important growth of the skin-care products market observed in recent year (*Global Wellness Economy Monitor*). In fact alterations in skin appearance result in unpleasant psychological and social impact among individuals [57]. The term “cosmeceutical” was coined in the nineties by Albert Kligman Montgomery, an American dermatologist who had contributed to the studies on tretinoin as a cure against acne, to indicate a new class of cosmetic formulations with therapeutic activity [58]. Despite its wide use in the scientific literature, the term “cosmeceutical” is still a source of debate and regulatory bodies, such as the FDA (Food and Drug Administration) do not officially recognize the use of the term, as they distinguish between compounds that are tested *in vivo* according to clinical trial procedures (drugs) and compounds which are not subjected to such controls before being placed on the market (cosmetics) [59], [60]. Particularly in the last 50 years dermatologists, cosmetologists and the cosmetic industry have felt the need to discriminate between a cosmetic with a simpler hygienic function, from one with the ability to change the skin physiology. Although the most adequate way to describe one ingredient that characterizes a cosmetic formulation, is the term "claim ingredient" [61], the scientific literature widely reports the term “cosmeceutical” both for an ingredient that shows a biological activity and a final cosmetic product that contains an ingredient able to have a certain biological activity. Moreover, the terms cosmeceutical is used as a marketing strategy to capture the attention and to be differentiated from other cosmetic products. To draw conclusions, as this PhD thesis is developed in the context of academic scientific research, with an eye toward the technology transfer, the term cosmeceutical will be used e.g., to refer to biologically active anti-ageing peptides.

Generally speaking, cosmeceuticals are topical use products specifically aimed at improving skin conditions, usually free from dyes and containing minimal concentrations of perfumes and preservatives, and often containing UV radiation protection factors [62].

Cosmeceuticals not only counteract the signs of skin aging, but can also provide protection to skin, nails, hair, and can have lightening, anti-wrinkle, or sun protection properties; actually the literature reports a wide range of active ingredients effective for the formulation of cosmeceuticals, intended to be used as whiteners, depigmentation agents, moisturizers, emollients, anti-aging, anti-photoaging and photo-protectors, marketed in several kind of formulations such as creams, ointments, lotions, gels, serums, perfumes, lipsticks, nail polishes, toothpastes, and preparations for facial and eye makeup [63], [64].

1.4 PEPTIDES AS ACTIVE INGREDIENTS

Peptides have a wide range of functions, and thus a large number of potential applications, ranging from active pharmaceutical ingredients to innovative nanomaterials. In particular, the cosmetic industry showed in recent years an increased interest toward the use of peptides as cosmeceutical ingredients [62], boosting a field whose growth has been constant for many years. Peptides entered the cosmeceutical field in 1973 when Pickart proposed the synthetic peptide GHK as a signal peptide enhancing collagen production and acting as a carrier peptide when complexed with Cu(II) [65]. Since then, due to their versatility, a plethora of peptides of cosmeceutical interest have been developed in response to the most frequent and not fully satisfied market requests. Initially, the cosmeceutical applications of peptides were limited to their use as carriers for larger molecules, enhancing their penetration (e.g., the above-mentioned copper tripeptide GHK-Cu). More recently, a deeper knowledge of the biological functions of many peptides enabled their use as regulators of cellular processes, as in the case of the well-known pentapeptide KTTKS, proposed as ECM stimulator. However, while some of the peptides used in cosmeceutical formulations are pharmacologically tested, in order to demonstrate the claimed bioactivity, it is relatively uncommon to find published data concerning their bioavailability and stability when applied topically on human skin [66]. Moreover, attention should be paid to the association between good topical care products and food supplements in which the term “peptide” is starting to be (ab)used to identify mostly not well characterized protein hydrolysates. Nevertheless, consumers today understand the importance of reading product labels and INCI (International Nomenclature of Cosmetic Ingredients) lists. In fact, more and more costumers ask for specific information regarding the active principles used in cosmeceuticals and they are attracted by scientific data demonstrating the number of claims reported by the cosmetic industry. Furthermore, the pharmaceutical use of peptide active ingredients demonstrates that there are several possibilities to enhance their bioavailability (see Figure 8) and in some cases these approaches have been applied to peptides of cosmeceutical interest as well [67]–[70].

Actually, peptide as pharmaceutical ingredients are susceptible of a number of chemical modifications, such as cyclization, conjugation to different tags and insertion of non-natural amino acids, thus suggesting numerous opportunities to control either their efficacy to the designated clinical target or their pharmacokinetic properties, e.g., increasing the resistance to protease digestion or the permeability through the *stratum corneum* [71].

Peptides as active ingredients in cosmeceutical products are usually classified into three categories: neurotransmitter inhibitor peptides, carrier peptides and signal peptides. These classes, which have been the subject of several reviews in the last years, will be now briefly described, and some peptides as examples for each class will be shown in Figure 9 [72].

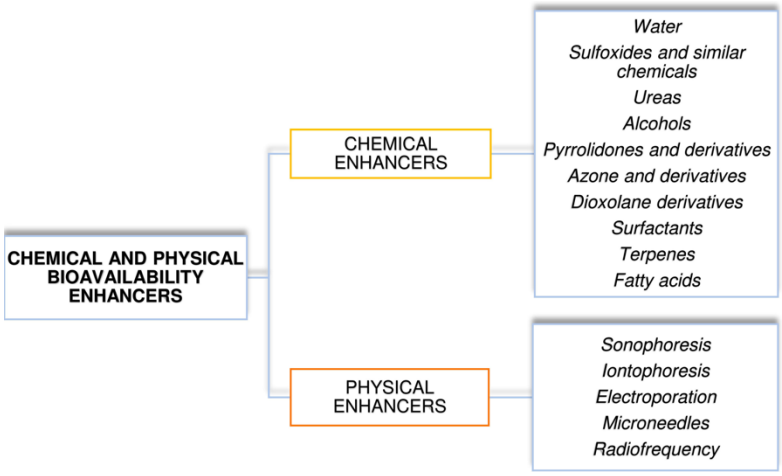

Figure 8 Chemical and physical bioavailability enhancers, according to the literature [67][68].

1.4.1 Neurotransmitter Inhibitor Peptides

Fine lines and wrinkles are getting formed, among other, due to the muscle cramps. These movements, provoked both involuntarily and knowingly, are closely connected with a large number of SNARE (Soluble N-ethylmaleimide-sensitive factor Activating protein REceptor) complexes. Acetylcholine (ACh), the main neurotransmitter involved in this process, is released from vesicles as the result of a reaction cascade mediated by SNAP (SyNaptosome-Associated Protein) receptor protein. This receptor controls directly the synaptic vesicle fusion for ACh release, involving SNARE complex formation [73]. Once ACh is released, it binds to the appropriate receptor and triggers muscle cramps. Some peptides with similar sequence to the synaptic proteins can potentially inhibit this reaction. Therefore, those are termed neurotransmitter inhibitor peptides [74]. SNAP-25 (molecular weight 25 kDa), which is essential for ACh release from vesicles with the presynaptic vesicle, is particularly targeted by the well-known botulinum neurotoxin type A. Botulinum neurotoxin type B has a different mechanism of action. In fact, it leads to VAMP (Vesicle-Associated Membrane Protein) cleavage, necessary for the release of ACh [75]. Botulinum toxins are widely used as a standard reference, in terms of activity, for new neurotransmitter inhibitor peptides tested as cosmeceuticals.

1.4.2 Carrier Peptides

Cu(II), one of the crucial metal ions in human body, can be stabilized or delivered into cells by peptides. It is incorporated in various processes, including enzymatic reactions, wound healing, and angiogenesis [76]. In the case of cosmeceuticals, copper is an essential cofactor for lysyl oxidase and can contribute to modulate collagen or elastin concentration in dermis.

The most important peptide of this class is Gly-His-Lys (GHK), which was shown to be able to reduce the activity of MMPs and collagenase, thus preventing premature skin-aging [75], [77].

1.4.3 SIGNAL PEPTIDES

In this class of cosmeceuticals, peptides able to modulate skin protein turnover are included, most of them enhancing collagen production. In fact, their name derives from the ability to signal or mimic the signals inducing the synthesis of ECM proteins. In this category, peptides promoting collagen production and released by the ECM are called matricins [74]. One of the first peptide used with a similar activity is the gastrin-releasing peptide, a bombesin-like neuropeptide that promotes wound healing by stimulating keratinocyte proliferation [78].

This part of this PhD project had the aim to design, synthetize and evaluate the *in vitro* activity, permeability and stability of specific signal peptides derived from SA1-III, a decapeptide (Ac-MGKVVNPTQK-NH_2) recently described by our group [79], [80], which modulates collagen turnover.

SELECTION OF COSMECEUTICALLY RELEVANT PEPTIDES

	PEPTIDE NAME AND SEQUENCE	COMMERCIAL NAME	BIOACTIVITY	ORIGINAL SYNTHETIC STRATEGY
NEUROTRANSMITTER INHIBITOR PEPTIDES	**ACETYL HEXAPEPTIDE-3** Ac-Glu-Glu-Met-Gln-Arg-Arg-NH_2	*Argireline*	Ca^{2+}-dependent catecholamine inhibitor, blocking SNARE complex formation (Blanes-Mira et al. 2002)	SPPS (Blanes-Mira et al. 2002)
	PENTAPEPTIDE-3 H-Gly-Pro-Arg-Pro-Ala-NH_2	*Vialox*	ACh receptor antagonist, disabling nerves function (Schagen 2017)	SPPS (Patent No.: US 2015/0361137 A1)
	PENTAPEPTIDE-18 H-Tyr-Ala-Gly-Phe-Leu-OH	*Leuphasyl®*	ACh decreased secretion in synaptic clefts (Dragomirescu et al. 2014)	N/D
	TRIPEPTIDE-3 H-β-Ala-Pro-Dab-NH-benzyl × 2·AcOH	*Syn®-Ake*	Muscular nicotinic ACh receptor antagonist (Reddy, Jow, and Hantash 2012)	N/D
	ACETYL OCTAPEPTIDE 1/-3 Ac-Glu-Glu-Met-Gln-Arg-Arg-Ala-Asp-NH_2	*SNAP-8™*	SNAP-8 competitive inhibitor, blocking SNARE complex formation (Lipotec s.a. SNAP-8 2020)	N/D
CARRIER PEPTIDES	**COPPER TRIPEPTIDE-1** Cu(II) H-Gly-His-Lys-OH	N/D	Collagen/elastase synthesis cofactor also involved in MMPs and collagenase decreased activity (Campbell et al. 2012; Pickart, Vasquez-Soltero, and Margolina 2015)	Isolated from HSA (Pickart and Thaler 1973)
	MANGANASE TRIPEPTIDE-1 Mn(II) H-Gly-His-Lys-OH	N/D	*Ibidem* (Hussain and Goldberg 2007)	N/D
SIGNAL PEPTIDES	**PALMITOYL HEXAPEPTIDE-12** Pal-Val-Gly-Val-Ala-Pro-Gly-OH	*Biopeptide EL™*	MMPs activity upregulator, elastin downregulator and collagen synthesis stimulator (Floquet et al. 2004)	LPPS (Senior et al. 1984)
	PALMITOYL PENTAPEPTIDE-4 Pal-Lys-Thr-Thr-Lys-Ser-OH	*Matrixyl®*	ECM proteins synthesis feedback modulator (Choi et al. 2014)	N/D
	PALMITOYL TRIPEPTIDE-1 Pal-Gly-His-Lys-OH	*Biopeptide CL™*	Collagen and GAG synthesis stimulator (Johnson et al. 2018)	N/D
	PALMITOYL TRIPEPTIDE-5 Pal-Lys-Val-Lys-OH	*Syn®-Coll*	TGF-β stimulator inducing collagen synthesis; MMPs inhibitor (Kim et al. 2017)	N/D
	LIPOSPONDIN Elaidyl-Lys-Phe-Lys-OH	N/D	TGF-β stimulator (possible role of elaidyl moiety in MMPs inhibition) (Cauchard et al. 2004)	N/D
	HEXAPEPTIDE-11 or PENTAMIDE-6 H-Pro-Val-Ala-Pro-Phe-Pro-OH	N/D	ATM and p53 downregulator, protecting fibroblasts against oxidative stress (Sklirou et al. 2015)	Isolated from *Saccaromices* yeast, then synthesized by SPPS (Sklirou et al. 2015)
	TRIPEPTIDE-10 CITRULLINE *N/D*	*Decorinyl®*	Collagen fibres diameter regulator, increasing endogenous collagen quality, without affecting its synthesis (Puig, Antón, and Mangues 2008)	SPPS (Puig, Antón, and Mangues 2008)
	PKEK H-Pro-Lys-Glu-Lys-OH	N/D	IL-6, IL-8, α-MSH, and TNF-α downregulator; involved in hyperpigmentation reduction (Marini et al. 2012)	N/D
	GEKG H-Gly-Glu-Lys-Gly-OH	N/D	Collagen synthesis stimulator (Farwick et al. 2011; Sommer et al. 2018)	N/D
	SA1-III Ac-Met-Gly-Lys-Val-Val-Asn-Pro-Thr-Gln-Lys-NH_2	*KP1*	Collagen turnover modulator by protease inhibition (Pascarella et al. 2016; Cipriani et al. 2018)	SPPS (Pascarella et al. 2016; Cipriani et al. 2018)

Figure 9 Relevant peptides in commercially available cosmeceuticals [72].

2. STATE OF THE ART

2.1 SERPIN A1 ROLE IN ECM

Once the importance of a proper balance between biosynthesis and degradation of type I collagen has been described, numerous studies have evaluated the potential use of small molecules, such as short peptides, for the treatment of pathophysiological and pathological conditions such as collagen related diseases, defects in wound repair, and skin aging. Peptides developed in the framework of this PhD project derived from the superfamily archetype of serin-protease inhibitors: serpin A1, also named A1AT or α1-antitrypsin, a single-chain glycoprotein 394 amino acids long (with a signal sequence of 24 amino acids) with a total weight of 52 kDa [81]. This protein is an excellent cosmeceutical lead as it is endowed with the ability to inhibit trypsin and elastase together with anti-inflammatory activity, useful in the presence of injuries especially due to UV radiations. Once produced by the liver, macrophages and respiratory epithelial cells, serpin A1 is released directly into the bloodstream. A1AT is involved in blood coagulation, fibrinolysis, apoptosis, general inflammation, and some studies report that its C-terminal portion also has an anti-HIV activity [82]–[85]. One of the main targets of serpin A1 is represented by the elastase released by neutrophils, phagocytic cells that constitute a first line of defense in case of pathogenic invasions [34]. The task of this enzyme is to digest connective tissue elements to allow infiltration of blood cells to perform defense and repair functions. It has been shown that the activity of this protease greatly increases in the fluids of the inflammatory phase of chronic wounds (from 3 up to 8 mU/mg protein) compared to the fluids of acute wounds (from 0.1 up to 0.3 mU/mg protein) [84], [86]–[88]. Elastase also degrades fibronectin, which intervenes in the processes of spontaneous healing of wounds. This protein is deposited at the wound interface in the first phase after the wound formation and subsequently becomes part of the provisional matrix [89]. Serpin A1 inhibits the activity of elastase during inflammation processes to avoid involvement of neighboring areas, which are not affected by the inflammatory process. To support this hypothesis, several studies have shown a difference in serpin A1 concentration in chronic injuries compared to acute injuries: in chronic conditions there are very low values of this inhibitor, meaning that there is a dysfunction in the turnover processes of the matrix components [86], [90], [91]. Serpin A1 is considered the most abundant serin protease inhibitor in blood [90], and it mediates multiple activities associated with tissue remodeling. Congote *et al.* showed that the sequence between amino acids 393-418, associated with a β-turn structure in the C-terminal region and reported in Figure 10, maintains pharmacological properties comparable to whole native A1AT [84], [85], [90].

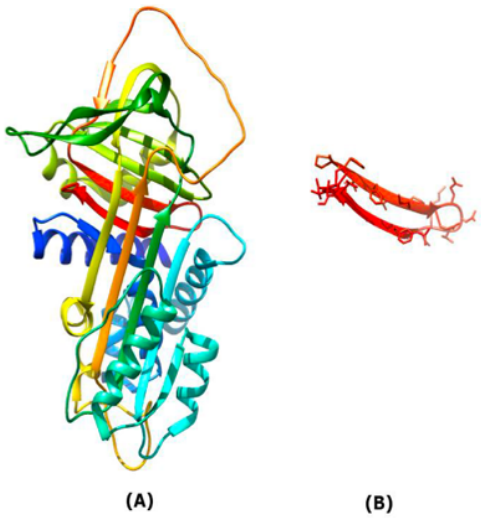

Figure 10 Serpin A1 whole protein (A) and the C-terminal portion investigated by Congote et al. (B) (PDB code: 2QUG).

Subsequently, Congote *et al.* compared the *in vitro* wound healing effect brought about by serpin A1 itself, a C-terminal portion (A1-C26) and a chimera between recombinant serpin A1 and insulin-like growth factor I (A1-IGF). They reported that peptide A1-C26 was effective in wound healing but even more in stimulating the increase of type I collagen *in vitro.* These data inspired the work of Pascarella *et al.* in our lab, aimed to verify whether shorter fragments could retain the above activities [79].

2.2 SA1-III PEPTIDE

Starting from the above-mentioned hydrophobic peptide sequence of serpin A1, A1-C26, Pascarella *et al.* selected three partially overlapping fragments, with the aim to isolate a smaller portion of the A1T1 with maintained ability as collagen turnover modulator. Shorter peptides, in fact, could be even more stable to protease activity, they could also show better permeability across the skin, and from a scale-up point of view they could be more attractive because of lower synthesis costs [92]. The peptides proposed by Pascarella *et al.* are reported in Table 3.

Table 3 Serpin A1 fragments chosen by Pascarella et al. [79].

Peptide name	***Serpin A1 fragments***	***sequence***
SA1-I	393-405	Ac-(PEG9)-PFVFLMIEQNTKS-NH_2
SA1-II	401-412	Ac-QNTKSPLFMGKV-NH_2
SA1-III	409-418	Ac-MGKVVNPTQK-NH_2

They synthesize overlapping fragments to include any active combination of amino acids; each fragment was C-terminally amidated and acetylated in N-terminal to avoid alterations in the net charges of each peptide, in order to reproduce the same properties observed for the whole protein. The initial choice to break down the A1-C26 sequence into three fragments consisting of 10 amino acids each, was later revised because of the strong hydrophobic region in the peptide SA1-I, localized in particular in the FVFLM sequence already investigated by Joslin *et al.* [93]. It was therefore necessary to modify SA1-I by pegylation; in addition, three other polar residues in the C-terminal portion were added, and for higher comparability, SA1-II was also elongated.
Collagen turnover modulation activity of the three peptides thus formed, was evaluated with SP-ELISA (Solid Phase-Enzyme-Linked Immunosorbent Assay) after treating with each peptide neonatal normal human dermal fibroblasts (neo-NHDF), in accordance with the studies carried out by Congote *et al.* [90]. The immunoenzymatic assay was designed using as positive controls TGF-β1 and L-ascorbic acid (vit. C), implicated in ECM remodeling processes [94], [95]. The results reported in Figure 11 showed that of the three peptides tested, SA1-III was the most active in increasing collagen concentration *in vitro*, and its activity was comparable to L-ascorbic acid.

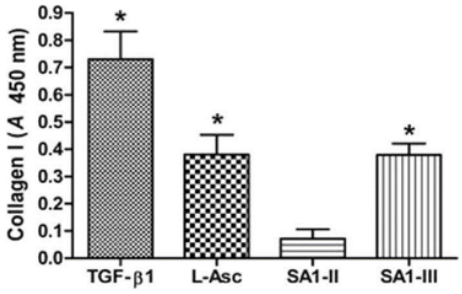

Figure 11 Type I collagen concentration evaluated with SP-ELISA after treatment of NHDFs with TGF-β1 (10 ng/mL), L-ascorbic acid (10 µM) and each peptide (40 µM) [79].

They calculated that the EC_{50} of peptide SA1-III was $9{,}75x10^{-7}$M and corresponded to a 33 % increase in collagen concentration in comparison with the basal collagen released by untreated cells. Subsequently, the activity of SA1-III in modifying collagen levels was analyzed in cell lysates (Figure 12) and in conditioned media using fibroblasts taken from human volunteers of different ages (C6: 36 years old (yo), C3: 57 yo, and C12: 84 yo) [80].

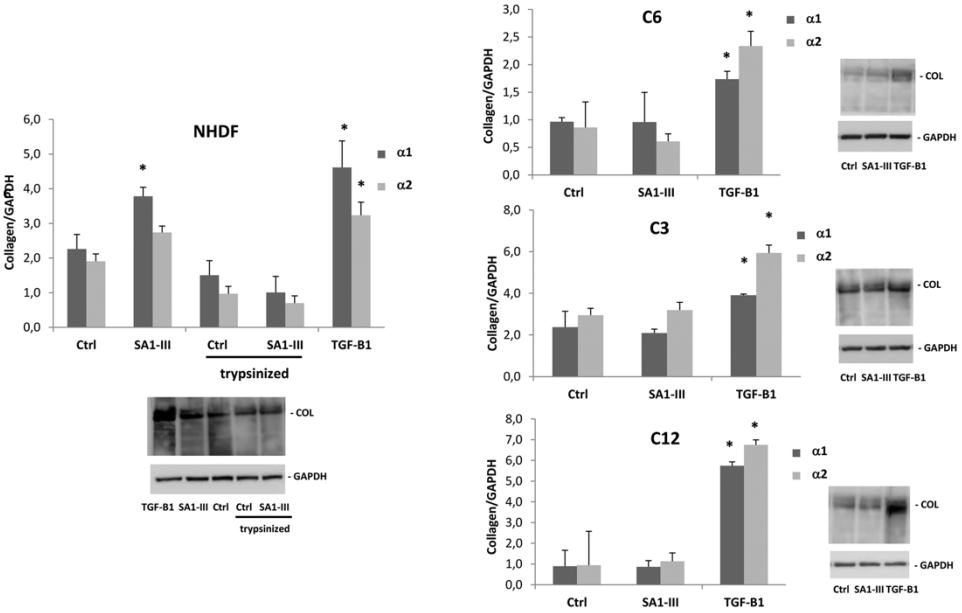

Figure 12 Effect of SA1-III (20µM) peptide and TGF-β1(10 ng/mL) on collagen concentration in cell lysates of different kind of fibroblasts after 72 h treatment. Trypsinized NHDFs were also used to analyze the truly intracellular collagen forms and to exclude any possible form of soluble collagen released by cells in their media. (Ctrl: untreated cells) [80].

It was demonstrated that the NHDFs cells are a good model to study collagen modulation: in fact, this kind of cells grow up faster than those obtained from adult subjects, have a better morphology, and reflect the conditions found in adult fibroblasts of different ages. The trypsinized NHDFs showed lower global collagen concentration, as expected, and no difference between control and peptide treatment, indicating no effect of SA1III on intracellular collagen levels, i.e., on the synthesis. On the other hand, the collagen levels found in cell lysates without pre-treatment with trypsin can be assimilated to a representation of the soluble collagen that fibroblasts were releasing in their media. Furthermore, it was shown that the peptide increased the level of the intact procollagen forms found in conditioned medium to a similar extent than TGF-β1. In addition, zymographic analysis carried out on SA1-III treated cell-conditioned media compared to media from untreated cells, showed a reduction in the gelatinolytic signal suggesting a reduced production of MMP-2 and MMP-9 induced by peptide SA1-III treatment in the fibroblasts in culture.

3. AIM OF THE PROJECT

In light of what Pascarella *et al.* observed [79], peptide SA1-III was chosen as a "cosmeceutical lead molecule" to obtain new bioactive peptides to be use, as a first approach, in cosmetic formulations (see in Figure 13 for peptide structure). Nevertheless, collagen turnover modulators are interesting from a therapeutic point of view in all those conditions where a defect in collagen induces pathologies, including problems of chronic wound healing.

3.1 SA1-III PROPERTIES

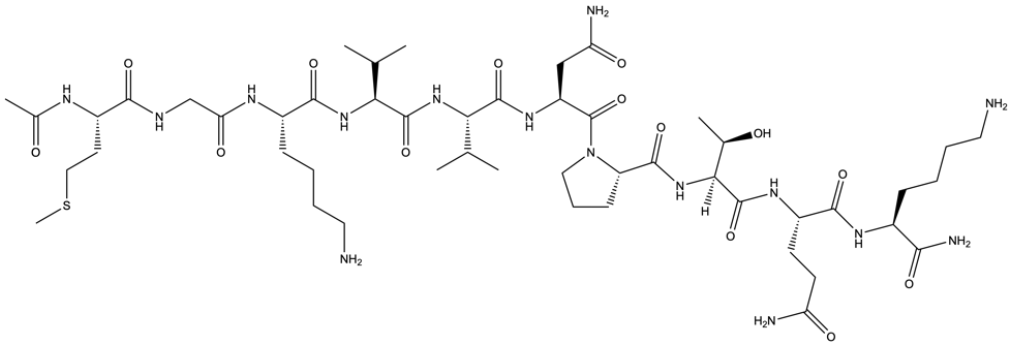

Figure 13 Peptide SA1-III structure, with the amidation in C-terminal and the acetylation in N-terminal.

To this purpose, a first goal will be to perform *in vitro,* or *ex-vivo* experiments in order to demonstrate SA1-III Mechanism of Action (MoA) and to describe SA1-III pharmacokinetic properties i.e., permeability through the skin, and both chemical and enzymatical stability.
The supposed MoA of SA1-III at that time was an inhibition of proteases, hypothesized by Cipriani *et al.* based on evidence obtained by zymography, but this needed to be detailed and confirmed.
Skin properties, like multilayering, lipophilicity, and the presence of numerous active enzymes, lead to the formation of a very effective barrier to the permeation of major ingredients in drugs or cosmetics. For this reason, it is mandatory to evaluate the ability of peptide SA1-III to pass through the *stratum corneum* to reach the ECM and the fibroblasts in the *dermis*.
As recently reported by Nguyen *et al.*, it is important to give the cosmeceutical buyers and consumers the opportunity to have access to research shreds of evidence supporting the claimed activity of cosmeceutical ingredients used topically [96], among which stability information related not only to the final formulation (i.e., shelf life of cream) but also and most importantly, to every single active ingredient [97]. To date, there were no robust analytical methods specifically designed to evaluate peptides of cosmeceutical interest for their enzymatic stability against dermal protease, and this is a great limit particularly when

aiming to produce formulations with pharmacologically active peptides for therapeutic purposes.

Moreover, considering that collagen-related pathologies are often associated to an inflammatory state, an additional goal will be the evaluation of the putative anti-inflammatory properties associated to peptide SA1-III.

3.2 SA1-III ANALOGUES

A second important step, to be carried out in parallel to the study of SA1-III pharmacokinetic properties, will be the design, synthesis, analytical characterization, and *in vitro* evaluation of new peptides derived from SA1-III.

Some modifications to the peptide backbone will be introduced to obtain second-generation peptides, more suitable for the cosmeceutical market. Among other aspects, this could be achieved by trying to increase SA1-III above-mentioned pharmacokinetic properties.

A first possible modification to peptide SA1-III is to shorten the amino acids sequence: this was the same reasoning of Pascarella *et al.* [79], as it will endow the molecule with a more feasible industrial scale-up process (also associated to low-price production costs). Moreover, active peptides with reduced sequence could also help in answering to the questions: what is the effective MoA of the SA1-III peptide and which sequence is actually implicated in the modulation of collagen turnover?

Whenever SA1-III should show poor intrinsic ability to pass through the *stratum corneum*, a second possible modification will be the palmitoylation (i.e., a conjugation with a fatty acid). In fact, in the case of macromolecules, transdermal delivery can be improved either by the incorporation in their composition of different moieties such as alcohols, free fatty acids, or surfactants (chemical enhancers), or by using physical enhancers, such as microneedles, ultrasonic waves, and low electrical current. Additional systems, e.g., nanoparticles, liposomes, nanostructured liquids, microemulsions, lyotropic liquid crystals, hydrogels, and polymer-based techniques can also be applied [98]. It goes without saying that the maintenance of collagen turnover modulation activity for the conjugated peptide must be demonstrated with *in vitro* assays.

Lastly, a third possible modification is the introduction of non-natural amino acid in order to increase the intrinsic peptide enzymatic stability to proteases.

4. RESEARCH DEVELOPMENT

4.1 RESEARCH WORKFLOW

This PhD project on peptide collagen turnover modulators derived from serpin A1 is divided into different branches, which are illustrated in Figure 14 in order to have a clear picture of what will be described step by step through the RESULTS and METHOD sections. To this purpose, recalls to paragraphs numbers are reported in the scheme.

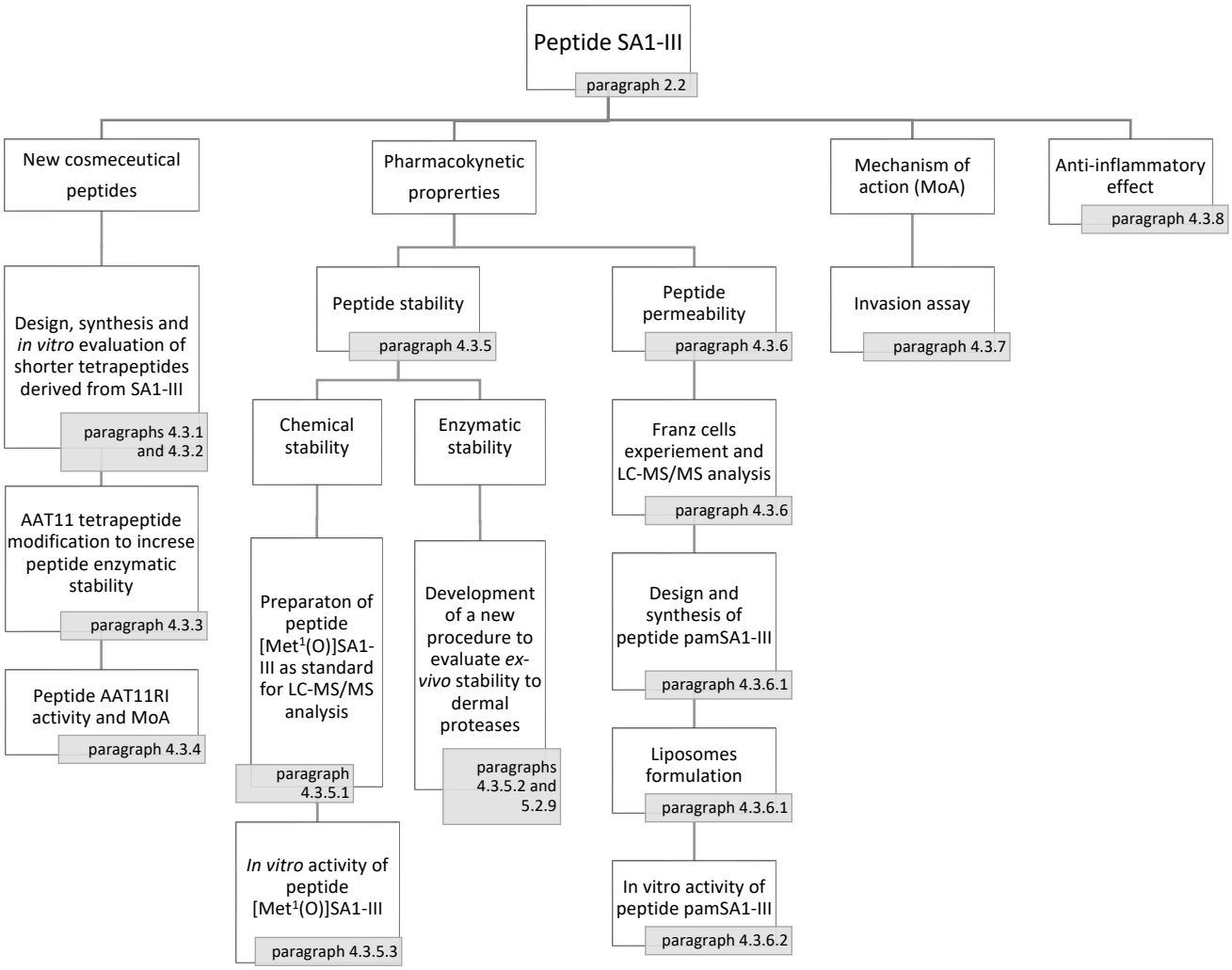

Figure 14 Workflow scheme of the research development.

Briefly, starting from peptide SA1-III (Ac-MGKVVNPTQK-NH_2), new shorter peptides were designed, synthetized and *in vitro* evaluated to be used as cosmeceutical active ingredients. Four overlapping fragments of SA1-III were chosen for this purpose.

One peptide of particular interest, AAT11 (Ac-KVVN-NH_2) was further modified in order to give rise to a second-generation family of smaller pseudopeptides with high stability to proteases. D-amino acids were introduced into the peptide sequence in place of the native L-amino acids and, in particular, two peptides were proposed: the one made of all D-amino acids (AAT11-allD), and its so-called "partial *retro-inverso*" analogue, named AAT11RI. The latter showed particularly interesting data in collagen turnover modulation when tested *in vitro*, so that due to this properties and taking into account its innovative sequence, it was patented [99].

A second purpose was to study peptide SA1-III stability in terms of chemical stability to oxidation (due to the Met^1 residue), and enzymatic stability to dermal proteases. To do this, an innovative methodology of LC-MS/MS analysis of peptides incubated with human skin homogenates (HSH) was developed [100]. This approach can be usefully applied to all peptides of cosmeceutical use. Moreover, peptide [Met^1(O)]SA1-III was obtained to be used as a standard in a more dedicated exploration of SA1-III oxidation in *ex-vivo* experiments conducted on human skin homogenates in which it was shown that peptide SA1-III is stable to this modification at least for 24 h.

In parallel to the description of SA1-III stability, peptide permeability across the skin was also evaluated using Franz cell assays. Unfortunately, peptide SA1-III does not show intrinsic ability to pass the *stratum corneum* by itself, and this means that its penetration must be adjuvated by other ingredients in the final cosmeceutical formulation. To improve this feature, a palmitoylated analogue of peptide SA1-III, termed pamSA1-III, was design and synthetized. Due to the lipophilic moiety, peptide pamSA1-III was then incorporated into liposomes to evaluate its activity in the collagen turnover modulation assay. Indeed, we were able to demonstrate in *in vitro* experiments that the activity observed in the case of SA1-III is maintained by its palmitoylated analogue pamSA1-III.

To confirm the hypothesis of a protease activity reduction demonstrated by both the studies of Cipriani *et al.* [80], and the preliminary observation of a reduction of collagen degraded bands in WB analysis conducted with SA1-III and its tetrapeptides, we studied the invasion ability of fibroblasts treated with SA1-III and AAT11RI peptides. This assay showed a significant decrease in protease activity, confirming the suggested mechanism of action.

Moreover, as final experiments, we evaluated the anti-inflammatory activity of peptide SA1-III, which brought about an interesting reduction of COX-2 protein level, ascribable to anti-inflammatory properties of this peptide.

4.2 INTRODUCTION TO METHODOLOGIES

4.2.1 PEPTIDE SYNTHESIS

Proteins are long polymers made up of the repetition of single units of amino acids linked by amide bonds between their α-carboxylic and α-amino groups. Peptides are smaller portions of proteins that can be more easily synthesized and therefore produced as unique molecules. Several synthetic peptides are relevant pharmaceutical products, ranging from the dipeptide sugar substitute aspartame to clinically used hormones such as oxytocin, adrenocorticotropic hormone, and calcitonin. The stepwise assembly of peptides from amino acid precursors has been described for nearly a century. The concept is straightforward, whereby peptide elongation proceeds *via* a coupling reaction between amino acids, followed by removal of a reversible protecting group. The first peptide synthesis, as well as the creation of the term "peptide", were reported by Fischer in 1901 [101]. Bergmann and Zervas created the first reversible Nα-protecting group for peptide synthesis, i.e., the carbobenzoxy group [102]. In 1954 Du Vigneaud *et al.* successfully applied early "classical" strategies to construct a peptide with oxytocin-like activity [103]. Classical, or solution-phase methods for peptide synthesis have an elegant history and have been well chronicled. Solution synthesis continues to be especially valuable for large-scale manufacturing and for specialized laboratory applications, even if nowadays large-scale synthesis assisted by microwaves in solid phase is an emerging and promising technology [104], [105]. The concept of solid-phase peptide synthesis (SPPS) stems from the possibility to take advantage of the chemistry that has been developed in solution, by adding a covalent attachment step that links the C-terminal amino acid to an insoluble polymeric support (resin), proposed in 1960s by Merrifield [106]. Subsequently, the anchored amino acid is extended by a series of coupling cycles stepwise from the C- to N- terminus using Nα-protected amino acids. The excess of soluble reagents and amino acids can be removed by simple filtration and washing. Once chain elongation has been completed, the crude peptide is chemically released from the support. Therefore, SPPS not only simplifies and accelerates the synthetic process, but also reduces the loss of intermediates during crystallization and purification steps, which dramatically affects the final yield of peptide synthesis, when performed in solution [107]. SPPS was later modified to use the tertbutyloxycarbonyl (Boc) group for Nα-protection [108] and hydrogen fluoride (HF) as the reagent for removal of the peptide from the resin [109]. SPPS was thus based on "relative acidolysis", where the Nα-protecting group Boc was labile in the presence of moderate acid (trifluoroacetic acid; TFA), while both the benzyl (Bzl) based side chain protecting groups and the peptide-resin linkage were stable in the presence of moderate acid and labile in the presence of strong acid (hydrofluoric acid; HF). In 1970, Carpino and Han introduced the 9-

fluorenylmethoxycarbonyl (Fmoc) group for Nα- protection [110]. The Fmoc group requires moderate base for removal, and thus offers a chemically mild alternative to the acid-labile Boc group. Fmoc-based strategies utilized tert-butyl (tBu) based side chain protection and hydroxymethylphenoxy-based linkers for peptide attachment to the resin. This was thus an "orthogonal" scheme that requires a base for removal of the Nα-protecting group and an acid to remove side chain protecting groups and break the peptide-resin linkage. The milder conditions of Fmoc chemistry as compared to Boc chemistry, which include elimination of repetitive moderate acidolysis steps and the final strong acidolysis step, were more compatible with the synthesis of peptides that are susceptible to acid-catalyzed side-reactions, and this brought a great change in the chemistry employed by peptide laboratories. Moreover, the Fmoc/tBu strategy is currently used by numerous commercially available synthesizers among which microwave-assisted solid-phase peptide synthesis (MW-SPPS) instruments are noteworthy.

Kinetic reaction problems due to intermolecular aggregation or to steric hindrance of protecting groups can generate premature termination of the peptide sequence during the different steps of the solid phase synthesis pathway. Therefore, the desired raw products are contaminated by a series of structurally, and chemically very similar, compounds such as diastereomers formed after epimerization or mismatched and incomplete sequences [111]. Therefore, the isolation of the target peptide is sometimes very tedious, representing a major limit for a preparative scale purification procedure. To decrease chain aggregation during synthesis, in 1990s microwave energy was introduced to peptide chemistry [112]. The effects of microwave irradiation on a growing polypeptide chain are due to both the increased temperature and to the alternating electromagnetic radiation to which the polar backbone of the polypeptide continuously aligns. As this new technology was widely appreciated, chemistry-dedicated microwave automated instruments became commercially available, and they started to be equipped with direct temperature control, magnetic stirring, and software for temperature and pressure control. Two different kind of microwave instruments are available to date: multi-mode and single mode. Single mode cavities have a uniform energy distribution, and they are frequently used to couple small samples. Compatibility of polymeric supports to higher temperatures and dramatic decrease of reaction time, boosted this technology to become the most appreciated for solid phase peptide synthesis. The average time of a single amino acid coupling assisted by MW can be decreased to approximately 15 minutes, unlike the manual SPPS that requires at least 45 minutes for each coupling. In the literature it has been widely reported that the microwave method generated peptides in at least comparable crude purity to conventional methods and importantly in a fraction of the time [113]. Interestingly, in many cases the microwave method proved superior to the conventional synthesis technique, yielding the peptide in significantly increased purity.

As previously pointed out, SPPS is based principally on two synthetic strategies: Boc/Bzl, in which a weakly acidic environment is used for the removal of the Boc group, and HF is used for the final cleavage from the resin; and Fmoc/tBu, in which amino acids are Nα-protected with Fmoc, that is labile to basic conditions, and tert-butyl in the side chain, which is unstable in mild acidic conditions and therefore is removed during the cleavage of the peptide from the resin [110], [114].
In particular, in the most used orthogonal Fmoc/tBu strategy, this protecting group is removed via base-induced β-elimination that gives carbon dioxide and dibenzofulvene as shown in Figure 15.

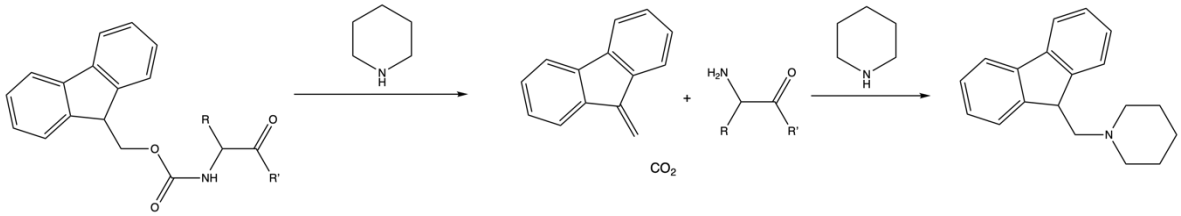

Figure 15 Removal of the Fmoc Nα-protecting group with piperidine in Fmoc/tBu SPPS.

Moreover, since the side product is a strong chromophore, the deblocking reaction can be also monitored by UV spectroscopy.
Fmoc group is also used to prepare several kinds of resins for SPPS e.g., the widely used rink amide resins (see Figure 16).

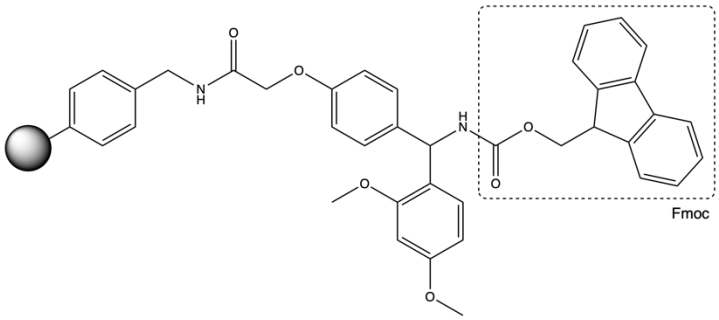

Figure 16 Rink amide AM resin (Fmoc-2,4-dimethoxy-4'-(carboxymethyloxy)-benzhydrylamine linked to Aminomethyl resin).

In these cases, once the resin of choice is swelled in N,N-Dimethylformamide (DMF) to expose all the anchorage site, the following step is the Fmoc removal from the resin, which give rise to a free amine group that will be available for the linkage with the first amino acid in C-terminal. Commonly, a solution of 20 % piperidine in DMF is enough for the deprotection step. The first amino acid will be then activated to be anchored to the resin; this activation consists in the transformation of the free carboxylic terminal group into more reactive forms, and it is carried out by using four different types of coupling techniques: carbodiimide, symmetrical anhydride, active ester, and coupling reagent.

Carbodiimides are one of the most popular *in situ* activators, since N,N'-dicyclohexylcarbodiimide (DCC) was used for the first time in 1950s [115]. However, due to its insoluble by-product dicyclohexylurea (DCU), it was used only in solution synthesis and not in SPPS where different kind of carbodiimides, producing DMF soluble urea, are preferred. In particular, in MW-SPPS a largely used couple of reagent is composed by N,N'-Diisopropylcarbodiimide (DIC) and Oxyma Pure. In fact, the highly reactive O-acylurea intermediate formed from DIC can induce side-reactions such as Asn and Gln dehydration or racemization [111], and for this reason auxiliary nucleophiles that capture the O-acylurea converting it in a less-reactive, but more selective form, are needed and recently, Oxyma Pure was identified as a potent and safe coupling additive [116], [117].
In Figure 17 the mechanism of action of DIC and Oxyma Pure to form a peptide bond is shown.

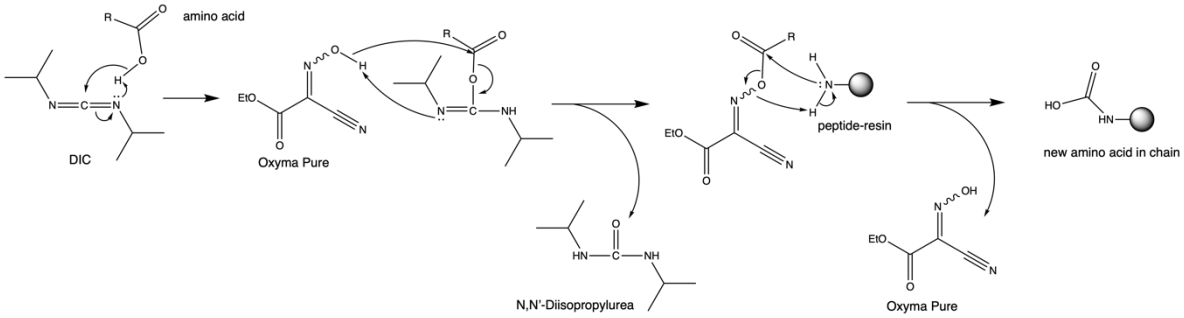

Figure 17 Peptide coupling reaction mediated by DIC and Oxyma Pure.

Preformed symmetrical anhydrides (PSA) may also be used in Boc chemistry, but they do not represent a first choice in peptide synthesis because they represent a great waste of material in comparison to the other techniques; in fact, they need two equivalents of protected amino acid to be formed and they must be used in excess.
A third way to obtain a peptide bond is to use amino acids preactivated esters [118], and to these days, only the pentafluorophenyl (OPfp) ones are used [119]. Thanks to their good stability in DMF and to the fact that they do not induce side reactions, they are preferable in those cases where longer coupling time is needed. OPfp esters are widely used in SPOT synthesis (which permits rapid and highly parallel synthesis of a large number of peptides and peptide mixtures) because the amide formation can be monitored in real-time using a dye, bromophenol blue, that form a blue ion-pair with the free amine group of the peptide in elongation, and as the reaction takes place, the color changes from blue to yellow [120].
The last class of molecules used to obtain a proper peptide bond, is the one of coupling reagents. They are the *in situ* activators, the use of which is generally easy and free of side reactions. The most used are phosphonium or aminium (also known as uranium) salts, e.g.,

HBTU, TBTU, BOP, and PyBOP (reported in Figure 18), that in the presence of a tertiary base convert an amino acid in the corresponding hydroxybenzotriazole (OBt) esters.
Moreover, there are other reagents that generate more reactive esters than OBt e.g., HATU (also reported in Figure 18), which generate OAt esters. However, they must be handled carefully as these triazoles (both OBt and OAt) are potentially explosive.

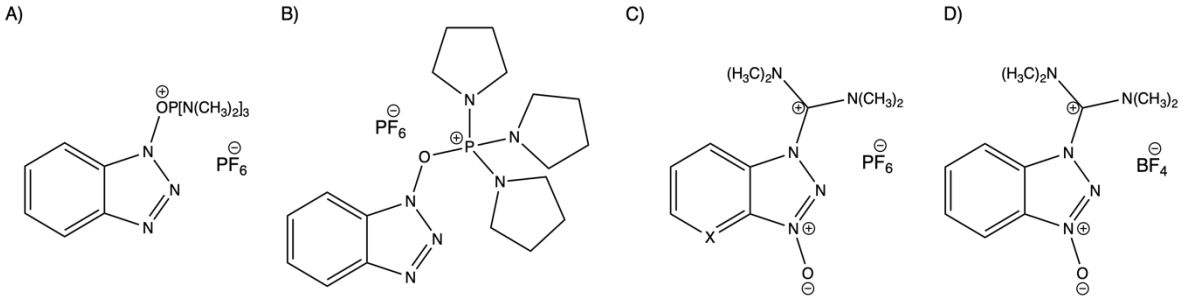

Figure 18 Coupling reagents structure. A) BOP; B) PyBOP; C) X= N HATU; C) X= CH HBTU; D) TBTU.

The above mentioned Oxyma Pure, indeed, led to a series of new coupling reagents that generate very reactive and safer esters [117].
Once the coupling strategy is chosen and the peptide on resin is ready, cleavage from the resin will occur upon treatment with TFA 95 % v/v in water, and, depending on the side chains protecting group, by adding a mixture of scavengers, reagents that can quench the reactive molecules deriving from side chain protecting group removal. Peptides recovered after a work-up step of repetitive ether precipitations, are then analyzed as raw material by HPLC-MS (high performance liquid chromatography coupled with mass spectroscopy). Finally, peptides are purified by chromatography (e.g., flash chromatography, semi-preparative or preparative HPLC) in order to obtain the desired HPLC purity grade.

4.2.2 PEPTIDE WITH MODIFIED BACKBONES

Human endogenous proteins are usually composed of natural amino acids, in the L-configuration. To overcome the disadvantages originating from the low bioavailability and short half-life of peptides with sequences derived from proteins, development of peptidomimetics can be an advantageous approach. In fact, strategies aimed to develop peptidomimetic may result in altering the physicochemical properties of a peptide, possibly increasing its biological activity [121]. Chemical synthesis plays a relevant role to give access to a much wider chemical diversity than peptide derivatives produced by recombinant technologies. In particular, there is space for a diversified intellectual property (in terms of new patentable chemical entities). Peptidomimetics very often contain non-peptide structural elements, such as peptide bond surrogates, which resist peptidase cleavage, a feature also found in natural peptidase inhibitors. Some strategies used in the field of cosmeceutical peptides to achieve good stability to skin proteases will be discussed below.
The use of non-coded amino acids in peptide analogs or peptidomimetics is a strategy to protect synthetic peptides from proteolytic enzymatic activity; in fact, peptidases are able to recognize only natural amino acids [122]. For example, replacement of His in the well-known GHK peptide by either L-4,5,6,7-tetrahydro-1Himidazo[4,5-c]pyridine-6-carboxylic acid (L-spinacine, Spi) or L-1,2,3,4-tetrahydro-isoquinoline-3-carboxylic acid (Tic) produces analogs that display good biological activity and better stability to the human serum proteases, as established in in vitro studies [123].
The use of modified peptide backbone is widespread in therapeutics, [124], [125] but also in the field of cosmeceuticals.
In 2009, Dalpozzo *et al.* introduced a partially *retro-inverso* analog of the natural growth factor GHK, with a reversal of the -CONH- bond between histidine and lysine that led to -NHCO- and resulted in the formation of a gem-diamino alkyl and a substituted malonyl residues [126]. This new peptide was shown to have enhanced enzymatic stability than the precursor, when tested *in vitro* in human plasma. One of the most common modifications reported in the literature for enhancing peptide stability is undoubtedly the cyclization of linear active peptides. Cyclic peptides are classified into homodetic, if the bridge that contributes to the ring is a peptide bond, and heterodetic, when the cyclization includes other bridges such as disulfide between two cysteine residues, ester (lactone), ether or thioether bridges. Furthermore, the two most common cyclization strategies are conducted by forming a linkage between the amino- and carboxy-groups in the N- and C-termini, or by forming a linkage between two amino acid side chains; the former is called head-to-tail cyclization (also known as end-to-end cyclization), the latter is called side chain-to-side chain. A third, lesser used way to obtain cyclic peptide is a compromise between the two and is called side chain to head [127] In fact, by reducing conformational flexibility,

cyclopeptides can display enhanced stability to proteolysis, and in some cases also better biological activity, if the bioactive conformation is stabilized [127], [128].

4.2.3 IN VITRO ASSAYS: CELL CULTURES

Peptides with HPLC purity over 95 % were then used to treat NHDFs to evaluate their *in vitro* activity. A picture of the cell used for the experiment is reported in Figure 19.

Figure 19 Untreated NHDFs; picture obtained in a Nikon TMS Inverted Microscope.

Cell cultures were established as a good method to reproduce, in a simplified system, the natural environment of various kinds of cell lines, in order to study biological phenomena such as cell growth and differentiation, structure and function of genes, including genetic manipulation. *In vitro* culture testing is the first steps required in the preclinical phase to obtain the marketing of a drug, and it is becoming a fundamental step for the evaluation of the activity of cosmeceutical raw materials too. Working with cell cultures requires specific skills, proper media, saline solutions and containers where to grow cells, and instrumentation that must ensure sterility, such as vertical laminar flow hoods, autoclaves or dry stoves for the sterilization of materials used [129], [130]. Among the most used media there are MEM (Minimum Essential Medium), DMEM (Dulbecco's Modified MEM) and RPMI (Roswell Park Memorial Institute), which differ from each other for saline composition and different nutrient content, while they all contain some essential amino acids, glucose, and inorganic salts essential for protein synthesis and cell growth in general such as Na^+, K^+, Mg^{2+}, Ca^{2+} and Cl^-. Conversely, this type of media does not contain antibiotics, L-Glutamine or fetal bovine serum (FBS), which could suffer instability, so it is necessary to add them at the time of cell culture. Cells are grown in incubators where a well-defined temperature, O_2 and CO_2 concentration is maintained; normally for mammalian cells standard parameters are used: 37 °C, 5 % CO_2 and 95 % O_2.

In order to measure the amount of protein present in each cell lysates sample, a protein dosing protocol was used. This procedure is essential to normalize the subsequent assays (e.g., Western Blot) according to the protein content of each sample. The protein assay is performed in 96 MW plates, using Bovine Serum Albumin (BSA) solutions to make a standard curve and H_2O as a blank sample. This is a colorimetric assay based on the Lowry method [131] and it is composed of two reagent (reagent A and reagent B) containing a saline solution of copper tartrate and an aqueous solution of phosphomolybdate and phosphotungstate, also called Folin-Ciocâlteu reagent, respectively. The reagents must be

mixed extemporaneously at the moment of the assay, and because of the copper tartrate, a highly alkaline environment is created in the well, which allows the proteins to react with copper. Once the complex is formed, this reduces the Folin-Ciocâlteu reagent. This reduction is particularly active if tryptophan and tyrosine are present, but to a lesser extent it is also determined by histidine and cysteine. The visible effect, even to the naked eye, is a change in the coloration of the blue-purple wells, which assumes different shades depending on the different protein concentration of the samples analyzed. Detection must be done by a spectrophotometer at the wavelength of 560 nm.

4.2.4 Immunoenzymatic Assays: Western Blot

The content of proteins (or enzymes) in cell conditioned media, and cell lysates can be evaluated thanks to the immunoenzymatic technique of western blot (WB).
This particular method of choice grants to obtain more precise data on protein concentrations if compared to the ELISA techniques previously used by Pascarella *et al.* [79]. In fact, WB allows to get specific information on the various forms of collagen (procollagen, mature collagen, degraded collagen), which is of great help in understanding the possible mechanism of action behind the activity of SA1-III and its derivatives. This differentiation is possible thanks to the combination between proteins separation mediated by electrophoresis, and the sensitivity of immunochemical techniques mediated by antibodies recognition [132].

4.2.5 Dermal Stability Assays

Bioactive peptides are highly appreciated in the cosmeceutical field for several reasons, mainly related to their high specific activity, which allows to use them in very low concentrations, usually micromolar [133]. However, peptides were once considered ineligible for drug development for many reasons, among which the most important was the presence within the human body of several proteases able to degrade them. In fact, as peptides are composed of many peptide bonds, they are susceptible to degradation by proteases, which are largely distributed in the skin, and intrinsic and extrinsic factors, such as age or exposure to UV-light, pollution, or extreme weather conditions, could mediate an increase of the enzymatic activity in the skin. [134]. To this purpose, it is necessary to set up the best experimental conditions to evaluate, by HPLC-MS/MS, the half-time of cosmeceutical peptides in skin homogenates.

4.2.6 Skin Permeability assays

As already discussed in paragraph 1.4, skin properties, like multilayering, lipophilicity, and the presence of numerous active enzymes, make skin a very effective barrier for the permeability of major ingredients in drugs or cosmetics. For these reasons, bioactive molecules, including peptides, should be characterized for their physicochemical features, such as molecular weight and melting point, average lipophilicity, and good water solubility [92].

A number of assays are available for skin permeability evaluation, including the commonly used Franz diffusion cell [135]. The Franz apparatus, reported in Figure 20, is designed to mimic the behavior of active principles and formulations when they are applied to skin.

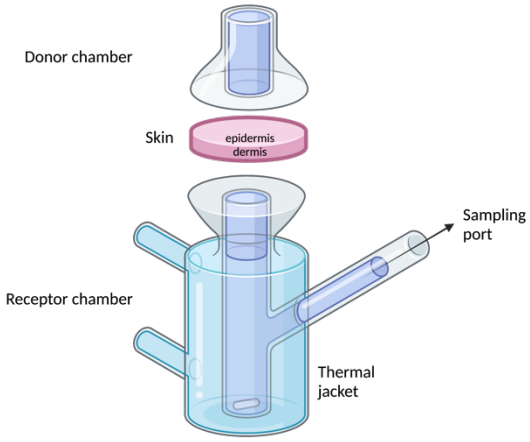

Figure 20 Scheme of a Franz cell apparatus with human skin as diffusion membrane.

Samples to be tested are placed in a donor chamber in contact with a membrane (artificial or real skin) and the rate of transfer is determined by collection of the permeate on the receptor chamber after different times of incubation. The solutions collected are then analyzed by HPLC-MS in order to describe a diffusion curve through the skin for the tested sample.

4.2.7 LIPOSOMES

Liposomes are sphere-shaped vesicles consisting of one or more phospholipid bilayers and widely used as a vehicle for drug delivery to their site of action, being used even for clinical applications [136]. Nowadays liposomes are also used to improve solubility and chemical stability of natural compounds [137], obtaining great visibility in the supplements and cosmetic markets, where the attention to “green” product is growing up. Liposome’s structure is characterized by the presence of one or more double layers of amphiphilic lipids mostly formed by phospholipidic molecules: those of the outer layer are regularly lined side by side and expose their polar head (hydrophilic portion of the molecule) to the aqueous environment that surrounds them; the apolar tail (lipophilic portion of the molecule) is instead directed inwards, where it intertwines with that of the second lipid layer, which has a specular organization in comparison to the previous one. In the internal phospholipid layer, in fact, the polar heads are directed towards the aqueous environment contained in the cavity of the liposome. The preparation of liposomes, and of nanomicelles in general, can be classified into two categories: chemical and physical methods. Chemical methods involve the covalent coupling of the drug to the polymer, after which the drug is

encapsulated into the core by self-assembly. The preparation process consists of a series of chemical reactions, which can be challenging and complicated. Thus, most of nanomicelles are prepared by physical methods, which include direct dissolution method, dialysis method, self-assembly solvent evaporation method and thin-film hydration method. The thin-film hydration method is most often used due to its simplicity and practicability, and its ability to yield small and uniform particles [138].

4.2.8 Invasion assays: The Boyden Chambers

In order to establish peptide mechanisms of action, invasion assays in Boyden invasion chambers have been performed. This apparatus is composed of two different compartments (donor and acceptor chamber), which are separated by a microporous membrane (or filter) coated with Matrigel® matrix in order to reproduce the ECM conditions. The invasion assay is widely use to quantitatively describe the migratory responses of cells, including chemotaxis, haptotaxis, and chemokinesis [139] and for each experiment some important parameters need to be optimized i.e., the number of cells to load on the chamber, the pore size of the membrane, the type and concentration of the attractant (if needed), and the incubation time. Cells are placed inside the upper chamber and induced to migrate through the pores, to reach the other side of the filter where a chemo-attractive substance enriches the medium. After an appropriate time of incubation, migrated cells are fixed to the filter and counted in an optical phase contrast microscope. The number of migrated cells that were previously treated with peptides is then compared to the number of migrated untreated cells, in order to underline possible differences in the migration ability that is in turn proportionally related to the protease ability of degrading the ECM components reproduced by the Matrigel® matrix.

4.3 RESULTS

Results obtained using the above-described techniques will be hereon described, with reference to the EXPERIMENTAL PART that includes each protocol.

4.3.1 SA1-III AND SHORT DERIVATES SYNTHESIS

An overlapping approach (offset: 2, overlap: 2) was applied to design four tetrapeptides derived from SA1-III, an active portion of serpin A1, as reported in Table 4.

Table 4 Serpin A1 fragments derived from overlapping strategy operated to peptide SA1-III.

serpin A1 fragments	***sequence***
SA1-III (409-418)	Ac-**MGKVVNPTQK**-NH_2
AAT09 (409-412)	Ac-**MGKV**-NH_2
AAT11 (411-414)	Ac-**KVVN**-NH_2
AAT13 (413-415)	Ac-**VNPT**-NH_2
AAT15 (415-417)	Ac-**PTQK**-NH_2

Peptides were named after A1AT protein (serpin A1) and the relative position of the sequences; each fragment was acetylated and amidated according to what has been already discussed in paragraph 2.2. All peptides were synthetized as reported in paragraph 5.2.1 and crude peptides were purified as reported in paragraph 5.2.2 to reach at least 95 % HPLC purity to be tested *in vitro* on NHDFs. Analytical characterization of the final products is reported below in Table 5.

Table 5 Analytical characterization of purified peptides SA1-III, AAT09, AAT11, AAT13, and AAT15. All the analysis were carried out on a HPLC Waters with a 2.7 µm (100 x 3.0 mm) Bioshell A160 C18 column working at 0.6 ml/min. Solvent lines were (A) H_2O (0.1 % v/v TFA); (B) acetonitrile (ACN) (0.1 % v/v TFA). [a] Retention time expressed in minutes. The analytical gradients were: [b] 10-60 % ACN in 5 min; [c] 05-50 % ACN in 5 min; [d] 05-40 % ACN in 5 min; [e] 03-15 % ACN in 5 min.

Peptide	***Sequence***	***RP-HPLC Rt [a]***	***Purity grade (HPLC)***	***ESI-MS MH^{+1} (m/z) Calc / (found)***
SA1-III	Ac-MGKVVNPTQK-NH_2	3.63 [b]	≥ 95 %	1142.6 / 1142.7
AAT09	Ac-MGKV-NH_2	4.05 [c]	≥ 98 %	475.3 / 475.3
AAT11	Ac-KVVN-NH_2	2.60 [c]	≥ 98 %	500.3 / 500.4
AAT13	Ac-VNPT-NH_2	3.04 [d]	≥ 98 %	471.3 / 471.4
AAT15	Ac-PTQK-NH_2	3.20 [e]	≥ 98 %	514.3 / 514.3

4.3.2 IN VITRO TETRAPEPTIDES ACTIVITY

Firstly, the new tetrapeptides were used for the MTS assay (protocol described in paragraph 5.2.4) in order to evaluate their potential mitogenic properties. None induced a significant increase in cell proliferation (< 10 % as compared to the control cells).

Cell lysates derived from the treatment protocol described in paragraph 5.2.4 were used for western blot experiment (see protocol in paragraph 5.2.6) to evaluate collagen concentration considered as the two kinds of procollagens already described by Cipriani *et al.* with both amino- and carboxy-terminal portions (170 kDa) or with one of the two (150 kDa), that reflect the concentration of procollagen in the ECM according to previous interpretations described in paragraph 2.1 [80]. Indeed, the 130 kDa band related to tropocollagen, or rather one of its α chain, was not included in the graph below as the absorption values associated with it were not particularly high.
The data reported in Figure 21 show the average values of four WB assays performed on NHDFs cell lysates recovered after treatment for 72 hours with peptide SA1-III, its tetrapeptide derivatives, TGF-β1 and with mere DMEM 0 % FBS (CNTRL).

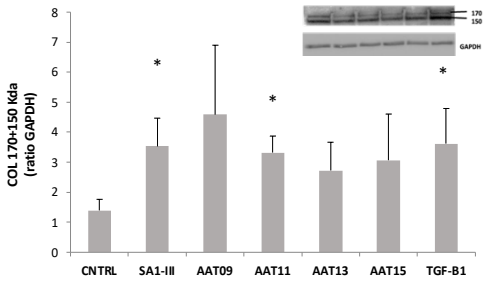

Figure 21 Bar chart showing the values for type I collagen concentrations measured through WB. Values are the average of four experiments carried out on cell lysates of NHDFs treated for 72 hours with the peptides reported in the x-axis (20 μM), with TGF-β1 (10 ng/mL), and untreated fibroblasts (CNTRL). At the top right: an example of a membrane with protein bands corresponding to the procollagen forms at 170 kDa and 150 kDa, and the reference band chosen (GAPDH) at 37 kDa. In the y-axis the values for the volume of protein bands procollagen (170 kDa and 150 kDa) in relation to the reference value (37 kDa) are reported. SE (standard error) value are also reported, and star data indicate a statistically significant increase in comparison to CNTRL cells (Student's t test, p < 0.05).

The absorbance values of each sample were compared to the value obtained for GAPDH (glyceraldehyde-3-phosphate dehydrogenase; housekeeping protein of 37 kDa) used as a reference.
These experiments on cell lysates confirm the activity of SA1-III in increasing collagen concentration when used as *in vitro* treatment at comparable level of what observed for TGF-β1, and both values are statistically significant (ANOVA, $p < 0.05$) as compared to CNTRL collagen level which represent the basal collagen concentration. All the new tetrapeptides show collagen levels higher than the CNTRL one, with AAT11 showing a statistically significant effect (Student's *t* test, $p < 0.05$).
Information on the different forms of extracellular collagen were obtained analyzing the conditioned media of fibroblasts that underwent the treatments. In this case, protein band quantification was made on:

- procollagen with C- and N-terminal (170 kDa) or with only one of the two (150 kDa),
- protease-degraded collagen bands present in the ECM (100 kDa, 75 kDa and 60 kDa).

The graphs in Figure 22 refer to the type I collagen concentration values acquired as procollagen bands and collagen degradation bands separately.

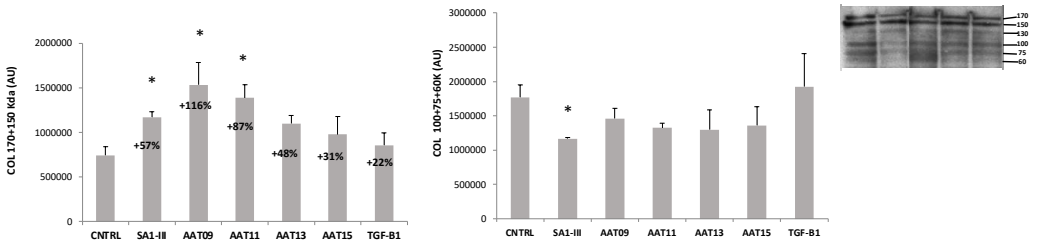

Figure 22 Bar chart showing the values for type I collagen concentrations measured through WB. Values are the average of three experiments carried out on conditioned media released by NHDFs treated for 72 hours with the peptides reported in the x-axis (20 µM), with TGF-β1 (10 ng/mL), and untreated fibroblasts (CNTRL). At the top right: an example of a membrane with protein bands corresponding to the procollagen forms at 170 kDa and 150 kDa (graph on the left), and collagen degraded forms at 100 kDa, 75 kDa and 60 kDa (graph on the right). In the y-axis the values for the volume of protein bands are reported. Percentage values in the graph on the left indicate the increase of procollagen concentration compared to the basal procollagen concentration observed for the CNTRL. SE (standard error) are also reported, and star data indicate statistically significant values (Student's t test; $p < 0.05$).

The activity of TGF-β1, as positive control, is clearly visible also in the culture media, even if to a lower extent. Peptide SA1-III shows an increase greater then 50% of procollagen, thus confirming the ability of this peptide to increase the concentration of collagen I also in the extracellular environment. Concerning the tetrapeptides, the data on the general increase of collagen remains consistent, especially associated with the peptides AAT09 and AAT11. The values associated with the degradation bands are particularly interesting, since they suggest a first hypothesis on the possible mechanism of action of the peptides analyzed. As expected, treatment with TGF-β1 does not affect collagen degradation products, if compared to the CNTRL. In fact, in accordance with the data in the literature, TGF-β1 is only implicated in the ECM components synthesis and not in degradation [19], [94].
The data found for SA1-III, however, show interesting decreases in the concentration of degraded collagen, as compared to the control, thus supporting the hypothesis that the mechanism of action with which the peptide increases the concentration of collagen type I is a reduction of protease activity on the produced collagen. This activity is also reported for all the tetrapeptides.

Taken together these experiments give a first suggestion on the mechanism of action of SA1-III, that have to be further investigated with specific assays.
Moreover, two peptides results stand out among the others: peptides AAT09 and AAT11.
As peptide AAT09 contains a methionine residue, which may be the cause of chemical instability due to oxidation of its side chain, in a first instance this will be considered a second-choice peptide. For this peptide, further modification might be done, e.g., an exchange between Met^1 and Nle^1 (Norleucine), a homologus amino acid that is not subject to the oxidation.

The results obtaine with AAT11, indeed, are robust (in terms of statistical significance) and its sequence does not contain chemically unstable amino acids. Thus, considering a bio-inspired approach, peptide AAT11 was chosen to be a new cosmeceutical lead to be further modifyed to enhance, e.g., peptide stability to proteases.

4.3.3 AAT11 D-SERIES SYNTHESIS

Chemical degradation of cosmeceutical peptides remains one of the major challenges, due to their limited bioavailability attributed to their high susceptibility to the proteases widely abundant in the skin. In order to develop active peptides derived from AAT11, with increased resistance to the action of peptidases, two analogues were designed, introducing D-amino acids instead of L-amino acids following the scheme shown in Figure 23.
Peptides AAT11-allD with sequence Ac-kvvn-NH_2 (lower-case letters indicate D-residues, e.g k indicates D-Lys, etc.) and peptide AAT11RI with sequence Ac-nvvk-NH_2 were synthetized as described in paragraph 5.2.1 and purified as reported in paragraph 5.2.2. The D-series tetrapeptides analytical characterization by HPLC-MS is reported in Table 6.

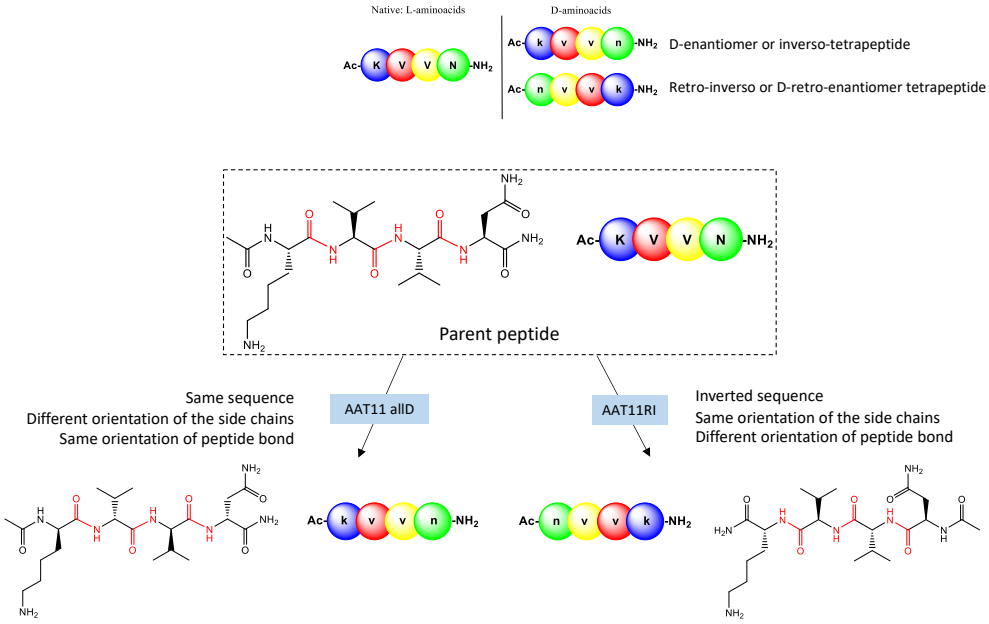

Figure 23 Design of more stable peptides derived from AAT11 fragment of serpin A1.

Table 6 Analytical characterization of purified peptides AAT11-allD and AAT11RI carried out on a HPLC Waters with a 2.7 µm (100 x 3.0 mm) Bioshell A160 C18 column working at 0.6 ml/min. Solvent lines were (A) H2O (0.1 % v/v TFA); (B) ACN (0.1 % v/v TFA). (a) Retention time expressed in minutes. The analytical gradient was (b) 5-30 % ACN in 5 min.

Peptide	***Sequence***	***RP-HPLC Rt [(a)]***	***Purity grade (HPLC)***	***ESI-MS MH^{+1} (m/z) Calc / (found)***
AAT11-allD	Ac-kvvn-NH_2	2.28 [(b)]	≥ 95 %	500.3 / 500.2
AAT11RI	Ac-nvvk-NH_2	3.47 [(b)]	≥ 95 %	500.3 / 500.2

4.3.4 D-ANALOGUES ACTIVITY

Given the fact that both peptides were obtained at an acceptable HPLC purity grade, they were used for a preliminary *in vitro* screening of their activity, by treatment of NHDFs, as described in the protocols reported in the experimental methods. As shown in Figure 24, experiments were carried out on peptides SA1-III, AAT11, AAT11-allD and AAT11RI, using 20 µM concentration. Moreover, their potential mitogenic properties were also evaluated with the MTS assay (protocol described in paragraph 5.2.4), and they showed no significant increase in cell proliferation (< 10 % compared to the control cells).

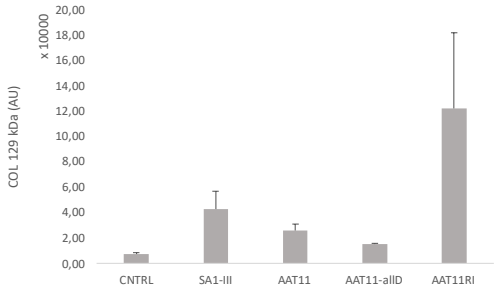

Figure 24 Bar chart showing the values for type I collagen concentrations measured through WB. Values are the average of three experiments carried out on conditioned media released by NHDFs treated for 72 hours with the peptides reported in the x-axis (20 µM) and untreated fibroblasts (CNTRL). In the y-axis the values for the volume of protein bands are reported. SE (standard error) value are also reported.

The results were very promising and surprising, as they showed that both D-analogues were able to increase collagen concentration, particularly peptide AAT11RI, which appeared to be a more potent collagen turnover modulator, as compared to the precursor peptide AAT11.

A remarkable fact is that, while usually the introduction of D-amino acids greatly improves their resistance to proteolytic degradation in comparison to the L-amino acids parent peptides, this transformation does not always reproduce the bioactive conformation, and could lead to the formation of less active analogues (as observed for peptide AAT11-allD) [125], [140]–[142]. Indeed, the great variability of AAT11RI effect (indicated by the high value of SE) can be associated to differences in cell proteolytic activity among different experiments and/or to the possible variability in the isolation of the media, as protein concentration involved several centrifugation passages. To this purpose, also taking into account what was already observed by Cipriani *et al.* [80] and described in paragraph 2.1, further experiments will be performed on cell lysate' proteins.

On the basis of these data, a patent application was filed in collaboration between the University of Florence and Espikem srl, an ex-spin off company of the University of Florence that invested in this project [99].

In order to consolidate this evidence, more detailed investigations were conducted and peptide SA1-III and AAT11RI were used again for *in vitro* treatment of NHDFs. Results showed in Figure 25 confirm, as expected, the finding of an increased activity of AAT11RI compared to SA1-III, as suggested by the preliminary data on AAT11RI shown above.

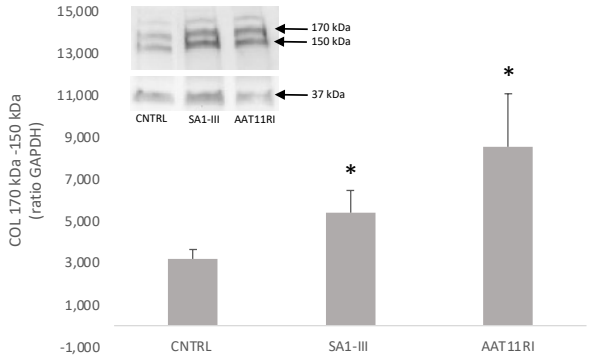

Figure 25 Bar chart showing the values for type I collagen concentrations measured through WB. Values are the average of eight experiments carried out on cell lysates of NHDFs treated for 72 hours with the peptides reported in the x-axis (20 µM), and untreated fibroblasts (CNTRL). At the top left: an example of a membrane with protein bands corresponding to the procollagen forms at 170 kDa and 150 kDa, and the reference band used (GAPDH) at 37 kDa. In the y-axis the values for the volume of protein bands procollagen (170 kDa and 150 kDa) in relation to the reference value (37 kDa) are reported. SE (standard error) value are also reported, and star data indicate a statistically significant increase in comparison to CNTRL cells (Student's t test; p< 0.05).

Moreover, increasing the number of experiment replicates (i.e., eight different WB acquisitions), and the use of cell lysates, where we can normalize values with reference to a housekeeping protein used as an internal reference, greatly improved the statistics associated to both peptides.

4.3.5 SA1-III STABILITY

Peptide bioavailability is a critical parameter, mainly due to their susceptibility to enzymatic activity, even when the route of administration is topical; in fact, several issues related to the presence of proteolytic enzymes in the skin should be taken into account [2], [143]. Moreover, when considering the *in vivo* bioavailability of a molecule, beside enzymatic stability, chemical stability should be considered, as well.

The most accurate and foremost technique to obtain this information is a quantitative combination of liquid chromatography and mass spectrometry. To this purpose, we developed a simple and reliable assay to determinate peptide stability, based on *ex-vivo* experiments on human skin homogenates (HSH) [100]. The protocols used to prepare samples will be described in paragraph 5.2.7. The stability studies were firstly optimized using a reference peptide, i.e. pal-KTTKS (palmitoyl-KTTKS-OH; synthesis and purification described in paragraph 5.2.1 and 5.2.2, and characterization reported in Table 7), whose enzymatic stability to proteases was already described [144], and then extended to peptides SA1-III.

Table 7 Analytical characterization of purified peptide pal-KTTKS carried out on a HPLC Waters with a 2.7 µm (100 x 3.0 mm) Bioshell A160 C18 column working at 0.6 ml/min. Solvent lines were (A) H_2O (0.1 % v/v TFA); (B) ACN (0.1 % v/v TFA). [(a)] Retention time expressed in minutes. The analytical gradient was [(b)] 50-80 % ACN in 5 min.

Peptide	***Sequence***	***RP-HPLC Rt [(a)]***	***Purity grade (HPLC)***	***ESI-MS MH^{+1} (m/z) Calc / (found)***
pal-KTTKS	palmitoyl-KTTKS-OH	3.76 [(b)]	≥ 95 %	802.01 / 802.1

The stability results of SA1-III reported in Figure 26 show that the peptide is stable in HSH up to 8 h, while after 8 h we observed a significant loss of analyte signal. The same degradation profile was also observed in HEPES solution. This peptide's behavior can be ascribed to a possible oxidation mechanism that occurs at longer incubation time (i.e., on the methionine residue present in position 1). The oxidation of this amino acid, which leads to methionine sulfoxide, has been frequently observed in proteins [145] and may occur in the presence of many factors, such as light and hydrogen peroxide. Moreover, it has been known for a long time that, when exposed to ambient light, HEPES produces hydrogen peroxide [146], and it has also been shown that hydrogen peroxide levels in the buffer slowly decrease upon storage in darkness.

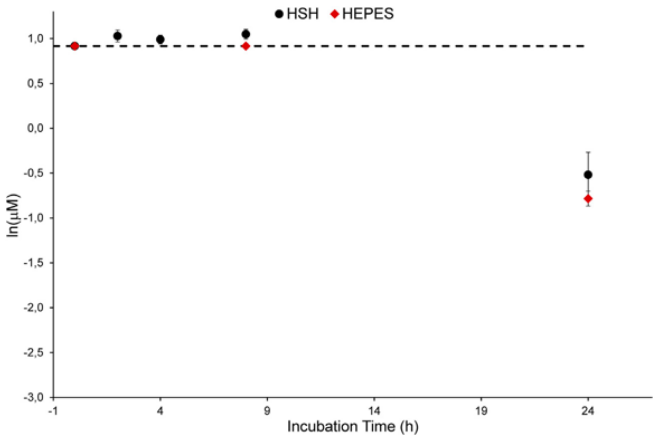

Figure 26 Degradation profile in HSH for SA1-III; HEPES solution also reported and substrate addition in dashed line [100].

4.3.5.1 Preparation of Peptide [Met[1](O)]SA1-III

Considering the hypothesis that the side chain of the methionine residue in the N-terminal position of peptide SA1-III could be oxidized in the experimental conditions used, peptide [Met[1](O)]SA1-III was prepared starting from a < 95 % purity batch of SA1-III (as described in paragraph 5.2.1) to characterize the MS/MS ions profile of the oxidized form. The oxidation reaction was monitored by UHPLC as reported in Figure 27.

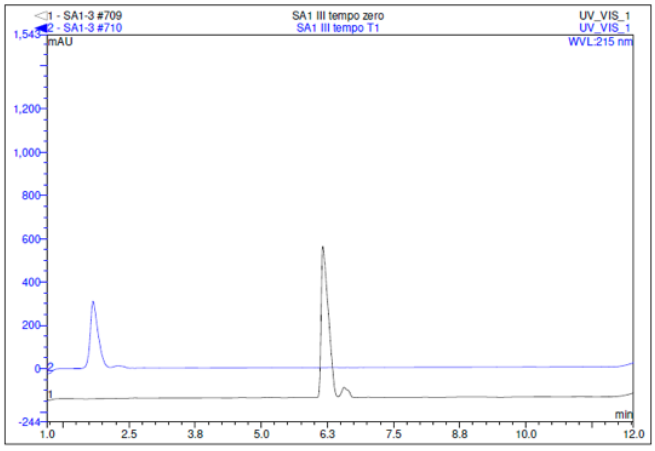

Figure 27 Oxidation test of SA1 III (m/z= 1142.635) to obtain [Met [1](O)]SA1 III (m/z= 1158.6). The reaction was monitored by UHPLC Thermo Dionex UltiMate 3000 at t0 (in black) and t1 (in blue) with an analytical method that goes from 8 to 20 % of ACN in 10 min, and a flow rate of 0.5 mL/min.

Peptide after oxidation was then purified as described in 5.2.2 and the resulting analytical characterization is reported in Table 8.

Table 8 Analytical characterization of purified peptide [Met[1](O)]SA1-III carried out on a HPLC Waters with a 2.7 µm (100 x 3.0 mm) Bioshell A160 C18 column working at 0.6 ml/min. Solvent lines were (A) H_2O (0.1 % v/v TFA); (B) ACN (0.1 % v/v TFA). [(a)] Retention time expressed in minutes. The analytical gradient was [(b)] 05-40 % ACN in 5 min.

Peptide	***Sequence***	***RP-HPLC Rt [(a)]***	***Purity grade (HPLC)***	***ESI-MS MH^{+1} (m/z) Calc / (found)***
[Met[1](O)SA1-III	Ac-M(O)GKVVNPTQK-NH_2	3.85 [(b)]	≥ 95 %	1558.6 / 1558.6

4.3.5.2 SA1-III enzymatic and chemical stability

A new LC-MS/MS assay was developed in order to describe the enzymatic and chemical stability of peptide SA1-III, taking into account the previously optimized experimental conditions [100].

The advantages of using a bidimensional HPLC system coupled with ion trap are several and principally related to the need of exclude any "matrix effect" linked to the complexity of the biological matrix used (HSH). Moreover, in addition to this cleaner HPLC separation, by using the ion trap more important information on the ion pattern will be obtained, thus resulting in a higher sensitivity, which is fundamental for stability evaluation analysis.

Peptide [Met[1](O)]SA1-III was used to monitoring the possible oxidation of the methionine residue in position 1 of peptide SA1-III. Moreover, a scrambled sequence, i.e., peptide SA1-III-sc (Ac-PVNTKMQVKG-NH_2), was designed and synthetized to be used as new ISTD (internal standard).

In fact, a perfect internal standard candidate is a molecule with characteristic as similar as possible to the analyte, in terms of chemical nature and possibly with the same molecular weight [147].

Peptide synthesis and purification methods are reported in paragraphs 5.2.1 and 5.2.2, while peptide characterization is reported in Table 9.

Table 9 Analytical characterization of purified peptide SA1-III-sc carried out on a HPLC Waters with a 2.7 µm (100 x 3.0 mm) Bioshell A160 C18 column working at 0.6 ml/min. Solvent lines were (A) H_2O (0.1 % v/v TFA); (B) ACN (0.1 % v/v TFA). [(a)] Retention time expressed in minutes. The analytical gradient was [(b)] 05-40 % ACN in 5 min.

Peptide	***Sequence***	***RP-HPLC Rt [(a)]***	***Purity grade (HPLC)***	***ESI-MS MH^{+1} (m/z) Calc / (found)***
SA1-III-sc	Ac-PVNTKMQVKG-NH_2	3.45 [(b)]	≥ 95 %	1142.6 / 1142.7

Thanks to the ion profile of each peptide, obtained following the protocols described in paragraph 5.2.7 and 5.2.9, the degradation profile of peptide SA1-III in HSH and in HEPES buffer was obtained, as shown in Figure 28.

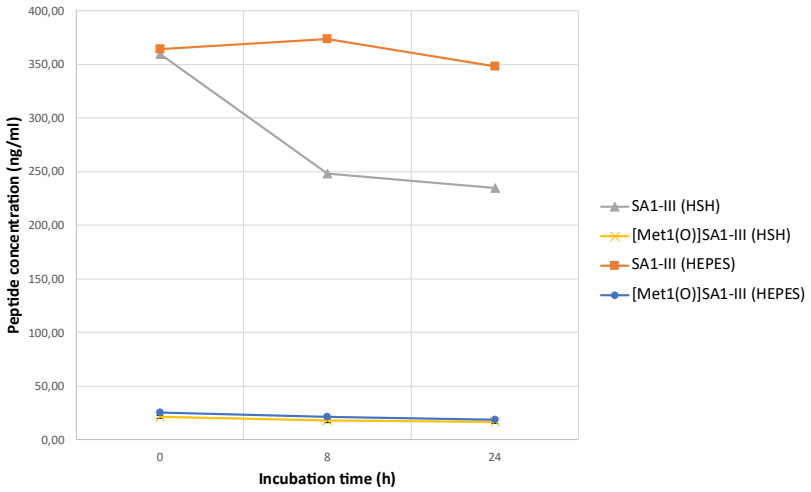

Figure 28 Degradation profiles observed until 24 h of incubation for SA1-III in HSH (gray line) and HEPES solution (orange line). [Met1(O)]SA1-III profiles in HSH (yellow line) and in HEPES solution (blue line) are also reported.

These new LC-MS/MS experiments highlight peptide SA1-III stability in HSH, showing that the concentration of the peptide in the homogenates decreases after 8 hours of incubation (69 % with reference to the initial concentration) and remains quite unmodified after 24 h (65 % with reference to the initial concentration). As shown, the concentration of the ions related to the oxidized form of peptide SA1-III does not increases, thus indicating that the peptide is chemically stable to the oxidation that can occur during sample preparation and more importantly during the exposure to the skin homogenates (at least in these experimental conditions). Moreover, peptide SA1-III appears to be stable in HEPES (the ions concentration does not decrease) and therefore the previously observed data are ascribable to HEPES ageing and consequent peroxide production, as mentioned above; in fact, for these new experiments fresh HEPES salt was purchased and prepared.

4.3.5.3 [Met^1(O)]SA1-III activity

Although it was observed that no oxidation occurs in the experimental condition, it cannot be excluded that the peptide get oxidized during formulation (i.e., preparation of the cream), or during the product shelf life; in fact, this is a well-described problem for cosmetic products [148], [149].

In light of this, the oxidized form of peptide SA1-III was also tested *in vitro* on NHDFs with the protocol described in paragraph 5.2.4. Peptide [Met^1(O)]SA1-III resulted to be non-mitogenic in the cell proliferation assay (MTS).

Results of the WB experiments in Figure 29 (protocol in paragraph 5.2.6) showed that the oxidation does not dramatically affect peptide SA1-III activity; in fact, peptide [Met^1(O)]SA1-III still maintains a tendency to increase collagen levels in comparison to the basal level produced by CNTRL cells.

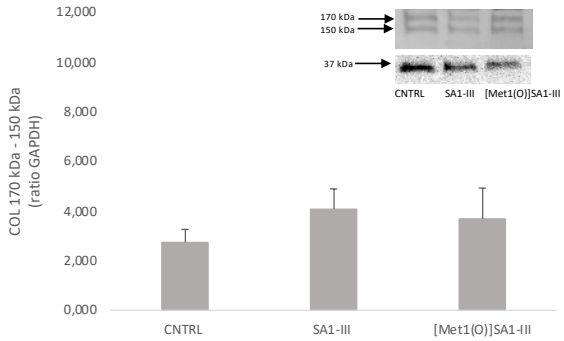

Figure 29 Bar chart showing the values for type I collagen concentrations measured through WB. Values are the average of three experiments carried out on cell lysates of NHDFs treated for 72 hours with the peptides reported in the x-axis (20 µM), and untreated fibroblasts (CNTRL). At the top right: an example of a membrane with protein bands corresponding to the procollagen forms at 170 kDa and 150 kDa, and the reference band used (GAPDH) at 37 kDa. In the y-axis the values for the volume of protein bands procollagen (170 kDa and 150 kDa) in relation to the reference value (37 kDa) are reported. SE (standard error) value are also reported.

4.3.6 SA1-III PERMEABILITY

In order to evaluate peptide SA1-III permeability through the *stratum corneum* of the skin, to reach the dermis, three Franz cell assays using human skin were performed as discussed in paragraph 5.2.8.
The LC-MS/MS analysis performed on samples taken at different time of incubation from the donor and receptor chambers, together with the analysis performed on epidermis and dermis slices chopped into pieces at the cryo-microtome, are reported in Figure 30.

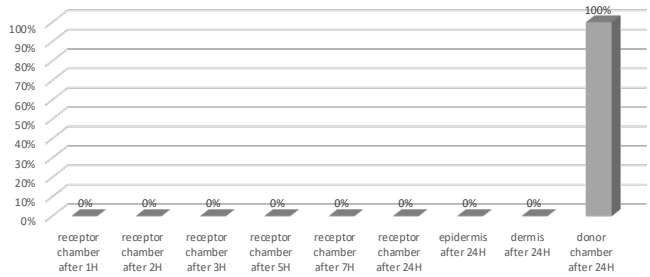

Figure 30 Franz cell experiments results reported as average of three experiments. Samplings at different time of incubation and from different areas are reported in the x-axis, while in the y-axis values are expressed as percentage of concentration in respect to the initial concentration of peptide in the donor chamber.

Unfortunately, it was observed that peptide SA1-III was not able to across the *stratum corneum* by itself, as its concentration level in the acceptor chamber never rises above 0 %; in fact, at the end of the experiment all the peptide was found in the donor chamber.

4.3.6.1 pamSA1-III Synthesis and Liposome Formulation

In order to ameliorate peptide SA1-III low lipophilic profile, we designed a second-generation peptide, potentially endowed with enhanced permeability through the skin. Inspired by the observation that one the main chemical modification used in the cosmeceuticals field to enhance the lipophilicity of bioactive peptides is the conjugation with a fatty acid [71], peptide SA1-III was conjugated with palmitic acid, giving rise to peptide pamSA1-III.
Synthesis was carried out as reported in paragraph 5.2.1 and crude peptide was purified as reported in paragraph 5.2.2 to reach at least 95 % HPLC purity to be tested *in vitro* on NHDFs. Analytical characterization of the final product is reported below in Table 10.

Table 10 Analytical characterization of purified peptide pamSA1-III carried out on a HPLC Waters with a 2.7 µm (100 x 3.0 mm) Bioshell A160 C18 column working at 0.6 ml/min. Solvent lines were (A) H_2O (0.1 % v/v TFA); (B) ACN (0.1 % v/v TFA). [(a)] Retention time expressed in minutes. The analytical gradient was [(b)] 50-100 % ACN in 5 min.

Peptide	***Sequence***	***RP-HPLC Rt [(a)]***	***Purity grade (HPLC)***	***ESI-MS MH^{+1} (m/z) Calc / (found)***
pamSA1-III	palmitoyl-MGKVVNPTQK-NH_2	4.30 [(b)]	≥ 95 %	1338.8 / 1339.0

The lipophilic properties of the peptide conjugated with a fatty acid provide on one hand a chance for the peptide to penetrate the skin and reach the ECM, where the target collagen-degrading enzymes are located, but on the other hand this modification decreases the solubility of the product in aqueous environment, thus limiting the possibility to use *in vitro* activity assays, performed in a water-based medium, DMEM. To overcome this problem, peptide pamSA1-III was incorporated into liposomes, prepared by the film hydration method [150], [151], according to the protocol described in paragraph 5.2.10. Empty liposomes (EL), to be used as negative control, and loaded liposomes (LL) were characterized by Dynamic and Electrophoretic Light Scattering (DLS and ELS) in terms of vesicle size (nm), homogeneity (polydispersity index; PDI) and the surface charge (zeta potential; mV), as described in Table 11, while in Figure 31 a graphical comparison between EL and LL is reported.

Table 11 Empty and loaded liposome parameters recovered by DLS analysis.

Liposome	***Z-Average (d.nm)***	***PdI***	***Z-potential***
Empty	135.4 ± 1.06	0.27 ± 0.024	-10.1 ± 1.08
Loaded (pamSA1-III)	107.6 ± 0.6028	0.256 ± 0.004	+25.7 ± 1.14

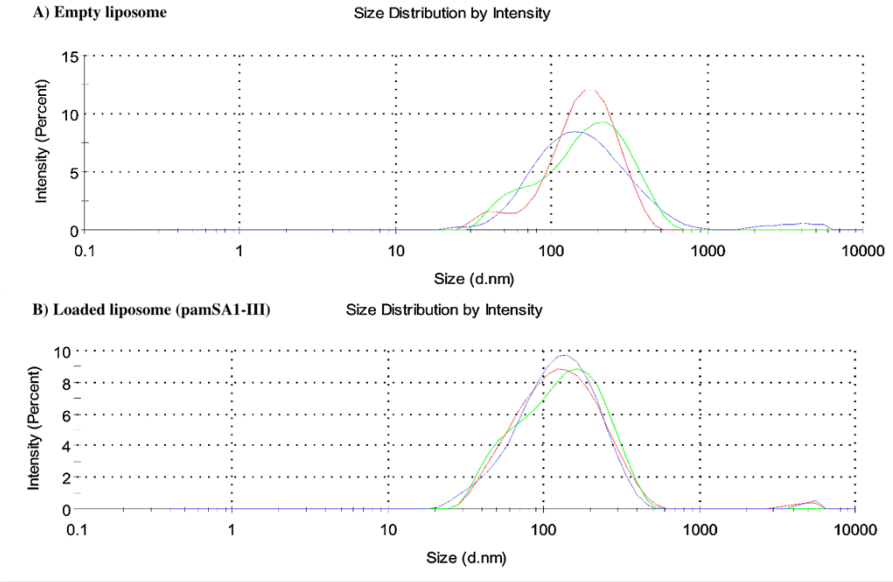

Figure 31 Comparison between empty (A) and loaded liposome (B) size distributions. Green, blue, and red lines indicate three different sampling of the liposome suspension. Images obtained by DLS analysis.

This characterization indicates that in liposomes loaded with peptide pamSA1-III (LL), both PDI and the average size slightly decrease, thus indicating that the system is more homogeneous and demonstrating pamSA1-III stabilizing and contracting capacity inside the bilayer. Moreover, the zeta potential positive value could be attributed to the protonated amino acids (i.e., lysine), and to the hypothetical position of the active principle inside the bilayer (probably the palmitic chain of pamSA1-III is inserted between the hydrophobic

chains which constitute the liposomal bilayer, while the peptide chain is positioned in the liposomal surface). A representation of the proposed spatial conformation assumed by peptide pamSA1-III in the liposome is reported in Figure 32.
The obtained EL and LL were used to evaluate if the conjugation with palmitic moiety affects the activity of peptide SA1-III towards collagen turnover.

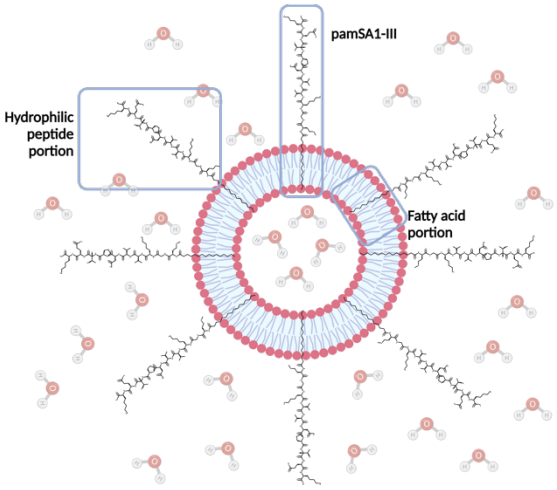

Figure 32 Loaded liposome conformation hypothesized from DLS values of characterization obtained.

4.3.6.2 pamSA1-III Activity

The results of WB experiments performed according to the protocol reported in paragraph 5.2.6 on NHDFs lysates derived from the 72 hours-treatment protocol, described in paragraph 5.2.4, are shown in Figure 33.

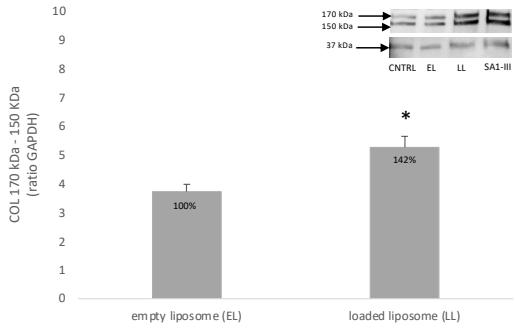

Figure 33 Bar chart showing the values for type I collagen concentrations measured through WB. Values are the average of three experiments carried out on cell lysates of NHDFs treated with empty liposomes (EL) and liposomes loaded with peptide pamSA1-III (LL; 20 µM final concentration) for 72 hours. At the top right: example of a membrane with protein bands corresponding to type I collagen at 170 kDa and 150 kDa, and the reference band (GAPDH) at 37 kDa. SE (standard error) values, and percentage of collagen level of LL in comparison to EL are also reported, and star data indicates a statistically significant value (Student's t test; $p < 0.05$).

Collagen concentration in untreated fibroblasts lysates (CNTRL) and fibroblasts treated with SA1-III lysates were also evaluated in order to check the robustness of the experiments (data not reported); additionally, the MTS cell viability test excluded possible mitogenic activity of peptide pamSA1-III.

As shown, peptide pamSA1-III loaded into liposomes increases type I procollagen concentration, as compared to empty liposomes. This means that the peptide can still modulate collagen turnover and that liposomes are actually a good vehicle for the solubility of the peptide in DMEM.

4.3.7 SA1-III AND AAT11RI MOA

Taking into account that the hypothesized mechanism of action of SA1-III is an inhibitory effect towards collagen degrading enzymes and considering AAT11RI as the most promising second-generation peptide, invasion assays were performed using fibroblasts treated with both peptides (separately), according to the protocol reported in paragraph 5.2.11.
These invasion assay experiments had the goal to demonstrate that a decreased ability to digest the Matrigel® matrix, measured as a decreased number of migrated cells, is closely related to the cell global proteolytic activity, possibly inhibited by the peptide.
As shown in Figure 34, upon cell treatment, both peptides were able to significantly decrease the number of migrated cells found into the acceptor chamber at the end of the experiment, as compared to untreated NHDFs, thus confirming the inhibitory activity against collagen degrading enzymes.

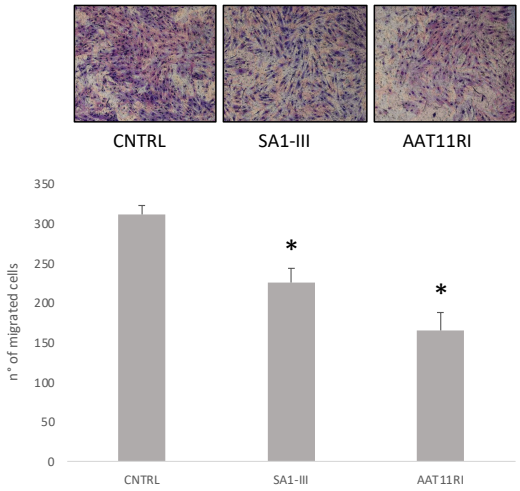

Figure 34 Top panel: Example of optical phase contrast microscope pictures taken in the same experiment for each experimental point, after fixing and staining phases. Bottom panel: Bar chart showing the number of migrated cells found as average of different Boyden chamber invasion assays carried out for 24 hours on NHDFs treated for 72 hours with the peptides reported in the x-axis at 20 μM concentration. In the y-axis the number of migrated cells is reported. SE (standard error) values are also reported, and star data indicate a statistically significant decrease in comparison to CNTRL cells (Student's t test; $p < 0.05$).

4.3.8 SA1-III ANTI-INFLAMMATORY PROPERTIES

As already pointed out in paragraph 1.2 and graphically described in Figure 7, collagen degradation and skin inflammatory state are regulated by the same signaling pathway; therefore, once the MoA of peptide SA1-III was demonstrated, it was of great interest to also evaluate its putative anti-inflammatory property. Giving the fact that COX-1 enzyme is constitutively expressed in many tissues, while COX-2 indeed is inducible and responds to pro-inflammatory stimuli, in these experiments cells were treated with a pro-inflammatory cytokine, TNF-α (tumor necrosis factor alpha), for the last 24 h during the 72 h-protocol, in order to induce inflammation [152].
Results of the WB experiments to measure COX-2 levels, conducted as reported in paragraph 5.2.6, are shown in Figure 35. It can be observed that the treatment induced a significant reduction of COX-2 expression in fibroblasts.

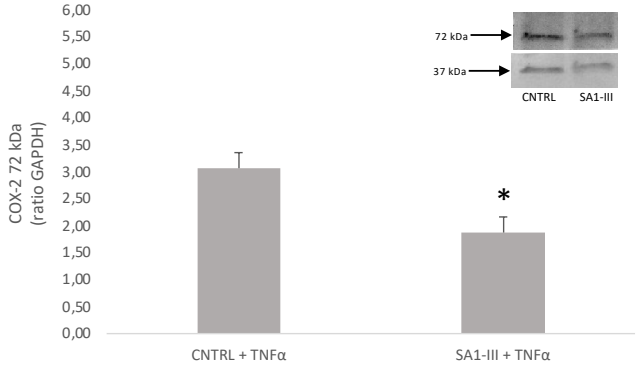

Figure 35 Bar chart showing the values for COX-2 protein measured through WB. Values are the average of three experiments carried out on cell lysates of untreated NHDFs (CNTRL) and NHDFs treated with peptide SA1-III (20 μM) for 72 hours; both were also treated with TNF-α (20 ng/mL) for the last 24 hours. At the top right: example of a membrane with protein bands corresponding to COX-2 at 72 kDa, and the reference band (GAPDH) at 37 kDa. SE (standard error) values are also reported, and star data indicate a statistically significant decrease in comparison to CNTRL cells (Student's t test; $p < 0.05$).

Considering these WB as preliminary results, it can be assumed that peptide SA1-III displays an anti-inflammatory activity, which could be of great interest from a cosmeceutical point of view, in all the conditions of skin inflammation, such as after cosmetic surgery.

5. EXPERIMENTAL PART

5.1 MATERIALS

Peptides were synthesized on a manual batch synthesizer PLS 4 × 4 (Advanced ChemTech, Louisville, USA).

Fmoc-L-amino acids, Fmoc-D-amino acids, palmitic acid puriss. ≥ 98.5 % (GC), dichloromethane (DCM), trifluoroacetic acid (TFA), piperidine, acetic anhydride (Ac_2O), N,N-diisopropylethylamine (DIPEA), diethyl ether (Et_2O), triisopropyl silane (TIS), N-methylmorpholine (NMM), and N, N-dimethylformamide (DMF) with purity grade suitable for peptide synthesis were purchased from Merck (Darmstadt, Germany).

Fmoc-Rink-Amide AM resin and Fmoc-L-Ser(tBu)-Wang Resin used for peptide synthesis were purchased from Iris Biotech AG (Marktredwitz, Germany).

N,N,N,N-tetramethyl-O-(1H-benzotriazol-1-y)uronium esafluorophosphate (HBTU) was bought from Advanced Biotech Italy (Milan, Italy).

HPLC-grade acetonitrile (ACN) was purchased from Carlo Erba (Milan, Italy). Methanol (Chromasolv), formic acid and ammonium formate (MS grade) and Verapamil Hydrochloride (analytical standard used as internal standard, ISTD) were purchased by Sigma-Aldrich (Milan, Italy). Solvents for HPLC were used without further purification steps. The milli-Q water was obtained with the Sartorius system (arium® 611 VF).

Peptides were purified by CombiFlash® NextGen 300 (Teledyne ISCO Genoa, Italy), coupled with an UV-visible detector, and equipped with a 15 g RediSep Gold® Reverse-phase (RP) C18 column, or by semi-preparative Water 600 HPLC system coupled with a Waters 2487 dual λ absorbance detector (λ=214 nm and λ=254 nm), using a reverse-phase Sepax Bio-C18 column (particle size 5 µm, 10 x 250 mm) column; in both cases with solvent system A (0.1 % TFA v/v in H2O) and B (0.1 % TFA v/v in ACN). The analytical HPLC system were analysis of raw and purified peptide were performed was Alliance Chromatography with a Phenomenex Kinetex C-18 column 2.6 µm (100 × 3.0 mm) working at 0.6 ml/min, with the indicated linear gradients, coupled to a single quadrupole ESI-MS (Micromass ZQ) and they were purchased from Waters (Milano, Italy). The peptides were lyophilized with an Edward Modulyo lyophilizer (5pascal, Milano, Italy).

The oxidation of peptide SA1-III was monitored in a RP-HPLC-ESI-MS system Thermo Scientific Ultimate 3000 equipped with a variable wavelength detector, and coupled with a Thermo Scientific MSQ Plus, using an ACQUITY UPLC CSH™ C18 column (particles size 1.7 µm, 1 x 100 mm).

Phospholipon® 90G (P90G) was from Lipoid GmbH (Ludwigshafen, Germany).

Cholesterol (CHOL) and Phosphate Buffered Saline (PBS 0.01 M) powder (pH 7.4) used for liposome formation were from Sigma Aldrich (Milan, Italy).

Liposome were sonicated in a Sonopuls HD 2200 ultrasound device with a KE 76 probe (Bandelin Electronic GmbH, Berlin, Germany).

The DLS and ELS evaluations were performed with a Zetasizer® NanoZS90 apparatus (Malvern Instruments, Malvern, UK) and ALV-60X0 software V.3.X provided by Malvern at 25 °C.

Killik™ medium was purchased by Bio-Optica (Milano, Italy).

Cell cultures (NHDFs) derived from the dermis of normal human neonatal foreskin (Clonetics, Lonza). Dulbecco's modified Eagle medium (DMEM), fetal bovine serum (FBS), Trypsin-EDTA with Phenol Red, RPMI 1640 medium (without L-glutamine and red phenol) and phosphate buffer saline (PBS) used for cell cultures were from EuroClone™ (Milano, Italy).

Penicillin-streptomycin, RIPA buffer, protease inhibitor, phosphatase inhibitor and bovine serum albumin were obtained from Sigma-Aldrich Chemicals Co. (St. Louis, USA).

DMEM was filtered employing Nalgene Rapid flow filter (Thermo scientific) system.

Cells were grown in Corning® Sterile 25cm^2 Rectangular Cell Culture Flask with Canted Neck & Phenolic Cap, TC-Treated Polystyrene, Graduated or Corning® cell culture flasks surface area 75 cm2, canted neck, cap (vented) purchased from Merck (Darmstadt, Germany).

For the cell viability assays, cells were seeded in 96-well microplates from VWR® International Srl (Milano, Italy). For peptide treatment experiments, and filters preparation for the Boyden chambers, 6-well, 12-well, or 24-well plates from VWR® International Srl (Milano, Italy) were employed depending on the needing.

Cell proliferation measurement was performed with CellTiter 96® AQueous One Solution Cell Proliferation Assay kit by Promega (Madison, USA). Recombinant human TGF-β1 was purchased from Peprotech (London, UK), while recombinant human TNF-α was purchase from Sigma Aldrich (Schnelldorf, Germany).

Protein content was determined according to the Bio-Rad® (Milano, ITA) system DC protein assay where reagent A is alkaline copper tartrate solution and reagent B is Folin reagent for colorimetric assays. Protein concentration was evaluated in a Perkin Elmer Wal-lac 1420 Victor 2 Multi-Label Microplate Reader.

Cell lysates and cell conditioned media were centrifuged in an Eppendorf centrifuge model 5417r (Milano, Italy).

The Mini-P tetra cell, 4precast gel apparatus, the 4-2 % MP TGX Stain-Free Gels (10 wells, 30µl), Trans-Blot Turbo Mini NC Transfer Packs, TRIS/GLYCINE/SDS 10x buffer, Non-Fat Dry Milk, and 2-mercaptoethanol ≥ 98 % pure (14.2 M) were purchased from Bio-Rad® (Milano, ITA).

NuPAGE™ LDS Sample Buffer (4X), and MagicMark™ XP Western Protein Standard were purchased from Invitrogen™ (Life Technologies supplier, Monza, Italy).

PageRuler™ Prestained Protein Ladder, and Sodium Chloride 99 % were purchased by Thermo Fisher Scientific™ (Life Technologies supplier, Monza, Italy).

Potassium Chloride approx. 99 %, Potassium Phosphate monobasic anhydrous; Sodium Phosphate dibasic heptahydrate 98-10 2%, and TWEEN® 20 were from Sigma Aldrich® (Life Technologies supplier, Monza, Italy).

Primary antibody rabbit anti-collagen type I polyclonal antibody (ab34710) used for the first set of tetrapeptides (AAT09, AAT11, AAT13, and AAT15) *in vitro* evaluation was purchased from Abcam (Amsterdam, Netherlands).

Primary mouse anti-COL1A2 (E-6) antibody (sc-393573) used for the preliminary screening of the AAT11 analogues (AAT11-allD and AAT11RI) was sent as a free sample from Santa Cruz Biotechnologies (Heidelberg, Germany).

Primary goat anti-collagen type I affinity purified polyclonal antibody (AB758) used for western blot for peptides pamSA1-III, [Met^{1}(O)]SA1-III and AAT11RI (final experiments) was from EDM Millipore Corporation (Massachusetts, USA).

Primary rabbit anti-GAPDH monoclonal antibody (14C10), and Anti-rabbit IgG HRP-linked antibody (7074) were purchased from Cell Signaling (Massachusetts, USA).

Primary rabbit anti-COX-2 polyclonal antibody (aa 584-598) was purchased from Cayman Chemical (Michigan, USA).

Anti-goat IgG (whole molecule) peroxidase conjugate antibody (A 5420) was purchased from Sigma Aldrich® (Life Technologies supplier, Monza, Italy).

Anti-mouse IgG (H&L) peroxidase conjugated affinity purified antibody was purchased from Chemicon International (USA).

Immobilon Western Chemiluminescent HRP Substrate was purchase from Merck Life Science S.r.l. (Darmstadt, Germany).

ImageQuant Capture mod.350 from GE-Healthcare (Little Chalfont, UK) was employed for the chemiluminescent acquisitions; while Quantity One® software from Bio-Rad® (Hercules, USA) was used to quantify protein bands.

HEPES ≥ 99.5 % (titration) was from Sigma Aldrich (Schnelldorf, Germany).

Specimens of human skin were taken from women patients subjected to breast surgery at Careggi University Hospital, Florence.

Rat and human skin homogenizations were performed in a POLYTRON®PT 1200 E handheld homogenizer from Kinematica Inc. (New York, USA).

A G-Therm 015 thermostatic oven was used to maintain the samples at 37°C during the degradation tests.

Eppendorf centrifuge 5415 D was employed to centrifuge skin homogenate samples.

The LC–MS and MS/MS analyses for the development of the dermal stability assays were carried out using a Varian1200 L triple quadrupole system (Palo Alto, CA, USA) equipped by

two Prostar 210 pumps, a Prostar 410 autosampler and an Electro-spray Source (ESI) operating in positive ions.

Once the experimental conditions were optimized, chromatographic separation of analytes for the final stability studies were carried out in a bidimensional LC system composed by a loading column Supelco Discovery® HS F5 Supelguard™ Cartridge (3 µm particle size, 20 mm x 2.1 mm) operating in isocratic mode and an analytical column Phenomenex Luna® PFP (2) (3 µm particle size, 50 mm x 2.0 mm) operating in gradient mode. For the MS/MS experiments used a Varian 500 ms ion trap equipped with Varian autosampler 410 and three pumps 210 and with an electrospray ionization source (ESI) operating in positive ion mode. Two pumps were used for the binary gradient and one pump was dedicated to the isocratic elution in the loading column. Samples were prepared for the LC-MS/MS run in Verex™ Cert+ Vial Kit, 9mm, Screw top, Polypropylene, 700 µL.

Raw data were collected and processed by Varian Workstation vers. 6.8 software.

Polycarbonate filters of 8 µm pores and 13 mm diameter used for the invasion assays were purchased from Neuro Probe Inc. (USA), while Matrigel® was purchase from Corning® (Darmstadt, Germany).

Diff-quick used to stain cells was purchased from Biomap (Milano, Italy).

All images, except those where references numbers are reported, were created with the BioRender on-line software with nominal license that allows their use for the present PhD thesis.

5.2 METHODS

5.2.1 MANUAL SPPS

All the peptides describe in this PhD project were synthetized according to manual SPPS procedures. A 0.1 mmol synthesis for each peptide was carried out on a manual batch synthesizer, in a teflon vessel with fritted disc and removable lid for SPPS, according to standard Fmoc/tBu strategy and employing HBTU (5 equivalents, eq) as coupling reagent and NMM (4-Methylmorpholine, 7 eq) as tertiary base. A Rink Amide AM resin 0.48 mmol/g loading was used to obtain all the C-terminus amidated.
Only in the case of peptide pal-KTTKS a Fmoc-Ser(tBu)-Wang resin 0.42 mmol/g was employed.
The following protocols will be described considering the formula reported below as a standard method to indicate a proportion between volumes of solvent used to solubilized 1 g of solid:

$$1\ volume\ (vol) = 1\frac{mL\ (solvent)}{g\ (solid)}.$$

As a first step, resins were swelled in DMF 10 vol for 30 minutes at RT. Deprotection of the Fmoc from N-terminal positions was performed with 10 vol of a solution of 20 % piperidine in DMF; two cycles of deprotection (5 minutes and 15 minutes) were performed for each positions except for the amino acids in second position, whose Fmoc was deprotected with two cycle of 5 minutes and 5 minutes, to avoid diketopiperazine formation [111]. Three washes in 5 vol of DMF were performed after Fmoc deprotection, and the following coupling step was performed with 5 vol of DMF and the above-mentioned coupling system, for 30 minutes. D-amino acid couplings were performed in the same conditions.
Conjugations with palmitic acid was performed in the same condition used for the coupling of the amino acids in terms of equivalents, but they were left for 50 minutes and the amount of DMF was brought to 20 vol due to the fatty acid swelling ability. After each coupling resins were washed three times with 10 vol of DMF. Peptide acetylation in α-N-terminus was carried out on the free α-amino function of the last residue anchored to the resin for all peptides, but pal-KTTKS and pamSA1-III. The resin was stirred in 1 vol of 10 % v/v Ac_2O (acetic anhydride) in DMF at room temperature (RT) for 10 minutes and then washed 3 times with DCM (dichloromethane) and dried in a lyophilizer. The peptides were cleaved from the resin, with concomitant deprotection of the amino acid side chains, by treatment with 15 vol of a cleavage mixture consisting of TFA/H_2O/TIS (triisopropyl silane) (95:2.5:2.5) or alternatively TFA/H_2O/TIS/EDT (ethane-1,2-dithiol) (94:2.5:1:2.5) if methionine residues were present (SA1-III, AAT09, SA1-III-sc and pamSA1-III). The resins were treated with the reaction mixture at RT, stirring at 400 rpm. After 3 h the resins were filtered off, and

peptides were precipitated from 100 vol of cold Et_2O and centrifuged at 3500 rpm (three cycles of ether addition and centrifugation) and finally they were solubilized in H_2O or H_2O:ACN (acetonitrile) 50:50 (peptides pal-KTTKS and pamSA1-III), and lyophilized.

5.2.2 PURIFICATION AND CHARACTERIZATION

Purification of the peptides after cleavage (raw or crude peptides) were performed by MPLC (Medium Pressure Liquid Chromatography) on a CombiFlash® NextGen 300+ Teledyne ISCO instrument with a Teledyne ISCO RediSep® Gold 15g column or by semi-preparative chromatography on an HPLC Waters 600 coupled with Waters UV DAD 2487 with a Sepax Bio-C18 Column to achieve a > 95 % HPLC purity grade. The purification methods employed for each peptide are shown in Table 12. Peptides SA1-III, SA1-III-sc, and [Met^1(O)]SA1-III were purified by MPLC, while the tetrapeptides, pal-KTTKS, and pamSA1-III were purified by semi-preparative HPLC.
Solvent used for the reverse-phase chromatography were, in both cases:

- solvent A: milliQ H_2O (hereon H_2O) with 0.1 % TFA v/v
- solvent B: ACN with 0.1 % TFA v/v

Table 12 Gradient of final purification used for peptides SA1-III, tetrapeptides (AAT09, AAT11, AAT13, AAT15, AAT11-allD, and AAT11RI), pal-KTTKS, [Met^1(O)]SA1-III, SA1-III-sc, and pamSA1-III. [(a)] MPLC method; [(b)] semi-preparative method.

Peptide	***Gradient***
SA1-III	10-50 % ACN in 16 min[(a)]
AAT09	10-50 % ACN in 30 min[(b)]
AAT11	05-40 % ACN in 30 min[(b)]
AAT13	05-40 % ACN in 30 min[(b)]
AAT15	05-25 % ACN in 30 min[(b)]
AAT11-allD	05-40 % ACN in 30 min[(b)]
AAT11RI	05-40 % ACN in 30 min[(b)]
pal-KTTKS	40-80 % ACN in 30 min[(b)]
[Met^1(O)]SA1-III	05-35 % ACN in 16 min[(a)]
SA1-III-sc	10-50 % ACN in 16 min[(a)]
pamSA1-III	50-90 % ACN in 30 min[(b)]

After the purification steps, peptides were characterized as reported in Table 5, Table 6, Table 7, Table 8, Table 9 and Table 10 described in the Results chapter.

5.2.3 PEPTIDE SA1-III OXIDATION

Peptide [Met^1(O)]SA1-III was obtained from the precursor peptide SA1-III by direct oxidation. 0.1 mmol of crude SA1-III was solubilized in 100 vol H_2O and mixed with 2 eq of a 30 % H_2O_2 solution and left at room temperature under magnetic stirring for 1 h. The reaction was monitored periodically (t0, t1= 1 h) in order to ensure that 100 % of the sulfoxide form has been obtained, by using the UHPLC Thermo Dionex Ultimate 3000

system and an Acquity column UPLCR CSH™ C18 (1.7 µm 2.1 x 100 mm) working at a flow rate of 0.5 mL/min.

5.2.4 In Vitro NHDFs Treatments Protocol

Neonatal Normal Human Dermal Fibroblasts (NHDFs) derived from the dermis of human neonatal foreskin were used for all the experiments reported in the Results chapter. NHDF were cultured in high glucose (4.500 mg/L) DMEM, supplemented with 10 % FBS, L-glutamine 1 % and penicillin/streptomycin to a final concentration of 100 U/ml.
DMEM was filtered prior to use to guarantee sterility. Cells were maintained at 37°C in 5 % CO_2 humidified atmosphere. Once at confluence, cultures were propagated by trypsinization, and the attained PDL was calculated according to the equation: PDL = 3.32 × log N/No (where N and No are the recovered and seeded cell numbers, respectively). The experiments were conducted with medium-high cycling cells (15< PDL<25), seeded into 96-MW (multi-well), 12-MW, or 6-MW plates depending on the needing and considering the scheme reported in Table 13.

Table 13 Parameters used for cell culture in the respective plates used.

Multi-well type	***Maximum volume for well***	***Cells for well***
6 MW	2500 µL	100000
12 MW	1200 µL	40000
96 MW	200 µL	3000

Cell seeding into MW plates from a 25 cm^2 or 75 cm^2 culture flask was accomplished according to the following procedure:

1. Removal of culture medium,
2. Washing cycles (2) with PBS to remove residual DMEM,
3. Incubation at 37°C in 5 % CO_2 humidified atmosphere with trypsin 0.05 %-EDTA 0.02 % in PBS (3-7 min),
4. Addition of DMEM 10 % FBS to block trypsin activity (double volume in respect to trypsin-EDTA),
5. Transfer into tube and centrifugation (1200 rpm, 5 min),
6. Supernatant removal and suspension in 1-2 ml of DMEM, through mechanical disaggregation of the pellet,
7. Cell count in Bürker counting chamber, performed on 20 µL of withdrawn suspension,
8. Pre-conditioning of the wells with DMEM 10 % FBS,
9. Cell seeding, equally distributing the suspension into the wells (depending on the parameter reported in Table 13),
10. Incubation until treatment at 37°C in 5 % CO_2 humidified atmosphere.

Cells seeded for the experiments in the proper multi-well were left in the incubator for 24 h or 48 h depending on cell passages (which influence cell growth speed), before the treatment with peptides. After that time DMEM was removed and cells were washed twice with PBS in order to eliminate FBS. Cell monolayers were then treated with each peptide at 20 µM solution in DMEM without FBS. The absence of FBS was a necessary condition for the further western blot acquisition of conditioned media derived from the peptide treatments in cell cultures; in fact, FBS proteins largely interfere with the electrophoresis course negatively contributing to the final acquisition by greatly increasing the background signal. At least one well of untreated cells was always used as a negative control (CNTRL) and added with DMEM w/o FBS.
TGF-β1 was employed as positive control at a concentration of 10 ng/mL (≈ 0.4 nM).
Depending on the final goal of the experiments, cells were then treated as described below.

5.2.4.1 Protocol for type I collagen quantification

Once NHDFs were treated with the peptide solutions, including empty and loaded liposomes, they were left for 72 h at 37°C in 5 % CO_2 humidified atmosphere. After that time, cells were observed under a NIKON TMS inverted microscope and no remarkable change in their morphology was observed. Conditioned media were recovered, centrifuged at room temperature (RT) at 250 g (Eppendorf centrifuge model 5417r) and then concentrated at the minimum volume (25-30 µL), by using protein concentrator centrifugal filters with a cut-off of 30 kDa, because of the great dilution of the proteins in the whole medium released by cells. Concentrated media supernatants were stocked at -20°C.
Once the media were removed, cells were washed twice with PBS in order to clean cell membranes from proteins released in the medium. After the washings cells were treated with RIPA (Radio-ImmunoPrecipitation Assay) lysis buffer added with 1 % proteases inhibitor and 1 % phosphatases inhibitor, and then recovered with a scraper. Cell lysates were then sonicated for 2 minutes, centrifugated at RT at 14000 rpm, collected in new tubes, and global proteins content was evaluated with the protocol described in paragraph 5.2.5. Cell lysates were stored at -20°C until use.

5.2.4.1 Protocol to prepare cells for invasion assays

NHDFs were treated with SA1-III or AAT11RI for 48 h at 37°C in 5 % CO_2 humidified atmosphere. After that time, cells were observed under a NIKON TMS inverted microscope and no remarkable changing in their morphology was observed. Cells were then treated as follows:

1. Removal of culture medium,
2. Washing cycles (2) with PBS to remove residual DMEM,

3. Incubation at 37°C in 5 % CO_2 humidified atmosphere with trypsin 0.05%-EDTA 0.02% in PBS (3-7 min),
4. Addition of DMEM 10 % FBS to block trypsin activity (double volume in respect to trypsin-EDTA),
5. Transfer into tube and centrifugation (1200 rpm, 5 min),
6. Supernatant removal and suspension in 1-2 mL of freshly prepared peptide solution (20 µM) in DMEM w/o FBS (or DMEM w/o FBS in the case of CNTRL),
7. Cell count in Bürker counting chamber, performed on 20 µL of withdrawn suspension,
8. Preparation of cell suspensions in DMEM w/o FBS, SA1-III or AAT11RI considering 18000 cells in triplicate (72000 cells in total) for each experimental point.

5.2.4.2 Protocol for COX-2 quantification

Once NHDFs were treated with SA1-III, they were left for 48 h at 37°C in 5 % CO_2 humidified atmosphere. After that time, a TNF-α solution was added to the wells to obtain a final concentration of 20 ng/mL in the media. Besides, the initial concentration of SA1-III solution in these experiments was of 25 µM, in order to have a 20 µM final concentration. After the addition of the TNF-α, cells were left at 37°C in 5 % CO_2 humidified atmosphere for 24 h.
At the end of the 72 h of total treatment, conditioned media were recovered, centrifuged at RT at 250 g (Eppendorf centrifuge model 5417r) and then concentrated at the minimum volume (25-30 µL), by using protein concentrator centrifugal filters with a cut-off of 30 kDa, because of the great dilution of the proteins in the whole medium released by cells. Concentrated media supernatants were stocked at -20°C.
Once the media were removed, cells were washed twice with PBS in order to clean cell membranes from proteins released in the medium. After the washings cells were treated with RIPA (Radio-ImmunoPrecipitation Assay) lysis buffer added with 1 % of proteases inhibitor and 1 % of phosphatases inhibitor, and then recovered with a scraper. Cell lysates were then sonicated for 2 minutes, centrifugated at RT at 14000 rpm, collected in new tubes, and global proteins content was evaluated with the protocol described in paragraph 5.2.5. Cell lysates were stored at -20°C until use.

5.2.4.3 Protocol for MTS

MTS assay was performed in order to detect changes in cell viability/number, possibly due to a cytotoxic or mitogenic effect associated with the synthetized peptides. The method is based on the reduction of MTS tetrazolium compound by viable cells to generate a colored formazan product that is soluble in cell culture media. This conversion is carried out by NADPH produced by NADPH-dependent dehydrogenase enzymes in metabolically active

cells. The formazan dye produced by viable cells can be quantified by measuring the absorbance at 490-500 nm.

Dedicated cells were seeded in a 96-MW plate in order to have triplicates for each experimental point (including the CNTRL cells) and treated as describe above.

After media withdrawal, the cell proliferation assay was performed according to the following steps:

1. Washing cycles with PBS (2 × 200 µL per well),
2. Addition of RPMI phenol-red-free culture medium with 5 % FBS (100 µL per well),
3. Addition of a ready-to-use MTS solution (20 µL per well),
4. Incubation at 37°C in 5 % CO_2 humidified atmosphere (visual check every 20 min until a brown color is developed),
5. Measurement of absorbance at 490 nm in a Victor 2 Multi-Label Microplate Reader.

Three empty additional wells underwent the same procedure and were referred to as blanks.

5.2.5 Cell Lysates Protein Dosage Protocol

The total protein content in fibroblast lysates was evaluated employing the Bio-rad® kit (DC Protein Assay), according to the Lowry method, in which proteins in the sample (mainly containing tryptophan and tyrosine, but also cystine, cysteine and histidine) react with an alkaline solution of copper tartrate and Folin reagent.

The assay was performed in 96-MW, adding in sequence:

1. 5 µL of each sample,
2. 25 µL reagent A (copper tartrate),
3. 200 µL reagent B (Folin reagent).

Other wells were prepared with increasing concentrations of BSA (bovine serum albumin) in milliQ H_2O (0.125, 0.25, 0.5, 1 and 2 mg/mL), and with milliQ H_2O (considered as a reference blank control). Each experimental point was made in triplicate. After incubation of the plate (37°C, 20 min), absorbance values were read at 560 nm in a Victor 2 Multi-Label Microplate Reader, and the protein content of each sample was determined through the calibration curve built up with values obtained from wells containing BSA at known concentration, after subtraction of the reference control value.

5.2.6 Western Blot Protocol

The NHDFs conditioned cell media and cell lysates prepared in accordance with paragraph 5.2.4 were used to quantify their type I collagen or COX-2 content by WB immunoenzymatic analysis.

WB protocol is articulated, and can be divided into 4 basic steps:

1. sample preparation,
2. separation of the protein mixture depending on their molecular weight (electrophoresis run),
3. blotting of the protein from gel to membrane,
4. antibody-mediated detection of protein bands.

In detail, after determination of the protein content, samples were prepared in order to have ≈ 10-30 μg of total proteins. Each sample was added with sample buffer 4X, containing SDS as denaturing agent, β-mercaptoethanol 10X (reducing agent) and H_2O to reach 25-30 μL in total as 30 μL is the well capacity for the gels employed for the assay. Once prepared as described, the samples underwent protein denaturation at 70°C for 10 minutes, were placed on ice for 10 minutes and centrifuged at 14000 rpm for 1 minute.

Pre-cast gels (Bio-rad®) were prepared in the electrophoresis apparatus, which was filled with Tris/Gly/SDS (TGS) buffer, then gel's wells were filled as well and loaded with the samples depending on the scheme adopted, considering at least one well for a chemiluminescence marker, and at least one well for a UV-vis marker, which will help in identifying protein bands depending on their molecular weight. To this purpose, 3 μL of Magic Mark, and 4 μL of Page Ruler were used respectively. Protein separation was performed at 165 V for 45-55 minutes, with 40-125 mA current. After that time, the blotting membranes were prepared in the Trans-Turbo cassette (Bio-rad®), gels were removed from the gel cassettes, washed in running buffer and placed above the membrane. The blotting sandwich was closed in the Trans-Turbo cassette and placed in the Trans-Turbo base (Bio-Rad®) where protein blotting from gels to membranes took place. The Bio-Rad® apparatus gives the opportunity to choose the proper protocol of blotting depending on the molecular weight of interest. For type I collagen acquisitions, proteins were blotted with the "HIGH MW" protocol, which last 10 min, while for COX-2 acquisitions, proteins were blotted with the "Mixed MW" protocol.

After recovering and washing the membranes, the transferred proteins were observed by treating them with Ponceau S stain (0.2 % solution in 3 % acetic acid) for 7 min (RT) with shaking, and then rinsed with deionized water. Protein bands colored in red also help cutting the membranes in strips for the subsequent incubation with different antibodies. Membranes were then washed with deionized H_2O (3 x 10 min) at RT in shaking.

Prior to incubation with primary antibodies, non-specific binding sites on the membrane were blocked by 1 hour treatment at RT with a solution of Non-fat dry milk 6 % in PBS. After the removal of the blocking solution, the membrane was incubated overnight (o.n.) at 4°C with shaking with primary antibodies used in dilution with PBS-Tween 0.05 % as follows:

- Primary antibody rabbit anti-collagen type I polyclonal antibody used for the first set of tetrapeptides (AAT09, AAT11, AAT13, and AAT15) *in vitro* evaluation, dilution 1:1000,

- Primary mouse anti-COL1A2 antibody used for the preliminary screening of the AAT11 analogues (AAT11-allD and AAT11RI), dilution 1:200,
- Primary goat anti-collagen type I affinity purified polyclonal antibody used for western blot for peptides pamSA1-III, [Met^1(O)]SA1-III and AAT11RI (final experiments), dilution 1:250,
- Primary rabbit anti-GAPDH monoclonal antibody, dilution 1:3000,
- Primary rabbit anti-COX-2 polyclonal antibody, dilution 1:200.

On the following day, membranes were washed with PBS-Tween 0.1 % (3 x 10 min) at RT with shaking, and exposed to the secondary antibodies, prepared in PBS-Tween 0.05 % as follows:

- Anti-goat IgG peroxidase conjugate antibody, dilution 1:3000,
- Anti-rabbit IgG HRP-linked antibody, dilution 1:4000,
- Anti-mouse IgG peroxidase conjugated affinity purified antibody, dilution 1:5000.

The incubation with the secondary antibodies lasted 1 h, at RT with shaking. After that time membranes were washed with PBS-Tween 0.1 % (3 x 10 min) with shaking at RT, and prepared, one by one, for the chemiluminescence acquisition. To this purpose, membranes were exposed to 500 µL of luminol and 500 µL of H_2O_2 for 3-5 minutes. Proteins were then revealed in a ImageQuant Capture 350 transilluminator, subsequently employing the Quantity One® software for band quantification. Bands corresponding to GAPDH (MW 37 kDa) were used as the internal control reference for the determination of type I collagen and COX-2 levels.

5.2.6.1 Statistics

Values were expressed as mean ± SE of 3-8 different experiments. The statistical significance of the differences was analyzed by one-way ANOVA for multiple comparisons, followed by the Student's *t* test for comparisons between two groups.

5.2.7 PEPTIDE STABILITY EVALUATION PROTOCOL

Peptide chemical and enzymatical stability to dermal proteases was evaluated in HEPES buffer solution, in rat skin homogenate as a first model to set up the experimental conditions, and finally in human skin homogenates (HSH). 10 mM pH 7.4 HEPES buffer solution was prepared with 238.31 mg of HEPES solubilized in 100 ml of milliQ H_2O to obtain a 10 mM concentration, and pH was adjusted to 7.4. Rat and human skin homogenates were prepared according to the protocol used by Choi *et al.* [144], with an optimized procedure here described.

5.2.7.1 Rat and Human Skin Homogenates Preparation Stability Assay Protocols

After wild type rats (F344 Charles River) of similar ages and different gender (11–12 months, 2 male and 2 female) were euthanized, dorsal skin was removed, deprived of adherent fat and cut into pieces of the same size (0.3 cm^2). Those pieces were put three by three in 1,5 mL Eppendorf tubes containing 1 mL of milliQ H_2O and kept on ice. Each different sample was homogenized with a POLYTRON®PT 1200 E handheld homogenizer (Kinematica Inc) for about 15 min and then centrifugated at 10.000 rpm for 30 min at 4°C. All supernatants were transferred in 15 mL Falcon tubes after filtration with Syringe Filters 0.2 µm and diluted with HEPES buffer solution (pH 7.4; 10 mM), to obtain a final volume of 7.5 mL. Homogenates were put at first at −80°C to stop the enzymatic activity and after 2 h were moved at −20°C, where they were at last stocked. Specimens of human skin were taken from 2 patients (50 years-old and 60 years-old women) subjected to breast surgery at Careggi University Hospital, Florence. Human skin homogenates (HSH) were pre-pared following the same protocol described above.

5.2.7.2 Sample preparation procedure

In Figure 36 a scheme for the sample preparation procedure used for the first LC-MS/MS analysis is reported:

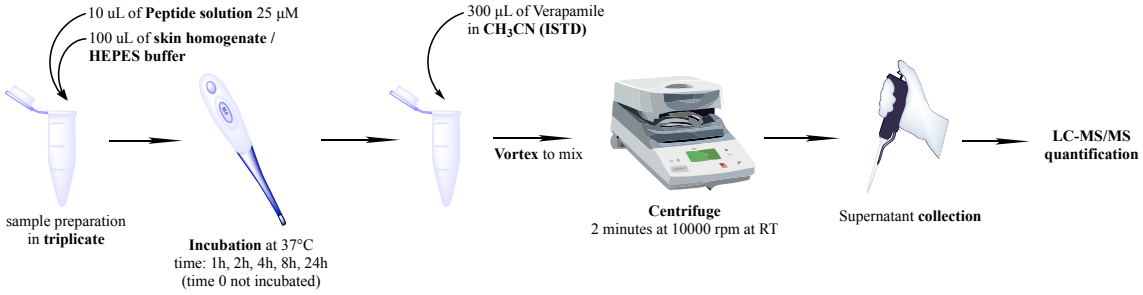

Figure 36 Schematic representation of the sample preparation procedure for the LC-MS/MS acquisition in triple quadrupole.

Peptide was prepared in stock solution at a concentration of 1000 ppm (part per millions) in H_2O/MeOH 50:50. Concentration of peptide solution, protein concentration, and skin homogenates dilution were optimized using rat skin homogenates and the peptide pal-KTTKS [100]. Verapamil was used as internal standard, due to its compatibility with the experimental conditions and with the operating HPLC gradient.
Once the analytical procedure was moved from the triple quadrupole quantification to the ion trap acquisition, the sample preparation protocol was readjusted as reported in Figure 37:

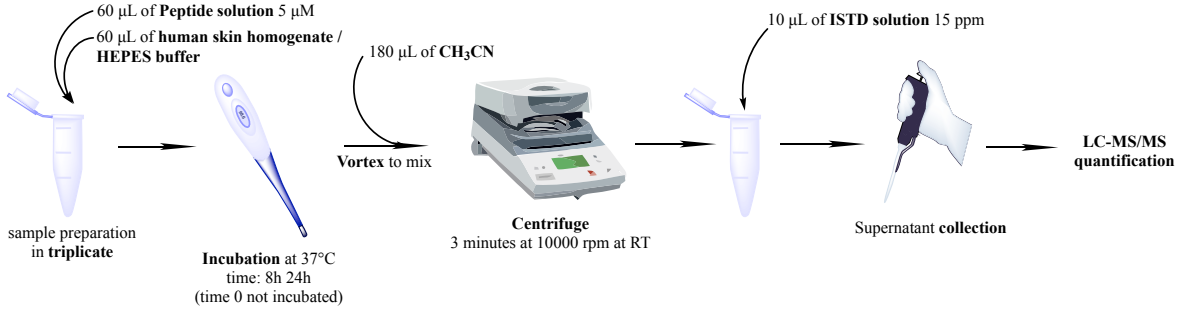

Figure 37 Schematic representation of the sample preparation procedure for the LC-MS/MS acquisition in the ion trap.

For the final experiments performed in the ion trap, the protein concentration of the human skin homogenates used was: 0.231 mg/mL, corresponding to aliquots of the same sample used for setting up the experiment in the triple quadrupole [100]. Moreover, in order to prevent possible peptide adsorption to glass, plastic vials were employed for all the analysis [153].
The LC-MS/MS analytical method adopted is reported in the corresponding paragraph 5.2.9.

5.2.8 Franz Cells

In vitro SA1-III skin permeability was investigated by the Franz cells apparatus, using human skin specimen taken from a patience subjected to breast surgery at Careggi University Hospital, Florence. Human skin was separated from the hypodermis layer before starting the assay.
Experiments were carried out according to the protocol recently reported by Vanti *et al.* [154].
Briefly, Franz cells consists of two compartments, donor, and acceptor, separated by a horizontally oriented membrane (skin in this case). The receptor compartment was filled with 7.5 mL of PBS solution, selected as release medium, and was kept under constant magnetic stirring (500 rpm), while the donor compartment was loaded with 1 mL of a solution of 50 ppm of peptide SA1-III in PBS. Cell diffusion area of 3.14 cm^2 was covered by the human skin and maintained hydrated by the acceptor solution. Finally, the cells were

clamped together. Donor chambers were closed with suited caps and sampling ports were sealed with parafilm, in order to avoid evaporation. During the experiment, the system was maintained at 35 ± 2°C by a thermostatic circulation bath and a water jacket around cells. Release medium samples (0.2 mL) were collected from the sampling port of the receptor compartment at established time points (1, 2, 3, 5, 7, 24 h) and were replaced with the same volume of fresh PBS solution. At the end of the diffusion experiment, a 0.2 mL sample was taken from the donor compartment.

At the end of the experiment, skin was recovered, washed three times with PBS, brought at +4°C, then cryoprotected by 5 min incubation in cold saccharose 10% in PBS, washed in PBS, embedded in Killik™ medium, quickly frozen by immersion in isopenthane and subsequently cut with a Reichert/Leica 2800 Frigocut cryostat (Wetzlar, Germany) into 10 µm thick horizontally oriented slices, in order to separate dermis from epidermis, which were then solubilized in MeOH (500 µL) and analyzed separately.

Collected samples were diluted with MeOH (100 µL of samples and 100 µL of MeOH) before being analyzed. LC-MS/MS analysis were carried out as describe in paragraph 5.2.9.

5.2.9 LC-MS/MS ANALYSIS

The setting up of the optimal experimental condition in the *ex-vivo* experiments conducted, in the first instance, in rat skin homogenates, was performed in a Varian1200 L triple quadrupole system (Palo Alto, CA, USA) equipped by two Prostar 210 pumps, a Prostar 410 autosampler and an Electro-spray Source (ESI) operating in positive ions.

The chromatographic parameters employed were tuned to minimize the run time. The column used was a Luna PFP, 30 mm length, 2 mm internal diameter and 3 µm particle size (Phenomenex, Italy), at constant flow of 0.25 mL/min, employing a binary mobile phase elution gradient. The eluents used were formic acid (10 mM) and ammonium formate (5 mM) (solvent A) and formic acid (5 mM) and ammonium formate (10 mM) in methanol (solvent B) according to the elution gradient as follows: initial at 90 % solvent A, which was then decreased to 10 % in 4.0 min, kept for 3.0 min, returned to initial conditions in 0.1 min and maintained for 3.0 min for reconditioning, to a total run time of 10.0 min. The column temperature and the injection volume were 30°C and 5 µL, respectively. The ESI source was operated in positive ion mode, using the following setting: -4.5 kV needle, 42 psi nebulizing gas and 20 psi drying gas at 280°C. The mass spectrometer was used in scan mode by acquiring the range from 300 to 1500 m/z. The optimal tandem mass spectrometry conditions, in terms of collision energy and specific product ions, were established through the ERMS experiment, and employed to set up the LC–MS/MS method. All the parameters that may affect the assay results, including substrate concentration, skin homogenate dilution, protein concentration, and batch-to-batch homogenates variation were evaluated in different experiments [100].

Despite the first LC-MS/MS method optimized in the triple quadrupole system was set up, in order to increase the chromatographic conditions (due to peptide high polarity) and minimize the "matrix effect" of the HSH complex matrix, a new bidimensional HPLC was developed. Moreover, to expand the analytes panel that can be analyzed in each run, an ion trap was employed. In fact, the ion trap gives higher quality level of the information obtained, providing higher sensitivity.

For this reason, chromatographic separation of all the samples collected during the final dermal chemical and enzymatical stability experiments, and during the Franz diffusion experiments (including skin layers samples), were carried out in a bidimensional LC system composed by a loading column Supelco Discovery® HS F5 Supelguard™ Cartridge (3 µm particle size, 20 mm x 2.1 mm) operating in isocratic mode and an analytical column Phenomenex Luna® PFP(2) (3 µm particle size, 50 mm x 2.0 mm) operating in gradient mode. These C18 PFP columns are composed of pentaflourophenyl groups and are largely used in case of hydrophilic analytes which are usually eluted with very low retention times, compromising peak resolution.

For the MS/MS experiments we used a Varian 500 ms ion trap equipped with Varian autosampler 410 and three pumps 210 and with an electrospray ionization source (ESI) operating in positive ion mode. Two pumps were used for the binary gradient and one pump was dedicated to the isocratic elution in the loading column.

We used the following elution solvents:

Solvent A) MQ H_2O + 20 mM HCOOH + 5 mM $HCOONH_4$

Solvent B) MeOH + 20 mM HCOOH + 5 mM $HCOONH_4$

Solvent C) H_2O/MeOH (9:1) + 20 mM HCOOH + 5 mM $HCOONH_4$ (only used to load peptide solutions in the first column).

As a first step, the best way to analyze our peptides with the mass spectrometer was evaluated, between scan, single ion monitoring (SIM) or product ions scan. The latter, which showed the best sensitivity and the best signal-to-noise ratio, was chosen.

Then, the best chromatographic conditions to obtain good resolution, in terms of well separated and solved peaks, were chosen and are reported in Table 14:

Table 14 Gradient used for the LC bidimensional mode.

Time	*A%*	*B%*	*C%*	*Flow (mL/min)*	*Valve Position*
00:00	*30.0*	*3.3*	*66.7*	*0.75*	*Load*
05:00	*30.0*	*3.3*	*66.7*	*0.75*	*Inject*
05:01	*45.0*	*5.0*	*50.0*	*0.50*	*Inject*
10:00	*32.5*	*17.5*	*50.0*	*0.50*	*Inject*
13:00	*5.0*	*45.0*	*50.0*	*0.50*	*Inject*
14:00	*5.0*	*45.0*	*50.0*	*0.50*	*Load*
14:01	*3.3*	*30.0*	*66.7*	*0.75*	*Load*
17:00	*3.3*	*30.0*	*66.7*	*0.75*	*Load*
17:01	*30.0*	*3.3*	*66.7*	*0.75*	*Load*
18:00	*30.0*	*3.3*	*66.7*	*0.75*	*Load*

Collision induced dissociation (CID) experiments were performed for peptides: SA1-III, [Met[1](O)]SA1-III and SA1-III scrambled peptide, to select the product ion to be followed in the ion trap. In Figure 38 is reported, as an example, SA1-III CID in which precursor ion (571.8 m/z corresponding to the bi-charged peptide $[M+2H]^{2+}$) and several product ions (or ion ranges) are shown.

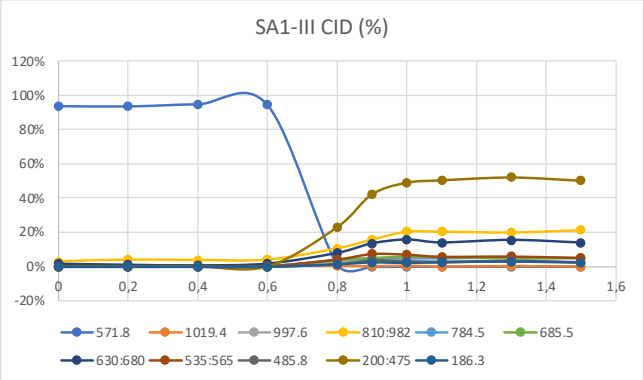

Figure 38 CID acquisition for peptide SA1-III.

A 600 ppb and a 6000 ppb solution of peptides SA1-III and [Met[1](O)]SA1-III together in H_2O/MeOH (50:50) were prepared starting from a 100 ppm solution derived by a the stock 1000 ppm solution (1 mg of each peptide solubilized in 1 ml of MQ H_2O), to minimized sample preparation errors.
600 ppb and 6000 ppb solutions were used to prepare 5 points for the calibration curve, described in Table 15:

Table 15 Preparation of the standard calibration curves for peptide SA1-III and [Met[1](O)]SA1-III.

ppb	***ISTD (SA1-III peptide scrambled)***	***SA1-III and [Met[1](O)]SA1-III***	***H_2O/MeOH (50:50)***
0	*15 µL of a 10 ppm solution*	*/*	*585 µL*
50	*15 µL of a 10 ppm solution*	*50 µL of a 600 ppb solution*	*535 µL*
100	*15 µL of a 10 ppm solution*	*100 µL of a 600 ppb solution*	*485 µL*
250	*15 µL of a 10 ppm solution*	*25 µL of a 6000 ppb solution*	*560 µL*
500	*15 µL of a 10 ppm solution*	*50 µL of a 6000 ppb solution*	*535 µL*

Once the calibration curves were ready, triplicate analysis of each experimental point were performed. In particular, the following samples were analyzed:

- samples deriving from the incubation of peptide SA1-III with HEPES buffer (10 mM pH 7.4) at different times (0, 8, 24 h),
- samples deriving from the incubation of peptide SA1-III in HSH at different times (0, 8, 24 h),
- samples deriving from the donor chamber of the Franz cells after 24 h incubation,
- samples deriving from the receptor chambers of the Franz cells at different time of incubations (0, 1, 2, 3, 5, 7, 24 h),

- samples deriving from dermis recovered after Franz cells experiments,
- samples deriving from epidermis recovered after Franz cells experiments.

Analytical data were then processed with the Varia Workstation vers. 6.8 software, and results were reported as average of the triplicates.

5.2.10 LIPOSOMES PREPARATION

The film hydration method was used to prepare the liposomal formulations according to [150], [151]. Various ratios of Phospholipon®90G (P90G) and cholesterol (CHOL) were dissolved in dichloromethane, while a small amount of methanol was added together with peptide pamSA1-III. The organic solvents were evaporated under vacuum at 37 °C to obtain a thin dry film, which was hydrated using 10 mL of PBS (pH 7.4). The liposomal dispersion was kept under stirring at 850 rpm for 30 min at 38°C. In order to obtain homogeneous small unilamellar vesicles the samples were ultrasonicated by a KE 76 probe. A Sonopuls HD 2200 ultrasound device was use for 1 up to 6 min with or without pulsed duty cycles of half of a second “on” and half a second “off”. The amplitude was 70%. Samples were maintained in an ice bath to prevent degradation of constituents. The peptide concentration in liposome (LL) was 2 mg/ml. Batches were always prepared in triplicate.
Dynamic and Electrophoretic Light Scattering (DLS and ELS) were used to provide vesicle size (nm), homogeneity (polydispersity index; PDI) and the surface charge by zeta potential (mV) of the liposomes. The evaluation was performed with a Zetasizer® NanoZS90 apparatus and ALV-60X0 software V.3.X provided by Malvern at 25 °C. Autocorrelation functions were analyzed by the Cumulants method, fitting a single exponential to the correlation function to obtain particle size distribution. ELS functions were executed to measure the zeta potential applying the Henry correction to Smoluchowski’s equation. Three runs were conducted for each sample.
Liposomes were stored at 4°C and used for the in vitro experiments the same day.

5.2.11 BOYDEN CHAMBER PROTOCOL

Invasion assays were performed on Boyden chambers in order to evaluate the peptide influence on the proteases ability to digest a matrix (Matrigel®) that mimics the ECM.
Polycarbonate filters of 13 mm diameter and 8 µm pores were covered with 50 µg of Matrigel® and left to dry overnight at RT under a laminar flow hood, considering three Boyden chambers (triplicate) each experimental point, including the CNTRL cells. The following day, filters were recovered in a 24-MW plate with a solution of 1 % denatured BSA in DMEM for at least 1 h (RT).
Lower Boyden chambers were filled with 200 µL of DMEM 2 % FBS and filters were settled over the meniscus of the solution paying attention to avoid bubble formation. Matrigel®

layer must be facing the upper chamber. Once filters are placed, the upper chamber is installed, creating a hole where the suspensions of cells, derived from the protocol described in paragraph 5.2.4.1, will be placed. Boyden chambers were then left at 37°C in 5 % CO_2 humidified atmosphere for 24 h. A schematic representation of the final aspect of the invasion experiment is reported in Figure 39.

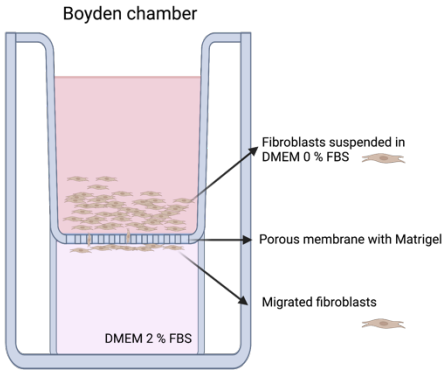

Figure 39 Schematic representation of the Invasion experiment carried out in the Boyden chamber.

After 24 hours of incubation time, filters were recovered in a 24-MW and fixed in MeOH for at least 1 h. In order to avoid interference, unmigrated cells were removed from the filter with a cotton swab. Migrated cells were then stained with Diff-Quick solution 1 and 2 (3-5 minutes each). Filters were then washed in milliQ H_2O and filter triplicates were recovered in the same histological grade glass to be observed and counted in a NIKON Eclipse E200 microscope (optical zoom 4x, 10x and 40x were employed). Images were collected at 10x at different visual fields and cells were counted at least in three visual fields for each experimental point. A comparative count between total cells contained in CNTRL cells filters and treated cells filters was also performed and the ratio between them was the same found by counting singular visual fields. In the light of this, considering the simplicity in acquiring visual fields, we decided to adopt this counting methodology.

6. CONCLUSIONS AND FURTHER DEVELOPMENT

"Cosmeceuticals" is becoming an ordinary term to define a new class of products, at the borderline between classic cosmetics and pharmaceuticals, which are influencing in large measure the cosmetic market [155].

Among the several families of cosmeceutical ingredients that have been developed, bioactive peptides play an important role, and their use constantly increased in the last decade. In fact, peptides are involved in many physiological processes, such as skin aging, and therefore they are interesting starting points for the development of attractive active ingredients with skin-related indications, particularly in anti-aging treatments.

Accordingly, within the last decades, several peptides targeting collagen production have been described, mainly as active ingredients to be included in cosmeceutical formulas to improve skin firmness and texture [75]. On the contrary, very little is known about signal peptides able to modulate collagen turnover by decreasing protease degradation activity, which is indeed a crucial aspect to guarantee collagen integrity, especially in the case of aged skin.

The aim of the present PhD project was to develop new peptides with proven activity in the modulation of collagen turnover, using as a starting point the peptide SA1-III, already developed by Pascarella *et al.* [79], and studying its pharmacokinetic properties, such as chemical and enzymatical stability, as well as its mechanism of action, an aspect that was only partially described previously [80]. Considering the great interest raised within the cosmetic market by the collagen modulating properties of peptides, we do believe that these molecules could be successfully employed in the development of novel cosmeceutical products.

As already introduced in the RESEARCH DEVELOPMENT chapter, several branches of the project were carried out in parallel.

Firstly, new shorter peptides were design and synthesized, starting from peptide SA1-III (Ac-MGKVVNPTQK-NH_2). Peptides were obtained by solid phase peptide synthesis, using a Fmoc/tBu strategy and employing NMM and HBTU as coupling system. All the syntheses were followed by a purification step, to achieve an HPLC purity > 95 %. Peptide activity was evaluated *in vitro* by treating normal human dermal fibroblasts (NHDFs), which are collagen releasing cells, with the peptide of interests for 72 hours, followed by the collection of both conditioned media and cell lysates. For each peptide, MTS viability assay was also performed in order to exclude any possible mitogenic or cytotoxic effect on fibroblasts. Collagen quantification was obtained from western blot experiments by using specific type I collagen antibodies. Once it was established that the evaluation of type I procollagen concentration in cell lysates was a good representation of collagen levels in the extracellular matrix, considering the complicated and error-prone media concentration passages

necessary to achieve a concentration of global proteins suitable for western blot experiments, all the quantifications were obtained using exclusively cell lysates.

One of the second-generation peptides, the partially *retro-inverso* tetrapeptide AAT11RI (Ac-nvvk-NH_2), showed interesting activity in the modulation of collagen turnover *in vitro*, in comparison with the parent peptide SA1-III. For this reason, taking into account the originality of the chemical modification of this sequence, at least in the field of cosmeceutical peptides, AAT11RI was patented [99]. This aspect is considered an added value of the present work, as technology transfer, that represents the third mission of the Italian Universities, is an important feature of a research project aiming at the valorization of the scientific results, in the framework of a fruitful collaboration between Academia and cosmetic companies.

Peptide SA1-III stability (both chemical and enzymatic) and permeability through the skin were also evaluated. In particular, a procedure to analyze peptide stability with *ex-vivo* experiments carried out on skin homogenates by LC-MS/MS analysis was firstly developed [100] and subsequently optimized. This procedure could be potentially applied to all those peptides, which are interesting for topical application. Moreover, as the chemical stability seems to be a pivotal aspect of cosmeceutical products already on the market, particularly those containing methionine residues were oxidations can occur [148], [149], it was mandatory to take into account this aspect. To this purpose, peptide [Met^1(O)]SA1-III was prepared and used as a standard to evaluate SA1-III oxidation in *ex-vivo* experiments conducted on human skin homogenates (HSH), meanwhile exploring peptide SA1-III enzymatic stability to the HSH proteases. The final results, conducted using a bidimensional HPLC system coupled with an ion trap mass spectrometer, showed that peptide SA1-III is chemically stable to Met^1 oxidation in HEPES buffer for up to 24. Moreover, considering the data on peptide SA1-III in HSH, it was interestingly showed that sample preparation and experimental conditions do not affect peptide chemical stability. In fact, there was no increase in [Met^1(O)]SA1-III concentration, while after 24 hours of incubation SA1-III concentration never declined below 65 %. Taken together, these results confirm that SA1-III is an attractive peptide to be used for topical application, e.g., for daily application creams, as its bioavailability in the 24 hours is more than acceptable. Although in the described experimental conditions peptide [Met^1(O)]SA1-III formation was not observed, an oxidation in the cream formulation or shelf life cannot be excluded. For this reason, the activity of the oxidized form of SA1-III was evaluate *in vitro* with the same protocol already described, and the results showed that oxidation does not dramatically affect peptide activity. Moreover, peptide Met^1(O)]SA1-III cytotoxicity was excluded by MTS evaluation.

Now that the analytical procedure to obtain dermal proteases stability profiles is optimized, it will be of great interest to evaluate the dermal protease stability of peptide AAT11RI and compare its degradation kinetics with that of SA1-III. In fact, AAT11RI was designed as a

peptide with increased stability to proteolytic enzymes: it is composed of D-amino acids with inverted sequence in comparison to the parent peptide AAT11 (Ac-KVVN-NH_2), resulting in a peptide where the spatial orientation of the amino acid side chains is the same, while the orientation of the peptide bond, that is usually subjected to proteases cleavage, is inverted. As peptide AAT11RI is a very short and polar peptide, the new instrumental set up, that includes a bidimensional HPLC system, will be of great help in increasing peptide retention time in order to further evaluate its enzymatic stability.

In parallel to the description of peptide dermal stability, SA1-III permeability across the skin was also evaluated. By means of 24-hours Franz cell permeation experiments performed with human skin placed between a donor and a receptor chamber, followed by LC-MS/MS analysis, it was demonstrated that peptide SA1-III is not able to pass the *stratum corneum* by itself, meaning that it has not the proper intrinsic permeation ability. To improve this characteristic, peptide pamSA1-III (palmitoyl-MGKVVNPTQK-NH_2) was design and synthetized. The use of a fatty acid to improve peptide permeation across the *stratum corneum* is a widely used technique for cosmeceutical peptides, considering that many relevant and extensively used second-generation peptides are to the palmitoylated version of their precursor peptides [144], [156]–[158]. As the new designed peptide pamSA1-III had to be tested *in vitro* to evaluate its activity in increasing collagen concentration, it was incorporated into liposomes. Liposomes loaded with peptide and empty liposomes used as negative control, were then used as a 72-hours treatment for fibroblasts and collagen levels were then measured by western blot assays. Collagen levels in fibroblasts treated with peptide pamSA1-III were much higher than the basal collagen found in the cells treated with empty liposomes (44 % increase), thus indicating that the modification made in the N-terminal of peptide SA1-III maintained the peptide property of modulating collagen turnover. Peptide pamSA1-III cytotoxicity was also evaluated by MTS tests and empty liposomes were employed as negative control, showing no significative change in cell proliferation.

Within the immediate future, pamSA1-III permeability through the skin will be tested in the Franz cell apparatus, making a comparison, e.g., with a cosmetic cream containing peptide SA1-III. Another possibility will be represented by PAMPA experiments, since the artificial membranes used in this system is certainly more accessible than human skin specimens; the kind of membranes used with this technique mimic the *stratum corneum*, which is the limiting barrier to access the dermis. However, the poor skin permeability is only a marginal problem in the case of an active principle for cosmeceutical uses, as this property can also be increased by other ingredients included in the final formulation or thanks to many innovative skin permeation strategies recently developed and widely employed in the cosmetic field [71].

Finally, fibroblasts invasion assays in Boyden chambers were performed. As peptide AAT11RI was considered the candidate of choice among the second-generation peptides derived from SA1-III, it was tested in invasion assays as well. In this type of test fibroblasts, which are collagen but also collagenase releasing cells, have to move side to side through a membrane (filter) covered with an artificial gel that mimic the extra-cellular matrix that divides two compartments with different concentrations of a chemoattractant used to induce cell migration. In these circumstances, their only way of moving from one compartment to the other is to degrade the matrix components by means of their proteolytic activity. Cells used for the experiments were treated with 20 µM solutions of SA1-III and AAT11RI for 48 hours, then trypsinized, solubilized again in 20 µM solutions of SA1-III and AAT11RI and left for 24 hours in the Boyden chambers. Control untreated cells were also employed. The results showed a significant decrease in protease activity, confirming both the suggested mechanism of action, and the increased activity of the shorter peptide in comparison to peptide SA1-III. These results are a confirmation of what was previously hypothesized [80] also taking into account that it was already described that a 44-mer peptide from serpin A1, from which SA1-III formally derives, known as SPAAT (short piece of α1-antitrypsin) and originally isolated from human placenta, is a competitive inhibitor of serin proteases [159], [160].
Moreover, as inflammation and proteolytic enzyme activity are modulated by the same cell signaling pathway, the potential anti-inflammatory activity of peptide SA1-III was also evaluated. After 48 hours of fibroblast treatment with peptide SA1-III (20 µM), TNF-α (20 ng/mL) was added to the cells media in order to induce an inflammatory state. Control cells were treated with the TNF-α as well. 24 hours later, conditioned media and cell lysates were collected and COX-2 levels in cell lysates were evaluated, showing that peptide SA1-III is able to decrease COX-2 levels, thus indicating a potential anti-inflammatory property which has to be further confirmed by increasing the number of experiments. Besides, the anti-inflammatory property of serpin A1 is largely known in literature as this protein is considered the most potent neutrophil elastase inhibitor and in light of this, it is not out of place trying to exploit this relevant characteristic, e.g., to promote wound healing [88], which represent a dermatologically relevant target.

In conclusion, it is undeniable that nowadays the discovery of novel active molecules of cosmeceutical interest has a strong added value in terms of technological transfer, as many ingredients obtained from academic research are exploited in the industrial environment to develop new cosmetic products for the market. Thus, the valorization of synthetic peptides as suitable entities to be employed as active ingredients in the cosmeceutical field attracts growing interest. In fact, peptides are largely used in the field of cosmeceuticals, giving rise in the last decades to a new class of active ingredients. Consequently, it is

mandatory that these molecules, like any other active substance, go through a full and accurate characterization at pre-clinical level, in terms of *in vitro* activity, mechanism of action, pharmacokinetic properties, and bioavailability.

To evaluate all these characteristics, several *in vitro* or *ex-vivo* experiments were employed over the course of this PhD project, and new analytical procedures were developed, whose general applicability enable their use in screening procedures, aiming to evaluate cosmeceutical peptides degradation profile.

In particular, this systematic approach shed light to some limits of the proposed cosmeceutical lead, peptide SA1-III, prompting us to develop new rationally designed second-generation peptides, such as AAT11RI, whose sequence was patented, in view of its cosmeceutical use. The biological evaluation of its collagen turnover modulation activity *in vitro* and the accurate study of its MoA revealed that this shorter sequence is even more promising than the previous peptides, demonstrating that there are many solutions to improve peptide characteristics. In fact, AAT11RI is the fruit of a backbone modification applied to peptide AAT11, which is part of SA1-III that itself is part of A1-C26, which derives from serpin A1. Therefore, which will be the next cosmeceutical peptide?

7. ACKNOWLEDGMENT

This work was supported by Tuscany Region [project: BIOPEPTIDI. Sviluppo di nuovi peptidi biologicamente attivi. PORCREOFESR 2007-2013].
I would like to thank Prof. Giovanna Caderni (Dep. Neurofarba, University of Florence), and Dr. Desirè Pantalone (Sect. Surgery, Dept. of Experimental and Clinical Medicine, University of Florence) for kindly providing samples of rat and human skin respectively.

SARS-COV-2 VIRUS ANTIGENS FOR DIAGNOSTIC AND VACCINAL USE

8. INTRODUCTION

8.1 SEVERE ACUTE RESPIRATORY SYNDROME CORONAVIRUS 2

Viruses are infectious pathogens composed, in general, of genetic material surrounded by a protein capsid and, in some cases, lipid. They can be composed of DNA or RNA and exploit the protein synthesis mechanisms of the organism that infect to replicate [161].
Coronaviridae are a family of viruses characterized by envelope, positive filament RNA genome and in particular by the presence of several large protuberant glycoproteins, called Spike proteins. The Coronavirinae sub-family is divided into four genera: Alpha Coronavirus, Beta Coronavirus, Gamma Coronavirus and Delta Coronavirus [162]. A classification of the coronavirus family is reported in Figure 40 starting from the order (Nidovirales), family, subfamily (Coronavirinae) and genus (α, β, γ, and δ).

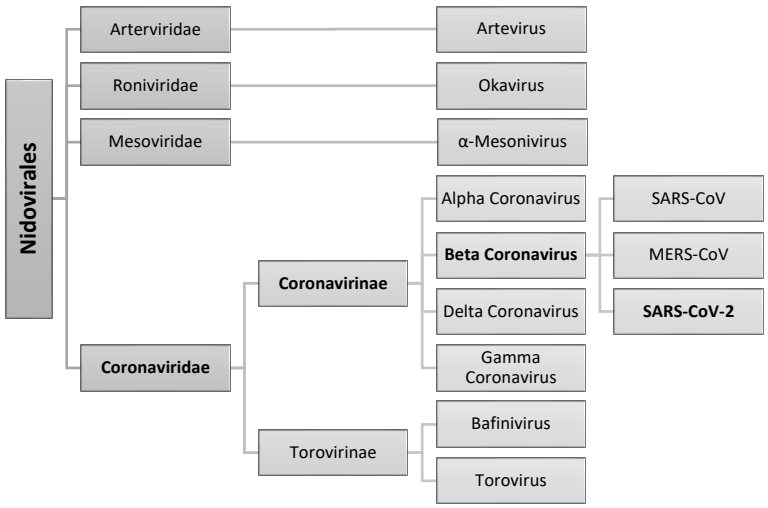

Figure 40 Classification of coronaviruses.

There are several species of Coronavirus belonging to this family, including six species that cause human disease: 229E, OC43, NL63, HKUI1, MERS-CoV (Middle Eastern Respiratory Syndrome Coronavirus), and SARS-CoV (Severe Acute Respiratory Syndrome Coronavirus) [163]. Among them, MERS-CoV and SARS-CoV viruses are zoonotic in origin and have been linked to respiratory problems causing sometimes fatal illness [164].
The first CoV outbreak, known as SARS-CoV, initiated in November 2002 in China and turned into global infection in 2003 with lethal rate of 10% in the world. After one decade, a second HCoV (Human Coronavirus) pandemic was caused by MERS-CoV, originated in June 2012 in Saudi Arabia, with a global fatality rate of 37%. To date, the latest HCoV is SARS-CoV-2, a

coronavirus that caused the outbreak of the COVID-19 pandemic in late December 2019 [165].

SARS-CoV-2 first cases were isolated in Wuhan (China), as a cluster of patients with pneumonia of unknown cause epidemiologically linked to a seafood and animal wholesale market. In fact, nine hospitalized patients were examined, eight out of the nine patients visited the Wuhan seafood market before the onset of the illness, while one patient stayed in a hotel close to the market [166], [167]. Several evidence based on genome sequences showed from the very beginning that SARS-CoV-2 human viral genome had high homology with bat-SL-CoVZXC21 (a bat CoV) and indicated bat as natural host (Figure 41; [168]).

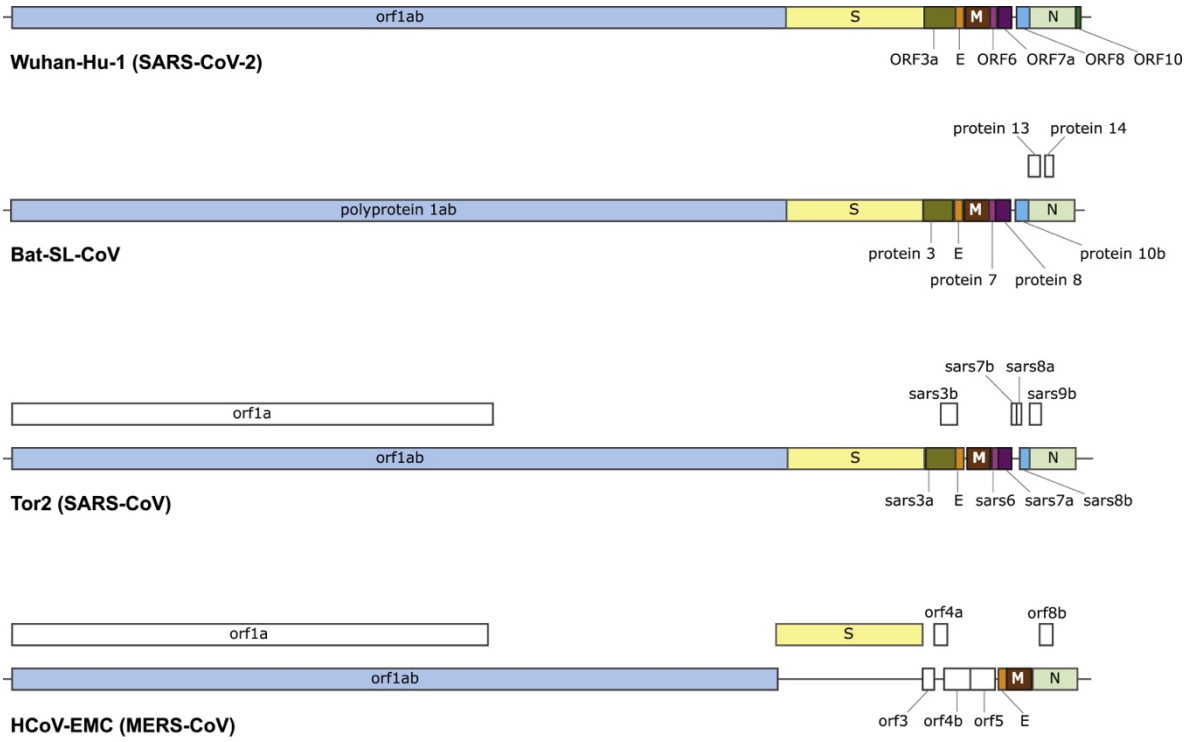

SARS-CoV-2	orf1ab	S	ORF3a	E	M	ORF6	ORF7a	ORF8	N	ORF10
Bat-SL-CoV	95%	80%	91%	100%	98%	93%	88%	94%	94%	-
SARS-CoV	86%	76%	72%	94%	90%	68%	85%	40%	90%	-
MERS-CoV	50%	35%	-	36%	42%	-		-	48%	-

Figure 41 Comparison of SARS-CoV-2 (Wuhan-Hu-1) genome structure with the closest coronaviruses (bat-SL-CoV indicates bat-SL-CoVZXC21) [168].

Therefore, even in the case of SARS-CoV-2, the hypothesis of human transmission was due to a zoonotic spillover event [169].

COVID-19 occurs with flu-like symptoms, especially fever and chills, coughing, difficulty in breathing, weakness, muscle pain, headaches, loss of smell and/or taste, nausea and diarrhea [166], [170]. Especially in immunocompromised individuals, COVID-19 is a very

dangerous pathology and may become fatal. SARS-CoV-2 has a high transmissibility: transmission can be through contact with respiratory droplets, direct contact with infected persons or contaminated surfaces. For this reason, and in order to slow down the infections, new hygiene standards were introduced widespread, such as wearing masks and paying attention to social distancing, in addition to the frequent use of sanitizing hand gels. The incubation period for COVID-19 was supposed to be of 14 days on average, which means that a seemingly healthy individual can be infectious for many days before presenting symptoms, increasing the chances that it will infect other people. In addition, it has been observed that the virus has participated in various "superspreading" events, meaning that a single infected individual can transmit the virus to a large number of healthy individuals in a short time. This phenomenon is due to the high efficiency of infection of SARS-CoV-2, which is thought to be able to infect a person with only 1000 viral particles [171].

8.2 SARS-COV-2 SPIKE PROTEIN

HCoVs (Human Coronaviruses) membranes contain four viral proteins:

- spike protein (S), a type I glycoprotein forming peplomers on the virion surface,
- membrane protein (M), spanning three times the membrane and having a short N-terminal ectodomain,
- small membrane protein (E), a highly hydrophobic protein,
- nucleocapsid protein (N), contained into the enveloped membrane, important to allow viral RNA packaging during host infection.

The β-coronavirus spike protein (S) is a glycosylated protein of 180/200 kDa covering the surface of SARS-CoV-2 and is strictly involved in host-cell penetration as it consists of two subunits: S1, mediating host cell hACE2 (human Angiotensin Converting Enzyme 2) receptor binding, and S2, responsible for the fusion with the host cell membrane [172]. S1 is a globular subunit consisting of various domains, including the receptor binding domain (RBD), the N-terminal domain (NTD) and the signal peptide (SP). Spike protein has a trimeric conformation (with homo-trimeric structure, as it is composed of three protomers) and is a class I fusion protein, i.e. it takes an initial pre-fusion conformation (Figure 42), which then passes to a post-fusion conformation as a result of a conformational change and proteolytic cut of the subunit S1 [173], [174].

Spike RBD mediates the binding with the PD domain (Peptidase Domain) of the ACE2 receptor and in the native conformation, at physiological pH, this region is hidden. In fact, as shown in Figure 42 the “down” conformation corresponds to the receptor-inaccessible state, whereas the “up” corresponds to the receptor-accessible state.

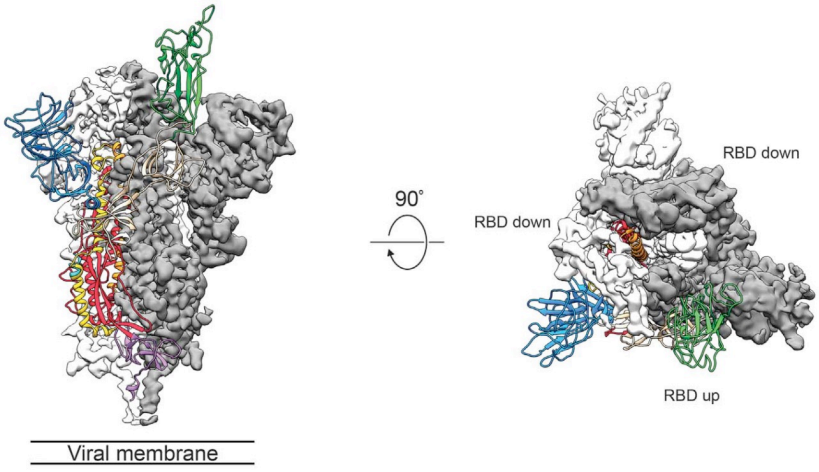

Figure 42 Side and top views of the prefusion structure of the SARS-CoV-2 Spike protein with a single RBD in the up conformation. The two RBD down protomers are shown as cryo-EM density in either white or gray and the RBD up protomer is shown in colored ribbons [173].

After the interaction with ACE-2 receptor, SARS-CoV-2 S protein changes its conformation and exposes the RBD domain, which can lead to host cell infection. Once anchored to the

host ACE2 receptor, Spike protein is subsequently cleaved at S1/S2 and S2' sites by TMPRSS2 (transmembrane Serine Protease 2), as shown in Figure 43. This leads to activation of the S2 domain and drives fusion of the viral and host membranes [175].

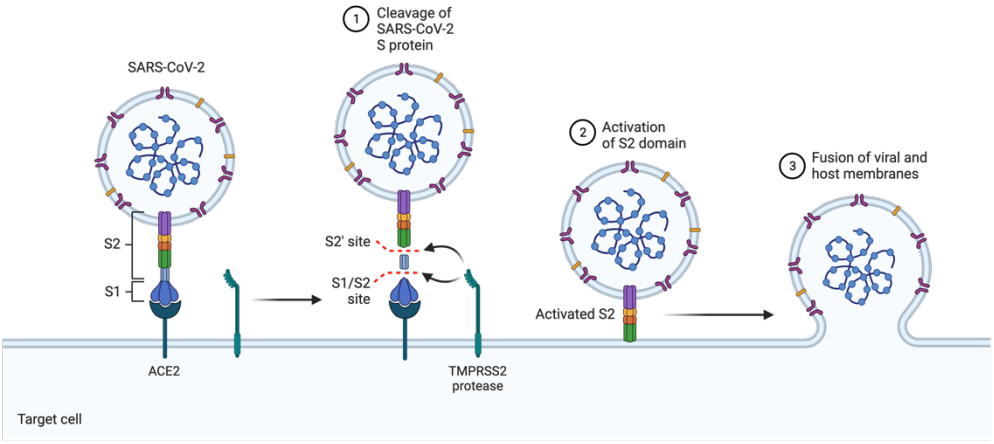

Figure 43 Mechanism of SARS-CoV-2 viral entry [175].

S protein is therefore a key factor in SARS-CoV-2 infection allowing virus entry into the cell through interaction with the human membrane protein hACE2, mainly present in the respiratory tract but also in various other anatomical districts. ACE2 is a transmembrane Zn-metalloprotein, which normally causes a reduction in blood pressure by acting against angiotensin 2 [176]. Angiotensin 2 is a proinflammatory hormone that raises blood pressure through vasoconstriction and increased saline concentration in the blood. A cleaved fragment of ACE2 modifies angiotensin 2, transforming it into angiotensin 1-7, which is instead a vasodilator. In healthy subjects, the amount of angiotensin 1-7 is much higher than that of angiotensin 2, which means that there are many more cleaved ACE2 receptors, that do not contain the anchorage point for the Spike protein. On the other hand, in subjects with diseases, for example chronic inflammation, angiotensin 2 will be predominant along with ACE2 presenting the un-cleaved portion, with whom the Spike protein can interact. This, together with other immunological factors, could be a reason why individuals with pre-existing diseases are much more susceptible to SARS-CoV-2 infection [177]
Among the other regions of the Spike protein, the RBD is the most interesting domain from the diagnostic/vaccinological point of view, as it is considered to play a relevant role in triggering the immune response.

8.3 IMMUNE RESPONSE

The immune system uses a complex group of protective mechanisms to control and usually eliminate exogenous organisms and toxins and this active answer to the external environment is defined immune response. It goes without saying that it is critical that the immune response avoid unleashing these destructive mechanisms against the mammalian host's own tissues, and indeed failure of self-tolerance underlies the broad class of autoimmune diseases [178].

In humans, two different immune responses exist: the innate and the adaptive immune response. The innate immune response is a non-specific and rapid response to any sort of pathogens and involves physical barriers such as skin and mucosa, but also soluble proteins and bioactive small molecules that are either constitutively present in biological fluids (such as the complement proteins) or that are released from cells as they are activated (including e.g., cytokines). The adaptive immune responses are instead triggered against specific antigens and are based primarily on the antigen-specific receptors expressed on the surfaces of T- and B-lymphocytes, and generate a strong and long-lasting response. When the organism interacts for the first time with a new pathogen, it starts producing T- and B cells effectors. The production of these effector cells can be divided into two different responses: the first, called "primary immune response", is the result of the first-time exposure to an antigen, and the second, called "secondary immune response", involves memory T- and B cells [179]. The rational to develop vaccines is based on the capacity to evoke a primary response without exposure to pathogens, using the relevant molecules triggering immunity. T cells are produced in the bone marrow and then migrate to the thymus, where their maturation takes place. From the same progenitor, T cells are differentiated into T-helper cells and T-cytotoxic cells, which express different receptors and serve different purposes. Both B cell generation and maturation indeed, take place in the bone marrow [180]. Even if innate and adaptive immune response are described separately, they have to be considered as opposite sides of the same coin and closely related to each other, where the innate response represents the first line of host defence, and the adaptive response becomes prominent after several days, as T and B cells have undergone clonal replication.

B- and T cells are responsible for the humoral and cell-mediated immunity, and they do not recognize the whole pathogen, but molecular components named antigens. These antigens are recognized by specific receptors exposed on the cell surface of both B- and T cells, and this recognition differs depending on the receptor-exposing cells. In fact, B cells recognize solubilized antigens through antigen receptors, named B-cell receptors (BCR), consisting of membrane-bound immunoglobulins [181].

In Figure 44 a schematic representation of the B cell receptors is shown.

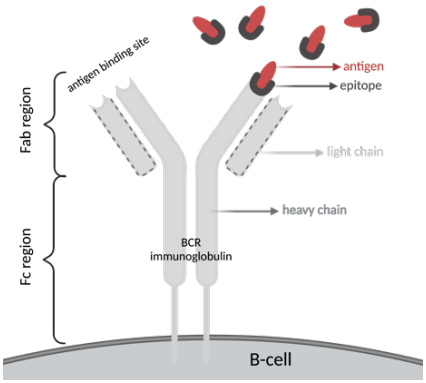

Figure 44 B cell receptor schematic representation, including the antigen binding site for the epitope recognition.

Following to this antigen-receptor interaction, which occurs at the epitope level, cells differentiate and secrete soluble forms of the immunoglobulins, also known as antibodies, that mediate humoral adaptive immunity. B-cell epitopes can be divided into two main categories, shown in Figure 45: linear epitope and conformational epitope. The former consists of sequential amino acid residues (continuous epitope), while the latter consists of non-sequential amino acid residues that interact one next to the other because of their spatial distribution in the solvent (discontinuous epitope).

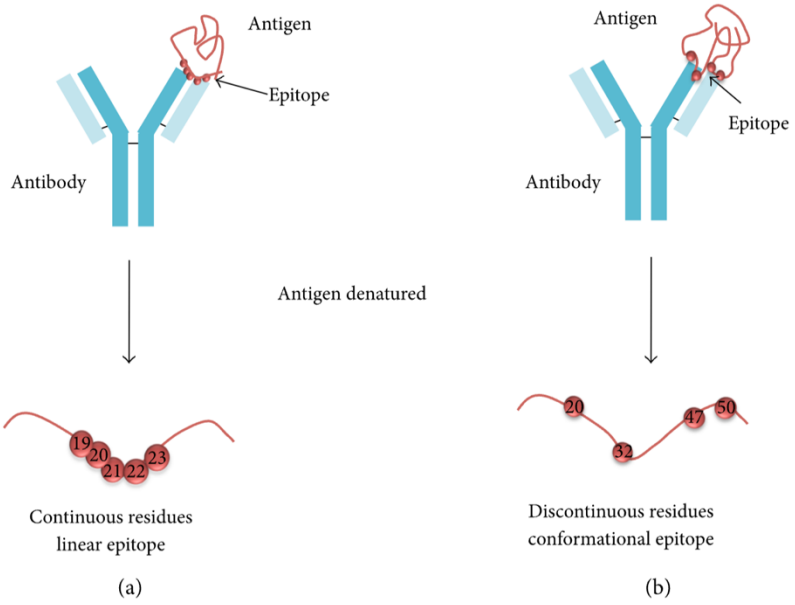

Figure 45 Linear and conformational B-cell epitopes. Linear B-cell epitopes (a) are composed of sequential/continuous residues, while conformational B-cell epitopes (b) contain scattered/discontinuous residues along the sequence [181].

For this reason, antibodies that recognize linear B-cell epitopes can recognize also denatured antigens, while due to the loss in protein conformation in denaturing environments, discontinuous epitope are no longer recognized [181].

B cell epitopes mainly belong to the conformational family, and they can be mapped thanks to conformational and functional studies such as crystallography, NMR (nuclear magnetic resonance), electronic microscopy, and western blot, dot blot or ELISA respectively.

T cell receptors (TCR), located on the T cells surface, enable the recognition of antigens presented on the surface of antigen-presenting cells (APCs) bound to major histocompatibility complex (MHC) molecules. The epitopes are presented by class I (MHC I) and II (MHC II) MHC molecules that are recognized by two distinct subsets of T cells, Cluster of Differentiation 4 (CD4+) and Cluster of Differentiation 8 (CD8+) T cells, respectively.

The presence of CD4+ and CD8+ memory T cells persist for several years as observed in SARS-CoV individuals. Since the high homology between SARS-CoV and SARS-CoV-2, SARS-CoV epitope mapping must be taken into consideration for the rational design of synthetic antigens, vaccines, and drugs [182]. Nowadays T cell epitopes can be predicted thanks to many bioinformatic tools, which facilitate peptide design for vaccinological and diagnostic purposes.

9. STATE OF THE ART

The recent pandemic from SARS-CoV-2, with its rapid spread, is a health emergency with a heavy impact on the health systems of all countries. Previously, there were two coronavirus outbreaks, the first caused by the SARS-CoV virus and the second from MERS-CoV, two members of the coronavirus beta family with whom SARS-CoV-2 shows a high structural homology (about 79% with SARS-CoV and 50% with MERS-CoV) [167], [168]. From the clinical and serological point of view, the previous epidemics have shown many similarities with the current pandemic, thus allowing the previously acquired knowledge to be adopted for the development of diagnostic and therapeutic tools against SARS-CoV-2 infection.

During the course of the coronavirus infection, a humoral and cellular immune response is developed and the production of IgM (M immunoglobulin) and IgA (A immunoglobulin) specific for SARS-Cov-2 is documented 7-10 days after the beginning of the disease, while the production of IgG (G immunoglobulin) is revealed after 10-15 days [183]. Convalescent subjects' plasma contains virus neutralizing antibodies and in some preliminary studies it has been used successfully to treat the illness [184]. Monoclonal antibodies able to inhibit virus-receptor interaction and neutralize the virus *in vitro* were obtained from B cells from infected and healed subjects [185], [186]. Another group of human monoclonal antibodies with neutralizing activity against SARS-CoV-2 was identified within a panel of clones obtained from subjects that were previously infected with SARS-CoV, thus demonstrating the relevance of the structural similarities between the two coronaviruses in the development of a protective immune response [187].

The target of neutralising monoclonal antibodies is mainly represented by sequences belonging to protein S (spike). The epitopes recognised by the neutralising antibodies described by Cao *et al.*[185] are situated in the contact surface between ACE2 and RBD, and the glycidyl group linked to RBD Asp^{165} is important for antibody binding. Similarly, the discontinuous epitope that is described to be targeted by one of the monoclonal antibodies isolated from Pinto *et al.* [187] contain fucose and other glycans bounded to Spike Asp^{343}.

In the immune response to the virus, the production of T cells is also of utmost importance: the presence of CD4+ T lymphocytes specific for viral antigens has been described in the peripheral blood of the totality of patients healed from SARS-CoV-2 infection and CD8+ T in 70 % of cases [188]. During the acute phase, however, specific lymphocytes are strongly reduced in circulation, probably seized in viral replication sites, which in fact are strongly infiltrated in the most serious cases [189]. Immunodominant epitopes recognised by T lymphocytes in all structural SARS proteins have been described.

The detection of anti-SARS-CoV-2 antibodies is currently carried out using recombinant proteins corresponding to the RDB region or larger portions of the S protein, or the entire N protein in solid phase-based techniques. With these methods anti-S1 antibodies of IgA

isotype were revealed in 83 % and IgG isotype in 67% of infected subjects [190]. All methods using recombinant proteins have the advantage of measuring antibodies directed against many epitopes, thus providing a high frequency of positivity in infected subjects and potentially in vaccinated people. However, only some of the measured antibodies may have neutralising activity and represent a potential surrogate of protection.

Analysis of a specific antibody response that can be obtained by the use of synthetic peptides, indeed, allows to distinguish specific from cross-reactive (unspecific) antibodies and to detect those which actually provide neutralization. A study of epitope mapping of the entire S protein, conducted in the Chinese population using overlapping peptides as antigens in a solid phase assay, identified some immunodominant epitopes that appears to be targeted by protective antibodies [191]. These epitopes, represented by linear sequences placed at the N- and C-terminus of the RBD, or in the S2 portion, are different from those recognized by neutralizing monoclonal antibodies, thus suggesting a high polyclonal immune response against SARS-CoV-2. The existence of many antigenic sites on S protein, also outside of the RBD, which can be targets of neutralizing antibodies has been confirmed by some recent studies [192], [193].

Concerning T cells specificity, an *in-silico* analysis using bioinformatics tools for the identification of epitopes predicted the existence of numerous T epitopes on the S and N SARS-CoV-2 proteins [168]. The probability that the identified sequences really match with T-epitopes is reinforced by the observation that many among them have high sequence homology with SARS-CoV epitopes and it has been experimentally proven that they are recognized by T cells in SARS-CoV infected subjects. Using "megapools" of synthetic peptides, Grifoni *et al.* demonstrated the existence of an anti-SARS-CoV-2 T response in all subjects infected with the virus [168].

10. AIM OF THE PROJECT

There are many analogies among SARS-CoV-2 and SARS-CoV, mainly due to the fact that both belong to the same virus family. Considering that patients infected by SARS-CoV developed long term immunology memory thanks to the synergy of B- and T cells, it was hypothesized that also in the case of SARS-CoV-2 infection a similar response could be triggered by CD4+ and CD8+ T cells. Moreover, SARS-CoV is the most closely related to SARS-CoV-2, for which a significant number of epitopes had been already described and reported to be a possible starting point for the individuation of peptide epitopes [168]. As shown in Figure 46 (left), a large number of SARS-CoV Spike protein residues was mapped as epitopes, meaning that the S protein has a key role in triggering the immune response. Thanks to the cryoEM structure of the SARS-CoV-2 S protein [173], which confirmed the overall structure homology with the SARS-CoV S protein, and helped by bioinformatic tools, Grifoni *et al.* indicated a number of putative immunodominant regions among this glycoprotein (Figure 46 on the right) [168].

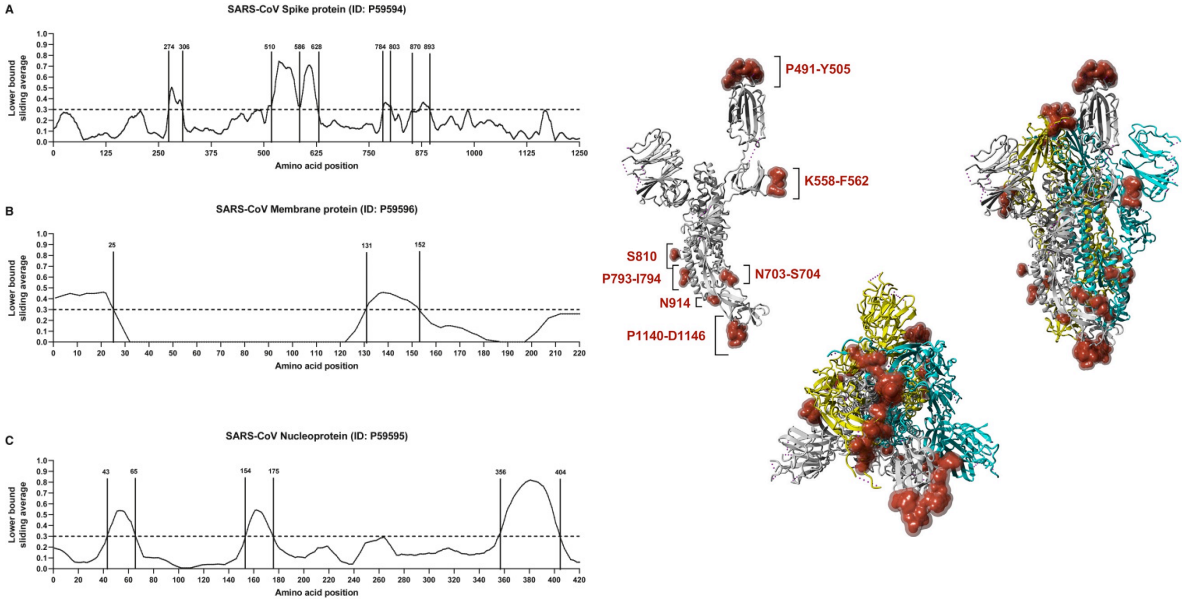

Figure 46 On the left: B Cell Immunodominant Regions Based on SARS-Specific Epitope Mapping. On the right: monomer and trimer conformation of SARS-CoV-2 Spike protein showing in red the calculated residues predicted to be B cell epitopes based on ranking performed with Discotope 2.0 [168].

Furthermore, several other studies reported the indication that RBD might be an immunodominant region of interest for the development of peptide epitopes [194]–[196], and Shrock *et al.* suggested that the immunodominant region included in the RBD might be enclosed in the N-terminal domain of the Receptor Binding Motif (RBM) [197].

Based on these recent research advances on the structure and function of S protein, a first series of peptides, *A* series, was selected from the S-ACE2 binding interface. In particular, sequence $RBM_{436-507}$ was selected as a region for putative epitopes. Together with this long peptide of 72 residues, named BIP (Binding Interface Peptide), 20-mer overlapping peptides (named P11, P12, P13, P14, P15 and P16) were also synthetized in order to map the entire RBM region.

Moreover, based on recent crystallographic studies involving a human monoclonal neutralizing antibody and the SARS-CoV-2 RBD region reported in Figure 47 [198], a new class of four peptides were designed to mimic a conformational epitope (*B* series).

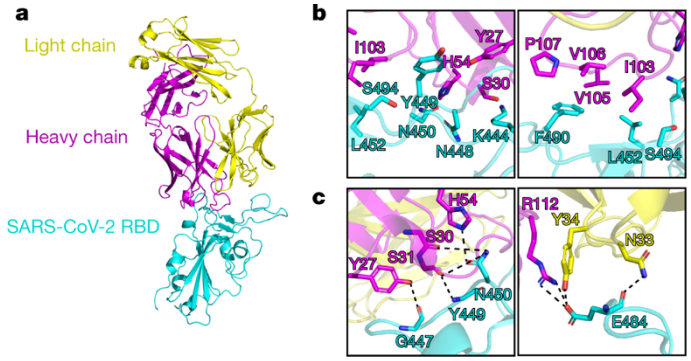

Figure 47 a, Overall structure of P2B-2F6 Fab in complex with SARS-CoV-2 RBD. b, Hydrophobic interactions around SARS-CoV-2 RBD residues Y449, L452 and F490 at the binding interface. c, Hydrogen bonds and salt bridges at the binding interface. The P2B-2F6 heavy chain is colored magenta, P2B-2F6 light chain is yellow, SARS-CoV-2 RBD is cyan and ACE2 is green [198].

Peptides of the first series were developed in the framework of an international collaboration between several research groups, i.e. the one in which this PhD project was developed (University of Florence, Profs. P. Rovero and A.M. Papini group), Italian clinical immunologists (University of Pisa, Prof. P. Migliorini group), a French bioinformatic group (CNRS Montpellier, Dr. A. Kajava), Swiss vaccinologists (University of Lausanne, Prof. G. Corradin group), Columbian vaccinologists (Caucaseco Scientific Research Center, Prof. M.A. Herrera group) and immunogenetists from Mali (University of Sciences, Techniques and Technologies of Bamako, Dr. S. Balam group). Moreover, circular dichroism (CD) analysis was performed at the University "Federico II" of Naples by Prof. A. Carotenuto group.

Peptides from the *A* series were tested along with recombinant proteins encompassing the full-length S-protein and the RBD to determine the potential role of $RBM_{436-507}$ in COVID-19 immunity.

A second class of peptides, *B* series, was developed in collaboration with Prof. A. Carotenuto from the University "Federico II" of Naples.

11. RESEARCH DEVELOPMENT

11.1 EPITOPE MAPPING

Antibodies have a high therapeutical and diagnostic relevance thanks to their characteristic to selectively recognize and bind antigens at the epitopes level. It is therefore of great interest to have detailed information concerning the epitope location and nature (linear or conformational). Specialized methods for mapping the two different classes of epitopes have been developed and defined as “epitope mapping”; they are based on a combination of protocols used to identify specific peptide sequences on antigens, which can provoke an immune response by interaction with antibodies (B cell response) or MHC molecules (T cell response) [199]. Historically, epitope mapping of protein antigens relied on enzymatic digestion or chemical cleavage to generate small fragments, which retained antibody binding [200]. The progress in structural biology techniques, e.g., 3D structure of the complex between antibodies and antigens, provided precious and detailed information about the binding interface, thus promoting the development of different epitope mapping techniques [201].

Among these techniques, the design of a series of overlapping synthetic peptides is a widely used strategy to identify linear immunogenic epitopes of various antigens, and a successful approach to find epitopes from potential target vaccine proteins [202]–[205]. The use of synthetic peptides as antigenic probes (by including the minimal epitope) to detect antibodies as biomarkers, instead of recombinant proteins, phage display or microarray technology, has several advantages such as the possibility to introduce post-translational modifications on amino acid side chains, lower time- and cost-consumes, and the possibility to introduce conformational constraints to mimic conformational epitopes. Indeed, not every recombinant protein can be produced with induced chemical modifications, because of several reasons:

- the organism chosen for the protein expression is not able to introduce the modifications,
- some post-translational modifications are only mediated by pathogens, such as in rheumatoid arthritis, in which citrullination is triggered by the pathogenic enzyme peptidyl arginine deiminase on arginine side chains,
- these modifications are not mediated by enzymes (such as glycation in diabetes),
- the antibody response linked to these modifications during the disease course are not constant [206].

When a peptide can really mimic an epitope structure and activate the antibody response, is defined as *mimotope* [207].

11.2 RESULTS

11.2.1 PEPTIDE SEQUENCES SELECTION

In order to study the interaction between S and ACE2 in detail, a focus was made on the surface of the RBD, which is involved in the ACE2 receptor binding. This binding segment should represent the target of the neutralizing antibodies. Dr. A. Kajava (CNRS of Montpellier) analysis of the 3D structure of the RBD-ACE2 complex showed that the large part of the RBD interacting surface, that is the Receptor Binding Motif (RBM), is composed of the 436-507 aa segment (Figure 48).

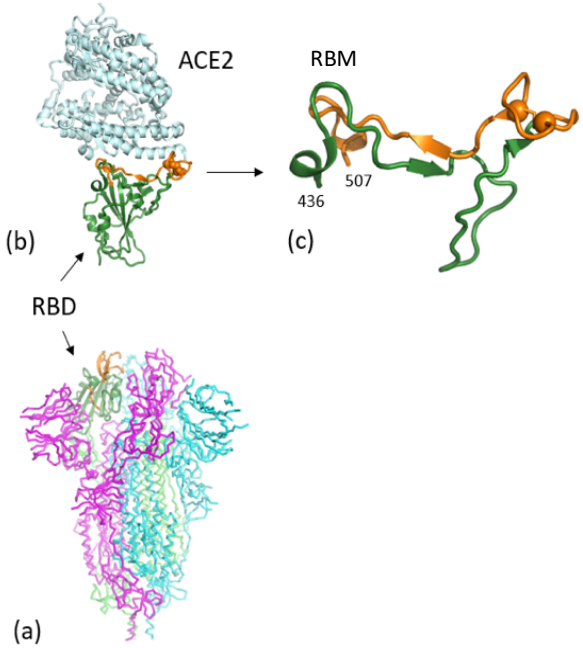

Figure 48 The atomic 3D structure of S trimer in the prefusion conformation [173]. RBD is shown in ribbon representation (dark green). Region 476-507 is in orange. (b) Complex between RBD (green-orange) and ACE2 receptor (light cyan) [172]. (c) Conformation of BIP peptide (436-507) within the RBD.

Since peptide synthesis technology has several advantages in comparison to the production of recombinant proteins, RBM region was selected for peptide synthesis and subsequent experimental studies. A first pool of peptides, hereon called *A* series, was selected as the central part of $RBM_{436\text{-}507}$ (peptide BIP), which contains a disulfide bridge that can be synthetically mimicked. This peptide sequence is specific to the SARS-CoV-2 and contains several predicted T-cell epitopes [168]. Moreover, overlapping 20-mer peptides derived from peptide BIP were also synthetized. Peptide names and sequences are reported in Table 16.

Table 16 Peptides of the "A" series sequences and positions on the SARS-CoV-2 Spike RBD region. Underlined sequences in peptides $RBM_{436-507}$ (BIP)and P12 represent disulfide bridges. Serine residues (S) highlighted in red in peptides P11 and P13 replace native cysteine.

Name	Sequence	Position
BIP	Ac-WNSNNLDSKVGGNYNYLYRLRKSNLKPFERDISTEIYQAGSTPCNGVEGFNCYFPLQSYGFQPTNGVGYQP-NH_2	436-507
P11	Ac-FNSYFPLQSYGFQPTNGVGYQP-NH_2	486-507
P12	Ac-GSTPCNGVEGFNCYFPLQSY-NH_2	476-495
P13	Ac-RDISTEIYQAGSTPSNGVEG-NH_2	466-485
P14	Ac-FRKSNLKPFERDISTEIYQA-NH_2	456-475
P15	Ac-GGNYNYLYRLFRKSNLKPFE-NH_2	446-465
P16	Ac-WNSNNLDSKVGGNYNYLYRL-NH_2	436-455

A second series of peptides, hereon *B* series, was proposed by Prof. A. Carotenuto from the University of Naples "Federico II" as linear peptides designed to mimic a putative conformational epitope derived from SARS-CoV-2 RBD. These sequences were chosen in the light of the observations described above concerning the interaction between the RBD region of SARS-CoV-2 Spike protein and the ACE2 receptor, and corroborated by the work of Ju *et al.* [198], where the crystallographic structure of the complex between a human monoclonal Ab and the SARS-CoV-2 RBD region showed which are the RBD amino acids involved in the binding. In particular, they are confined in a region of the RBD with ß-sheet conformation, where Y^{449} and N^{450} turns and meet S^{494} in spatial proximity. The amino acids fundamental for the binding, their spatial arrangement, position in the protein sequence, and the rational design of the first peptide sequence (S19) are reported in Figure 49.

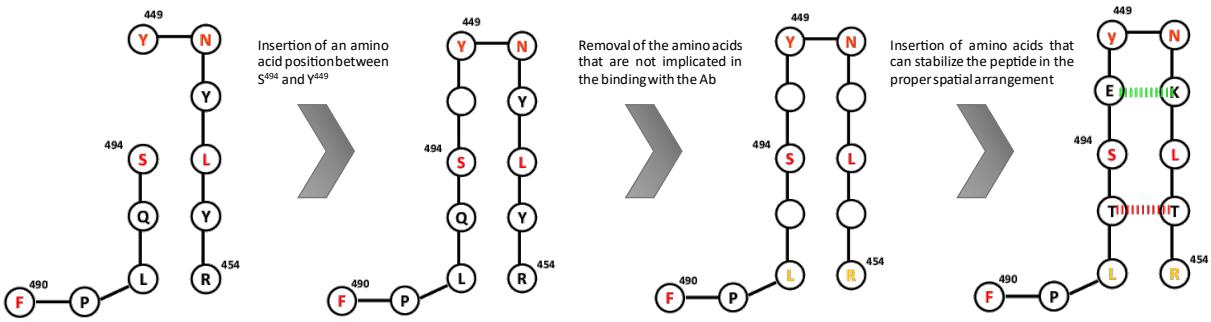

Figure 49 Design of peptide S19 from the B series.

Starting from the spatial arrangement of the amino acids in the crystallographic structure described by Ju *et al.* [197] and reported in Figure 49, the first step was to insert an amino acid position between S^{494} and Y^{449} in order to "close" the sequence and create a linear peptide that should mimic a conformational epitope (as the binding is mediated by non-contiguous amino acids). The amino acids implicated in the binding are F^{490}, S^{494}, Y^{449}, N^{450}, and L^{452}, while L^{492} and R^{454} seems to be exposed to the ACE2 receptor. These considerations led to a second step of peptide design in which amino acids not involved in the binding were eliminated. As last step, specific amino acids were proposed for the free positions in the sequence, in order to maximize the intramolecular interaction to maintain the spatial

conformation assumed by S protein. Moreover, Y^{449} (L-Tyr) was changed with y^{449} (D-Tyr) due to conformational improvement in order to have a positive ϕ angle.
The so designed first B series peptide S19, whose sequence is Ac-FPLTSEyNKLTR-NH_2 (in which lower case y indicates D-Tyr), was further modified with a biotinyl moiety (and β-Ala as spacer), in view of serological screening with streptavidin (or avidin) coated plates (Table 17). In addition, since it was observed that in some SARS-CoV-2 variants (e.g., Delta variant) there was the mutation L452R, peptides S21 and S22, bearing this mutation, were also designed (Table 17).

Table 17 Peptides of series B sequences and positions on the SARS-CoV-2 Spike RBD region. Red amino acids correspond to the virus mutation L452R.

Peptide name	***Sequence***
S19	Ac-FPLTSEyNKLTR-NH_2
S20	Biotin-βAla-FPLTSEyNKLTR-NH_2
S21	Ac-FPLTSEyNKRTR-NH_2
S22	Biotin-βAla-FPLTSEyNKRTR-NH_2

11.2.2 PEPTIDE SYNTHESIS, OXIDATION AND PURIFICATION

Peptide sequences of both *A* and *B* series corresponding to sequences described in Table 16 and Table 17, were synthesized and analyzed. Single cysteine residues in peptides P11 and P13 (Spike protein residues 486-507 and 466-485, respectively) were replaced with serine to avoid unwanted spontaneous formation of disulfide dimers. Peptides were prepared by microwave-assisted solid-phase peptide synthesis (MW-SPPS), biotin conjugation was performed by manual SPPS and, after acetylation or conjugation, peptides were cleaved from the resin and, in the case of $RBM_{436-507}$ and P12, oxidized in solution with H_2O_2 at pH 9.0. All sequences were N-terminal acetylated and C-terminal amidated to avoid the inclusion of terminal charged groups, which are not present in the native protein. The greater effort was spent in the synthesis of peptide BIP, composed of 72 residues, and containing a disulfide bridge. This stepwise synthesis was carefully optimized to obtain a crude product pure enough to enable further steps of purifications. The best strategy was to work on a 0.1 mmol scale, performing double coupling until 42^{nd} amino acid in the sequence. After the insertion of the 42^{nd} amino acid, the Fmoc-protected peptidyl-resin was split in two aliquots. Starting from 43^{rd} amino acid, synthesis was restarted using the same protocol, but working on half initial scale, resulting in an increased swelling volumes and in the use of double equivalents of reagents (as reported in Table 18).

Table 18 Peptide BIP synthesis cycles to optimize crude peptide purity.

Amino acid in sequence	***mmol scale***	***Amino acid Concentration***	***DIC concentration***	***Oxyma Pure concentration***
From 1^{st} to 42^{nd}	0.1 mmol	0.2 M	0.5 M	1 M
Form 43^{rd} to 72^{nd}	0.05 mmol	0.2 M	0.5 M	1 M

BIP synthesis quality was monitored by cleaving from the resin a small sample of peptide after coupling of amino acid 52, 62, and 72 and checking the resulting product by MALDI-TOF and High-Resolution Mass Spectrometry analysis at CISM laboratory (University of Florence). The relevant mass spectra are reported in Figure 50 as an example. Crude peptides purifications were performed by flash chromatography followed by semi-preparative HPLC to achieve purity > 70 %. (BIP and P16), > 87 % (P13) or > 93 % (P11, P12, P14, P15 and S19-S22), using the methods reported in paragraph 12.2.4. Final characterizations are reported in Table 19.

Table 19 Analytical characterization of purified peptides BIP, P11-P16, S19-S22. All the analysis were carried out on a UHPLC Thermo Dionex Ultimate 3000 system coupled with MSQ plus single quadrupole ESI-MS. Solvent lines were (A) H_2O (0.1 % v/v TFA); (B) acetonitrile (ACN) (0.1 % v/v TFA). [(a)] Retention time expressed in min.[(b)]25-60 % in 10 min; [(c)]5-95 % B in 10 min; [(d)] 5-95 % B in 5 min.

Peptide	***Disulfide bond***	***RP-HPLC Rt [(a)]***	***Purity grade (UHPLC)***
BIP	Cys^{480}-Cys^{488}	4.88[(b)]	≥ 70 %
P11	/	5.55[(c)]	≥ 93 %
P12	Cys^{480}-Cys^{488}	5.34[(c)]	≥ 93 %
P13	/	4.02[(c)]	≥ 87 %
P14	/	4.49[(c)]	≥ 93 %
P15	/	4.97[(c)]	≥ 93 %
P16	/	4.80[(c)]	≥ 70 %
S19	/	3.45[(d)]	≥ 93 %
S20	/	3.46[(d)]	≥ 93 %
S21	/	3.21[(d)]	≥ 93 %
S22	/	3.27[(d)]	≥ 93 %

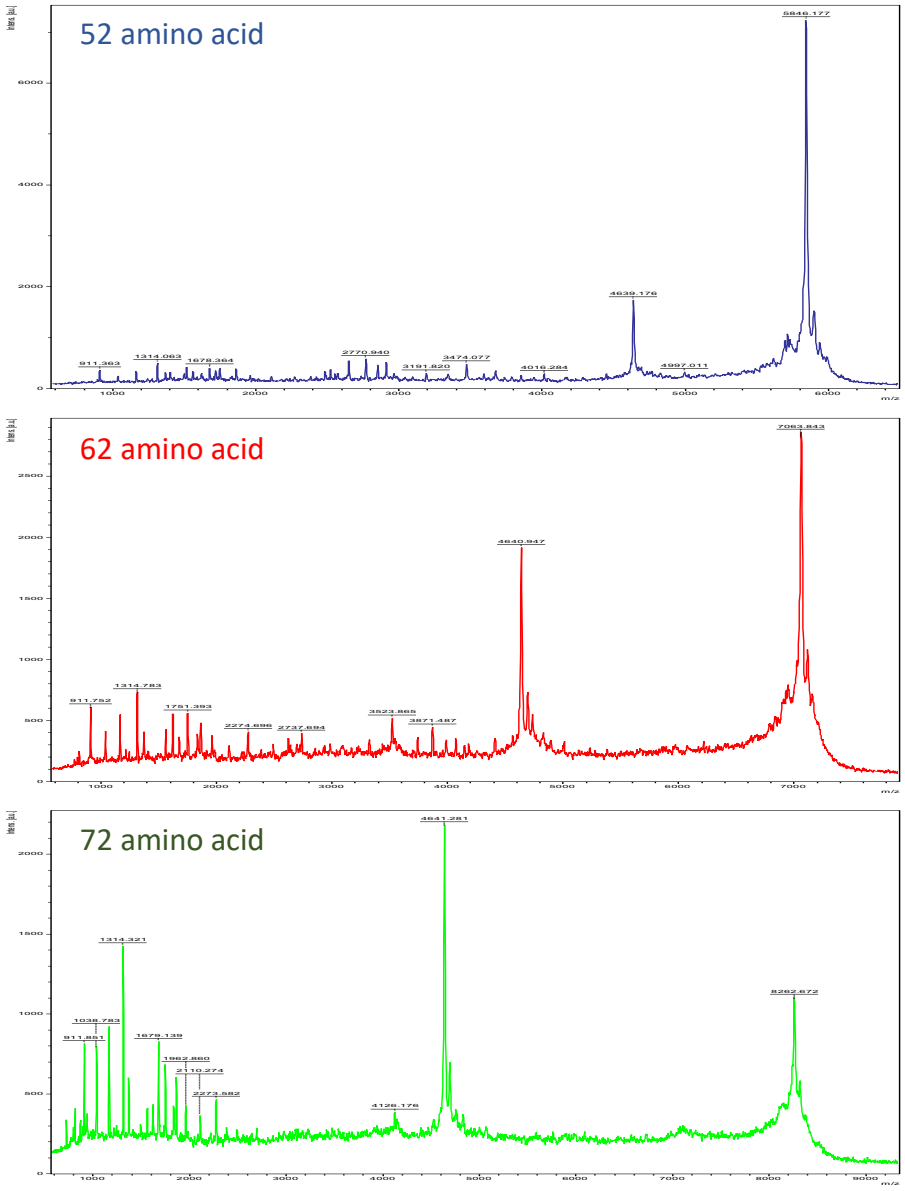

Figure 50 Mass spectra obtained by MALDI-TOF acquisitions in linear mode on peptide BIP in elongation after 52, 62 and 72 amino acids. Analysis were performed by CISM laboratory (Florence).

Pure peptides were then sent to the collaborators for the following serological and immunological screenings.

11.2.3 PEPTIDE BIP CIRCULAR DICHROISM

The conformation of peptide BIP in water at pH 7 was explored by circular dichroism (CD), as reported in Figure 51.

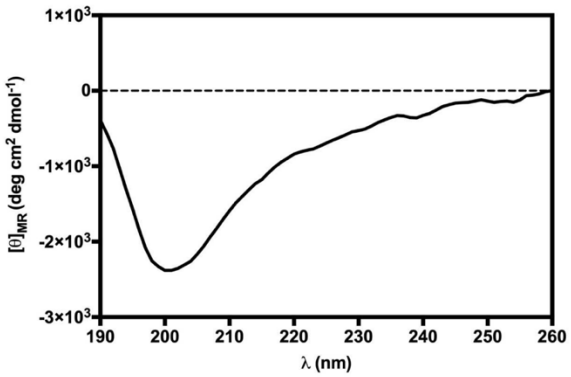

Figure 51 Circular Dichroism spectrum for peptide BIP.

The absence of a defined minimum around 200 nm, diagnostic of random coil conformation, is compatible with a certain degree of structuration of the peptide. The secondary structure content was predicted based on the CD spectrum using the online server for protein secondary structure analyses, DichroWeb [208]: 2 % helix, 30 % β-strand, 19 % β-turn, and 49 % random coil. The relatively high percentage of β-strand conformation suggests the intriguing hypothesis that $RBM_{436-507}$ peptide can partially preserve the extended conformation displayed along most of its sequence within the folded Spike protein (PDB code 6VXX) [209].

11.2.4 MICE IMMUNIZATION

Thirty BALB/c mice (female and male) were randomly divided in three group of ten that were sub-divided into two groups of five (five CNTRL and five test animals) in order to evaluate the immunization ability of recombinant Spike protein, recombinant RBD and synthetic peptide BIP. The immunization protocol, reported in paragraph 12.2.7, consisted of three subcutaneous injections (days 0, 20, 40) and blood was collected as schematically shown in Figure 52.

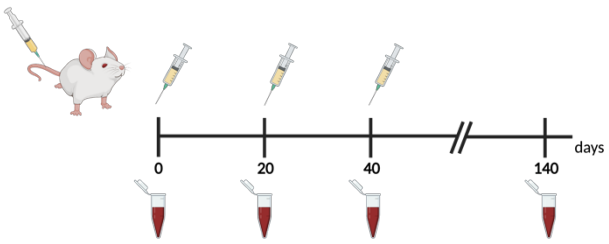

Figure 52 Schematic representation of the mice immunizing protocol and blood collection protocol adopted.

11.2.5 BIP REACTIVITY WITH MOUSE SERA

As shown in Figure 53, sera from all immunized animals, tested by ELISA at 1:100 dilution with the protocol reported in paragraph 12.2.8, using as antigen the S, RBD and BIP peptide (here named P3), indicated specific IgG seroconversion after the first immunization dose, and most of them displayed a boosting response after the second immunization dose. However, while animals immunized with BIP and RBD developed similar antibody profiles with high levels on day 40 (3.0 to 3.5 OD), mice immunized with the S protein displayed significantly lower responses (1.0 to 2.0 OD).

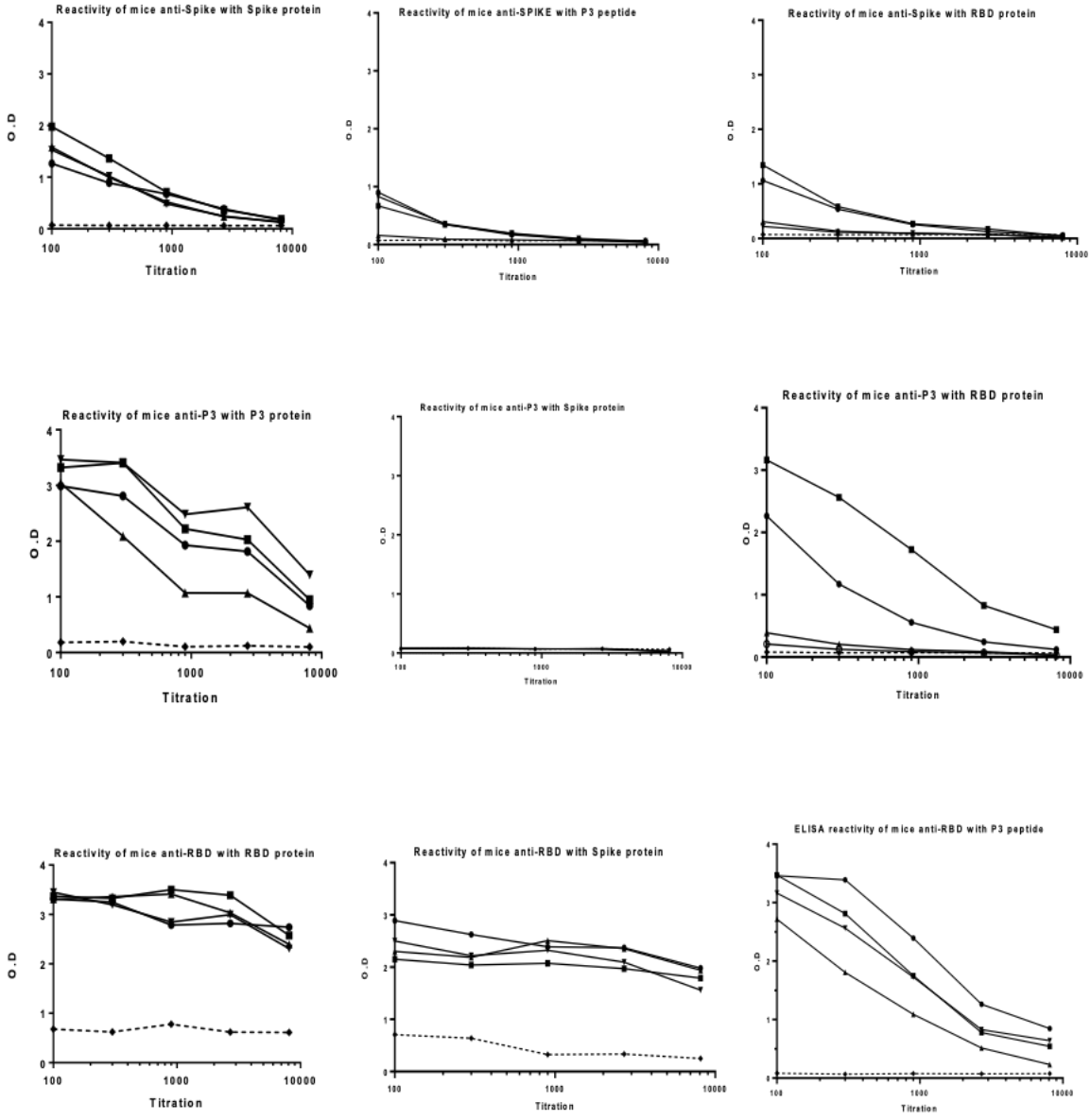

Figure 53 Mouse sera reactivity to Spike, RBD and BIP peptide (here named P3).

For BIP and RBD, antibodies remained at high levels (>2.0 OD) after day 140 whereas antibodies against S protein notably decreased (< 0.5 OD) during the same period. None of the control mice immunized with adjuvant alone seroconverted. The antibody titration (three-fold dilutions) on sera collected at day 140 indicated titers of 1:24,300 to BIP, 1:72,900 to RBD and 1:900 to S.

As shown in the upper panels of Figure 53, mouse antibody to S presented ELISA reactivity with the full-length S protein ranging from 1.2 to 2.0 OD when diluted to 1.100, whereas at the same dilution, the reactivity decreased to 1.1-1.3 OD for RBD, and to 0.9-0.7 OD for P3; however, the final reactivity titer of the anti-S antibodies was 1:10 with the S protein and $1.8x10^3$ with RBD and BIP (P3 in Figure 53). In the case of RBD, the mouse immunization elicited a vigorous antibody response (medium panels) with high optical densities even at 1:104 dilution. Although reactivity to the S protein and the BIP peptide were lower, the recognition remained significant even at dilutions of 1:104 and 5:103, respectively.

Sera from mice immunized with BIP peptide also displayed high reactivity with the homologous peptide and the RBD protein; however, these sera did not react with the S protein (lower panels).

11.2.6 EVALUATION OF ANTI BIP ANTIBODIES IN HUMANS

Patient sera were first screened by ELISA using S and RBD proteins and compared to a group of pre-pandemic normal sera (protocols reported in paragraphs 12.2.6 and 12.2.9). IgG antibody levels higher than the 97.5th percentile of normal sera were detected in 45 % (29/64) of patient sera on Spike protein and in 53 % (34/64) on RBD (Figure 54).

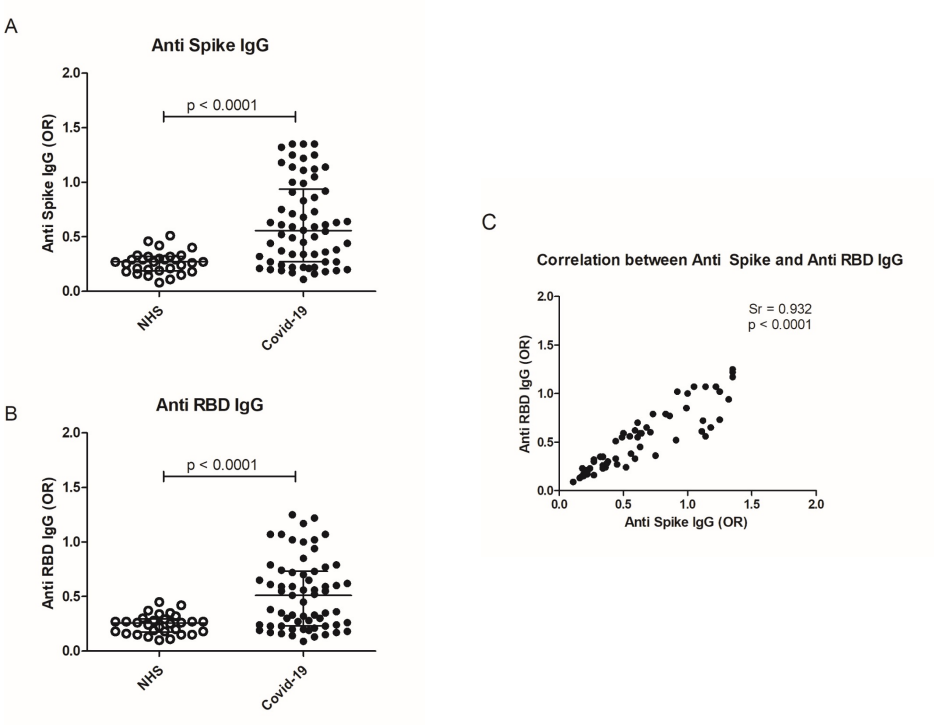

Figure 54 Anti-Spike and anti-RBD antibodies in Covid-19 patients. Distribution of anti-Spike IgG (A) and anti RBD IgG (B) in COVID-19 patients as compared with normal controls (NHS). Correlation of anti-S IgG and anti-RBD IgG in COVID-19 patients (C). p < 0.05 was considered as significative.

A strong positive correlation (p<0.0001) was observed between antibody levels on the two recombinant proteins (also reported in Figure 54).

It has been shown that low pH affects spike structure, favoring a closed conformation of the trimer [210] and affecting epitope exposure [211]. Thus, the ELISA assays were performed at acid pH, obtaining a similar level of antibodies in patient sera. Sera from COVID-19 patients and normal subjects were tested by ELISA on BIP immobilized on polystyrene plates. IgG anti BIP peptide higher than the 97.5th percentile of the normal population were detected in 21/60 (35 %) of the COVID-19 patients. As reported in Figure 55, antibody levels were significantly higher in patients than in controls (p<0.05) and were correlated with anti-Spike and anti-RBD antibody levels (p < 0.01). Anti BIP antibodies (indicated as anti-RBM$_{436-507}$ in Figure 55) of IgM and IgA isotype were also evaluated. IgM are detected in 7/60 (11.6 %) and IgA in 6/60 (10 %). IgM and IgA antibody levels are not significantly different in

COVID-19 patients with respect to controls. Co-expression of anti-BIP Ig isotypes in COVID-19 samples is also reported.

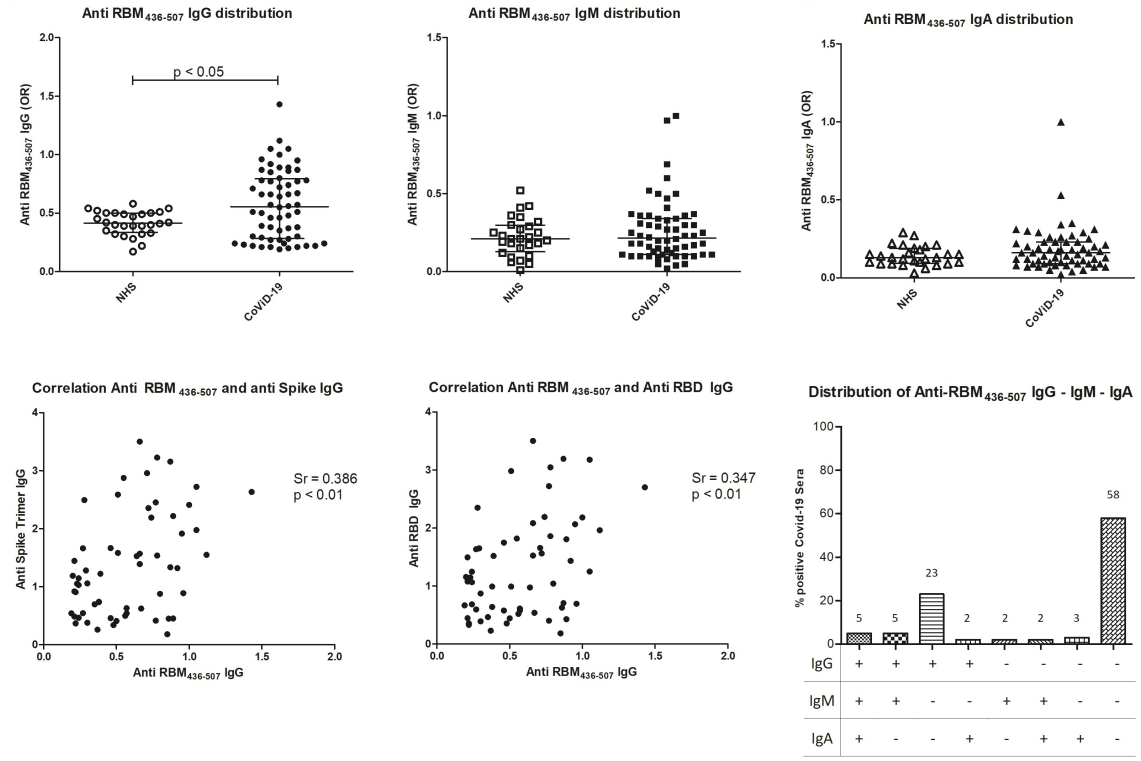

Figure 55 IgG, IgM and IgA response to peptide BIP (RBM $_{436-507}$) and their correlation with anti-Spike and anti-RBD antibodies.

11.2.7 EPITOPE MAPPING AND FUNCTIONAL ACTIVITY OF HUMAN ANTI BIP ANTIBODIES

Patient sera positive to BIP peptide were tested using the 20-mer overlapping peptides covering the entire BIP sequence (see Table 16). As shown in Figure 56, immune response mainly targets the N-terminal domain (P15-P16) rather than the C-terminal part (P11-P12), thus indicating that this confined region of the BIP peptide represents an interesting starting point for a peptide-based vaccine.

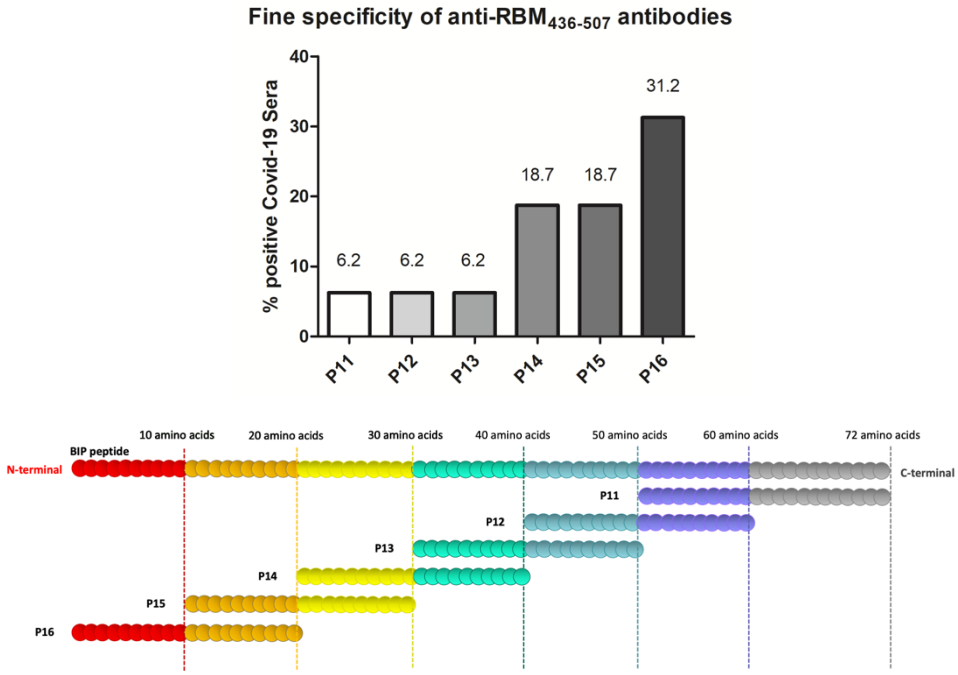

Figure 56 Overlapping peptides (P11-P16) response the BIP peptide responding Covid-19 positive sera.

12. EXPERIMENTAL PART

12.1 MATERIALS

Material used for peptide synthesis are reported below.

Peptide grade N,N-dimethylformamide (DMF), all Fmoc-L amino acids (and Fmoc-D-Tyr) were purchased from Sigma Aldrich (Milan, Italy). TentaGel® R RAM resin was purchased from Rapp Polymere GmbH (Tuebingen, Germany). Activators N,N'-diisopropylcarbodiimide (DIC), N,N-Diisopropylethylamine (DIPEA), 1-[Bis(dimethylamino)methylene]-1H-1,2,3-triazolo[4,5-b]pyridinium 3-oxide hexafluorophosphate (HATU) and Oxyma Pure were purchased from Sigma Aldrich (Milan, Italy). Trifluoroacetic acid (TFA), triisopropyl silane (TIS), and 2,2'-(ethylenedioxy)diethanethiol (DODT), diisopropyl ether (iPr_2O), 2-propanol, ammonium hydroxide 30 % (v/v) in water solution, hydrogen peroxide 30 % (v/v) in water solution and HPLC plus water were purchased from Sigma Aldrich (Milan, Italy). HPLC-grade acetonitrile (ACN) was purchased from Carlo Erba (Milan, Italy).

Material used to prepare the trimeric proteins and for the further biological investigations are reported in the respective methods.

12.2 METHODS

12.2.1 TRIMERIC SPIKE PREPARATION

Since the S trimer is described as the primary protein responsible for inducing an immune response towards the SARS-CoV-2 virus, first, a secreted and soluble form of this protein self-assembled in the trimer using Chinese Hamster Ovary (CHO) cells was [212].
Briefly, the transmembrane domain and the C-terminal intracellular tail were removed and replaced by a T4 foldon DNA sequence and a 8xHis tag. A signal peptide sequence was added. To stabilize the prefusion structure of the S trimer in this constructs, the original furin cleavage site RRAR was deactivated by changing it to RGSA and introduced amino-acid mutations K986P/V987P ("2P") as suggested by Wrapp *et al.* [173]. The construct used had the D614G mutation shared by most of the SARS-CoV-2 Variant of concern (B.1.1.7 – Alpha, B.1.351 – Beta, B.1.617.2 – Delta, B.1.1.529 Omicron) spread in Europe during 2020-2021 pandemic (https://www.ecdc.europa.eu/en/covid-19/variants-concern). This S protein construct was established to form trimers predominantly folded in the prefusion conformation [212]. In addition, the RBD of S protein (aa 319-541) was also produced as a recombinant product.

12.2.2 PEPTIDE SYNTHESIS

Peptides were prepared by microwave-assisted solid-phase peptide synthesis (MW-SPPS) and were assembled using an optimized protocol based on the Fmoc/tBu strategy and N,N'-diisopropylcarbodiimide (DIC) / Oxyma Pure as coupling reagents on the automated MW-assisted synthesizer Liberty Blue™ (CEM, USA). Tentagel R RAM resin was employed, as it is specially designed for long and difficult peptide sequences, as it is based on a PEG polymer that space out growing peptide sequences, thus reducing steric problems, and featuring a low loading (0.18 mmol/g). Peptides from *B* series were synthetized on a Tentagel S RAM resin (0.23 mmol/g) using a high swelling protocol was used.
The Fmoc/tBu MW-SPPS cycle consisted of:

- swelling in DMF for 30 min,
- Fmoc-deprotection by 20% (v/v) piperidine/DMF (4 mL, 81 eq) for 45 sec,
- washings with DMF (4 × 4 mL),
- double coupling with the Fmoc-protected amino acids (5 eq, 0.2 M in DMF), Oxyma Pure (5 eq 1 M in DMF) and DIC (5 eq, 0.5 M in DMF) for 125 sec,
- washings with DMF (2 × 4 mL).

Peptide elongation was performed by repeating the MW cycle for each amino acid coupling and deprotection. In the case of the 72-mer BIP, starting from cycle 43 the molar excess of

the couplings was switched from 5 to 10 eq and the swelling volume was doubled. Both deprotection and coupling reactions were performed at 90 °C in a Teflon vessel, applying microwave energy under nitrogen bubbling and monitoring the reaction temperature by an internal fiber-optic sensor. Conjugation with biotin was preceded by the addition of β-Ala as spacer. Biotin was conjugated manually upon solubilization at 70°C in DMF and N,N-Diisopropylethylamine (DIPEA) and 1-[Bis(dimethylamino)methylene]-1H-1,2,3-triazolo[4,5-b]pyridinium 3-oxide hexafluorophosphate (HATU) were used as tertiary base and coupling reagent, respectively. Unconjugated peptides were N-terminal acetylated using 10% acetic anhydride in DMF. After the acetylation step, the resin was filtered, washed with DMF (3 × 4 mL) and 2-propanol (3 × 4 mL), and dried under vacuum to obtain the dry peptide-resin. Cleavage of the crude peptides from the resin, with concomitant deprotection of acid sensitive amino acid side chains, was achieved by treatment of the peptide-resin with the cocktail TFA/DODT/H_2O/TIS (10 mL, (94:2.5:2.5:1) for 4.5 h at room temperature under soft stirring. The resin was filtered and rinsed with fresh TFA. The peptide was precipitated from the cleavage mixture by addition of ice-cold iPr_2O (40 mL). The solid was isolated by centrifugation and dried under vacuum. Characterization of the crude thiol free linear precursor peptides was performed by analytical UHPLC-ESI-MS.

12.2.3 Disulfide Bond Formation

The crude peptides BIP and P12 were introduced in a round bottom flask and a mixture of water and ACN (1:1) was added, stirring for about 15 minutes. After complete dissolution, additional water was added to the reaction mixture to obtain a final concentration of 3.3 mg/mL. pH was adjusted to 8.5-9.5 adding NH_4OH 7.5 %. 0.1 mL per gram of crude peptide and then Hydrogen Peroxide (30 % v/v water solution) was added to the solution. After 1 h of magnetic stirring at room temperature, the reaction was quenched adding Formic Acid to adjust the pH to 3 and the reaction mixture was lyophilized without further evaporation.

12.2.4 Purification and Characterization

After cleavage (P11, P13-P16, S19-S22) or after oxidation (BIP and P12), purifications were performed by flash chromatography on a CombiFlash® NextGen 300+ Teledyne ISCO instrument with a Teledyne ISCO RediSep® Gold 15g column followed by semi-preparative chromatography in a HPLC Waters 600 coupled with Waters UV DAD 2487 with a Phenomenex Jupiter C4 column (BIP) or a Sepax Bio C18 column to achieve a UHPLC purity grade > 70 % (P3 and P16) or > 87 % (P11-P15 and S19-S22) with the methods reported in Table 20. Final products were analytically characterized in a UHPLC Thermo Dionex Ultimate 3000 system coupled with MSQ plus single quadrupole ESI-MS and an Acquity column

UPLCR CSH™ C18 (1.7 µm 2.1 x 100 mm) or Agilent ZORBAX SB-C8 (3.5 µm 4.6 x 75 mm) working at a flow rate of 0.5 mL/min, and/or by MALDI-ToF analysis.

Table 20 Gradient of final purification used for peptides from the A and B series. [(a)] semi-preparative method; [(b)] MPLC method

Peptide	***Gradient***
BIP	30-45 % ACN in 45 min[(a)]
P11	25-60 % ACN in 16 min[(b)]
P12	20-70 % ACN in 16 min[(b)]
P13	15-60 % ACN in 16 min[(b)]
P14	20-50 % ACN in 30 min[(a)]
P15	20-60 % ACN in 16 min[(b)]
P16	20-60 % ACN in 16 min[(b)]
S19	25-60 % ACN in 30 min[(a)]
S20	25-60 % ACN in 40 min[(a)]
S21	10-50 % ACN in 40 min[(a)]
S22	25-60 % ACN in 35 min[(a)]

12.2.5 CONFORMATIONAL STUDIES BY CIRCULAR DICHROISM

CD spectrum of the BIP peptide was recorded using quartz cells of 0.1 cm path length with a JASCO J-710 CD spectropolarimeter at 25°C. The spectrum was measured in the 260−190 nm spectral range, 1 nm bandwidth, 64 accumulations, and 100 nm/min scanning speed. The peptide was dissolved in water at a concentration of 12 µM. The secondary structure content of the peptide was predicted using the online server for protein secondary structure analyses DichroWeb [208]. Input and output units and the wavelength step were θ (mdeg) and 1.0 nm, respectively. The algorithm used was CDSSTR, and the reference database was set-7 [213]. The normalized root mean square deviation (NRMSD) was 0.035.

12.2.6 HUMAN BLOOD SAMPLES

A clinical protocol was developed, submitted and approved by the local Ethical Committee (CEAVNO, Approval # 17522) in Italy and (CECIV, approval # 04-2020) in Colombia. Whole blood (10 mL) was collected by arm venepuncture using dry tubes after hospitalization and upon the patient's written informed consent; socio-demographic data and clinical manifestations were recorded. SARS-CoV-2 infection was confirmed by RT-PCR. Blood was fractionated and sera collected and kept frozen at -20°C until use for serology.

12.2.7 MICE IMMUNIZATION AND SERA COLLECTION

A total of 30 male and female, 6-8 weeks old BALB/c mice of 20 ± 5 g of body weight were randomly selected and distributed in three groups (A, B and C) of 10 animals/each. Each group was further divided into test (Exp) and control (Ctrl) sub-groups of five mice each and were further immunized with SARS-CoV-19 recombinant S (group A), recombinant RDB

(group B) protein as well as with the synthetic BIP peptide (group C). Each group of mice was immunized subcutaneously (s.c.) at the base of the tail on days 0, 20 and 40 with 20 µg of each antigen diluted in 50 µL PBS and emulsified in Montanide ISA-51 adjuvant (Seppic Inc., Paris, France) according to the manufacturer's recommendations. Mice were bled from submandibular veins on days 1-2 before first and third immunization, 20 days after the third dose and every 60 days until day 140. Whole blood (~100 µL) was collected, and sera separated by centrifugation and stored frozen at -20°C until use for serological analyses. Animal studies were carried out in the Caucaseco Research Center in Cali (Colombia) and approved by the Animal Ethics Committee of MVDC in Colombia. Animal care, housing, and handling were performed according to institutional guidelines and following the National Institutes of Health Guide for the Care and Use of Laboratory Animals.

12.2.8 Reactivity of Mouse Antibodies to S And RBD Proteins And BIP Peptide

The ELISA reactivity of sera from mice immunized with the S, RBD and RBM436-507 was determinate, using as antigens the specific immunogens. Briefly, 96-well plates (Nunc-Immuno Plate, Maxisorp, Roskilde, Denmark) were coated with one µg/mL BIP peptide, RBD and Spike Trimer protein, pH 7.4 at 4°C, o.n.. After plates were blocked with 5 % skim milk solution [PBS 1X, 0.05 % Tween 20, (PBS T)], serum samples were added at 1:100 or at three-fold serial dilutions starting at 1:100 in 2.5 % skim milk in PBS-T and were incubated for 1 hour. After the reaction, plates were washed and incubated with alkaline phosphatase-conjugated anti-mouse IgG antibody (Sigma Chemical Co., St Louis, MO) at a 1:1000 dilution for 1 hour. Reactions were revealed with para-nitrophenyl phosphate substrate (p-NPP) (Sigma Aldrich) and read at 405 nm wavelength (Dynex Technologies, Inc., MRX Chantilly, VA).

12.2.9 Elisa Assays to Analyze Anti-Spike, Anti-RBD, and Anti-BIP Human Antibodies

Nunc Maxisorp polystyrene plates were coated with Spike protein or RBD at 1 µg/mL in PBS pH 7.4 (50 µL/well) overnight at 4°C; peptide BIP was coated at 2 µg/mL in Carbonate buffer, pH 9.6; 20-mers P11-P16 at 10 µg/mL in PBS, pH 7.4. After blocking for 1 hour at RT with PBS pH 7.4, BSA 3 % (A4503 - Merck KGaA, Darmstadt, Germany), sera diluted 1/100 in PBS pH 7.4, BSA 1 %, Tween-20 0,05 % were incubated on the plate (50 µL/well) for 2 hours at RT. After 3 washings with PBS Tween-20 0,05 % (150 µL/well), goat anti-human IgG HRP (A0293 - Merck) diluted 1:5000 in PBS BSA 1 % Tween-20 0,05 % was added to the plates at 50 µL/well and incubated for 2 hours. For IgM and IgA determination, goat anti-human IgM HRP conjugated (A0420 – Merck) or goat anti-human IgA HRP conjugate (A0295 - Merck) diluted 1:20000 in PBS, BSA 1 %, Tween 0.05 % were added to the plates. After three

washings with PBS Tween-20, 0.05 %, enzymatic activity was measured at 450 nm after TMB addition (T4444 - Merck) and block by H_2SO_4 1M.

12.2.10 STATISTICAL ANALYSIS

Antibody titers were compared between mouse groups. A descriptive analysis was performed to evaluate differences in humoral immune responses within each group of mice. To compare the antibody response to each protein, Kruskal-Wallis was performed, followed by Dunn's multiple comparison test. Results of anti-S, anti RBD and anti-BIP antibodies were expressed as Odd Ratio (OR) of a positive internal control set at 1.0. A p value < 0.05 was considered statistically significant. Data were analyzed and plotted using GraphPad Prism software (version 5.01; GraphPad Software Inc, San Diego, California, USA).

13. CONCLUSIONS AND FURTHER DEVELOPMENT

The S protein, a large SARS-CoV-2 surface protein of about 1250 aa, which self-assembles in a homotrimer [214], was chosen as antigen for vaccine development by leading vaccine companies Pfizer and Moderna. Its RBD domain, that folds in the same stable 3D structure both as a part of the complete S protein and as a separate domain [215], is involved in the critical event of binding to the host ACE2 receptor and therefore it is target of neutralizing antibodies generated during a SARS-CoV-2 infection. It was shown that this monomeric domain of a smaller size (220 aa) represents another good candidate for the vaccine development [216]–[219]

The multiple vaccines currently approved worldwide are based on the full-length S protein, while using different technological platforms to present this antigen to the immune system of the host. Although most of them have displayed high protective efficacy, their efficacy and particularly the longevity of the antibody response and the virus neutralizing function, appear to be short lasting, demanding early boosting doses. In fact, within a period of less than one year, besides the two doses of a regular immunization schedule, at least a third booster dose is required to maintain a good protection level. Because of the wide virus propagation capacity, this scenario generates a significant logistic and economic global challenge. Therefore, alternative vaccine platforms are being envisioned. This PhD project's aim, as a part of an international scientific collaboration, was to search for smaller fragments of the S protein recognized by antibodies and suitable for production by the peptide synthesis technology, that may have similar or superior vaccine performances, as compared to the technologies currently applied. After analysis of the 3D structures of the S protein and of the RBD-ACE2 complex, the choice fell on a 72 residues segment (aa 436-507) of the RBD, called $RBM_{436-507}$ or BIP peptide. This sequence is conformationally constrained by a disulfide bond, is highly specific to SARS-CoV-2 and located within the RBD-ACE2 interface. Moreover, *in silico* studies predict the presence of multiple epitopes (B- and T cell epitopes) within this fragment [168].

According to Shrock *et al.* [197], COVID-19 patients produce antibodies to multiple sequences, such as S(412-431) and S(446-465), that overlap ACE2 contact residues, and S(432-451) and S(475-494), adjacent to critical residues contacted by ACE2; notably, all these sequences are contained within $RBM_{436-507}$. Moreover, after observations arising from a crystallographic study of the interaction between SARS-CoV-2 S protein and a neutralizing human antibody [198], a new series of short linear peptides were designed, as possible mimetic of a relevant conformational epitope. In the next future, conformational studies will be carried out on them, and their serological immune response will be evaluated.

A comparative analysis of the sero-reactivity and immunogenicity in rodents of the trimeric S protein, the RBD and its internal $RBM_{436-507}$ fragment (peptide BIP) was undertaken to

determine if the $RBM_{436-507}$ could represent a possible target of neutralizing antibodies with high specificity and affinity, which would represent an alternative path for developing a protective vaccine.
Sera from both humans and rodents allowed an extensive ELISA analysis on the reactivity of sera obtained from COVID-19 patients, and from immunized mice to compare the Ab response associated to the three antigens.
CD data suggest that BIP peptide can partially preserve the extended beta-conformation observed in the context of the native protein structure. However, anti-BIP antibody recognition is limited to only a fraction of pre-COVID-19 and COVID-19 donors. In COVID-19 patients, a polyclonal anti-BIP antibody response with IgM, IgG and IgA isotypes was detected in one third of the cases, in amounts correlated with the level of anti-RBD and anti-S antibodies.
The epitope mapping conducted on $RBM_{436-597}$, interestingly showed that different regions of BIP peptide display distinct reactivity, with the N-terminal portion of the fragment being more frequently recognized, thus this region may by exploited for further vaccine development.
In addition, peptide BIP is highly immunogenic in BALB/C mice, confirming that this sequence contains also T epitopes, as suggested by the analysis performed by Grifoni *et al.* [168]. Currently, reactivity studies, based on ELISA assays, of the anti-BIP mouse antibodies with its homologous peptide BIP, recombinant S and RBD proteins are still ongoing.

In conclusion, the comparative analysis of the immunological properties of the trimeric S protein, the RBD and its internal RBM fragment (peptide BIP) indicated that although the synthetic peptide has a reduced value of the sero-reactivity and immunogenicity in comparison to the S protein and the RBD, it still can be an alternative path for developing tools for the virus control, particularly vaccines. The basis for this potential is its small size, absence of the folding problems, easier incorporation in different multimeric carriers and benefits of the peptide synthesis production.

ABBREVIATIONS

Ac_2O: acetic anhydride
ACh: acetylcholine
ACN: acetonitrile
ACPs: antigen-presenting cells
ANOVA: analysis of variance
BCR: B-cell receptor
BIP: binding interface peptide
Boc: tertbutyloxycarbonyl
BOP: N-(Benzenesulfonyl)-L-prolyl-L-O-(1-pyrrolidinylcarbonyl)tyrosine sodium salt
BSA: bovine serum albumin
Bzl: benzyl
CD: circular dichroism
CD4+: cluster of differentiation 4
CD8+: cluster of differentiation 8
COX-2: cyclooxygenase-2
CTX: carboxyl-telopeptide
DCC: N,N'-dicyclohexylcarbodiimide
DCM: dichloromethane
DCU: dicyclohexylurea
DIC: N,N'-diisopropylcarbodiimide
DIPEA: N,N-Diisopropylethylamine
DLS: dynamic light scattering
DMEM: Dulbecco's modified minimum essential medium
DMF: N,N-Dimethylformamide
DODT: 2,2'-(ethylenedioxy)diethanethiol
ECM: extracellular matrix
EDT: ethane-1,2-dithiol
EGFR: epidermal growth factor receptor
ELISA: enzime linked immunosorbent assay
ELS: electrophoretic light scattering
FACIT: fibril-associated collagens with interrupted triple helices
FBS: fetal bovine serum
FDA: food and drug administration
Fmoc: 9-fluorenylmethoxycarbonyl
GAPDH: glyceraldehyde-3-phosphate dehydrogenase
hACE2: human angiotensin converting enzyme 2
HATU: 1-[Bis(dimethylamino)methylene]-1H-1,2,3-triazolo[4,5-b]pyridinium 3-oxide hexafluorophosphate
HBTU: *N,N,N',N'*-Tetramethyl-*O*-(1*H*-benzotriazol-1-yl)uronium hexafluorophosphate
HCoV: human Coronavirus
HEPES: (4-(2-hydroxyethyl)-1-piperazineethanesulfonic acid)
HF: hydrofluoric acid
HPLC: high performance liquid chromatography

IGF: insulin-like growth factor I
ISTD: internal standard
MEM: minimum essential medium
MERS-CoV: middle eastern respiratory syndrome Coronavirus
MHC: histocompatibility complex
MMPs: matrix metalloproteinases
MoA: mechanism of action
MPLC: medium pressure liquid chromatography
MW-SPPS: microwave-assisted solid phase peptide synthesis
MW: multi-well
NC domain: non-collagenous domain
neo-NHDFs: neonatal normal human dermal fibroblasts
NHS: normal heathy sera
NMM: 4-Methylmorpholine
NTD: N-terminal domain
NTX: ammino-telopeptide
o.n.: overnight
OBt: hydroxybenzotriazole
OPfp: pentafluorophenyl
OR: Odd ratio
p-NPP: para-nitrophenyl phosphate substrate
PAI-1: plasminogen activator inhibitor
pam / pal: palmitoyl
PBS: phosphate buffer saline
PD: peptidase domain
PDI: polydispersity index
PSA: preformed symmettical anhydrides
PyBOP: Benzotriazole-1-yl-oxy-tris-pyrrolidino-phosphonium hexafluorophosphate
RBD: receptor binding domain
RBM: receptor binding motif
RER: rough endoplasmic reticulum
RIPA: radio-immunoprecipitation assay
RNP: ribonucleoprotein complex
RP: reverse-phase
Rpm: revolutions *per* minute
RPMI: Roswell park memorial institute
RT: room temperature
RT: room temperature
s.c.: sub cutaneous
SARS-CoV: severe acute respiratory syndrome Coronavirus
SASP: senescence-associated secretory phenotype
SE: standard error
SLRPs: small leucine-rich repeat proteoglycans
SNAP: synaptosome-associated protein
SNARE: soluble N-ethylmaleimide-sensitive factor activating protein receptor
SP-ELISA: solid phase - enzyme-linked immunosorbent assay
SP: signal peptide
SPPS: solid phase peptide synthesis

SPs: serine proteinases
TBTU: 2-(1H-Benzotriazole-1-yl)-1,1,3,3-tetramethylaminium tetrafluoroborate
tBu: tert butyl
TFA: trifluoroacetic acid
TGF-β1: transforming growth factor
TIMPs: tissue inhibitors of metalloproteinases
TIS: triisopropyl silane
TNF-α: tumor necrosis factor alpha
TNF-α: tumor necrosis factor-α
u-PA: urokinase-type plasminogen activator
UHPLC: ultra-high performance liquid chromatography
v/v: volume to volume
VAMP: vesicle-associated membrane protein
vol: volume (1 vol = 1 mL/g)
w/o: without
WB: western blot
yo: years old

REFERENCES

[1] R. C. Fuhlbrigge and R. Chaiban, 'The Immune System, the Skin, and Childhood Rheumatic Disease', *Curr. Rheumatol. Rep.*, vol. 13, no. 2, pp. 103–109, Apr. 2011, doi: 10.1007/s11926-010-0158-2.
[2] S. J. de Veer, L. Furio, J. M. Harris, and A. Hovnanian, 'Proteases: common culprits in human skin disorders', *Trends Mol. Med.*, vol. 20, no. 3, pp. 166–178, Mar. 2014, doi: 10.1016/j.molmed.2013.11.005.
[3] 'Harper's illustrated biochemistry'. Lange Medical Books/McGraw-Hill, Estados Unidos, 2009.
[4] K. Gelse, 'Collagens—structure, function, and biosynthesis', *Adv. Drug Deliv. Rev.*, vol. 55, no. 12, pp. 1531–1546, Nov. 2003, doi: 10.1016/j.addr.2003.08.002.
[5] V. R. Sherman, W. Yang, and M. A. Meyers, 'The materials science of collagen', *J. Mech. Behav. Biomed. Mater.*, vol. 52, pp. 22–50, Dec. 2015, doi: 10.1016/j.jmbbm.2015.05.023.
[6] S. Ricard-Blum, 'The Collagen Family', *Cold Spring Harb. Perspect. Biol.*, vol. 3, no. 1, pp. a004978–a004978, Jan. 2011, doi: 10.1101/cshperspect.a004978.
[7] J. Parvizi and G. K. Kim, 'Collagen', in *High Yield Orthopaedics*, Elsevier, 2010, pp. 107–109. doi: 10.1016/B978-1-4160-0236-9.00064-X.
[8] J. A. Fallas, V. Gauba, and J. D. Hartgerink, 'Solution Structure of an ABC Collagen Heterotrimer Reveals a Single-register Helix Stabilized by Electrostatic Interactions', *J. Biol. Chem.*, vol. 284, no. 39, pp. 26851–26859, Sep. 2009, doi: 10.1074/jbc.M109.014753.
[9] A. V. Persikov, J. A. M. Ramshaw, A. Kirkpatrick, and B. Brodsky, 'Electrostatic Interactions Involving Lysine Make Major Contributions to Collagen Triple-Helix Stability', *Biochemistry*, vol. 44, no. 5, pp. 1414–1422, Feb. 2005, doi: 10.1021/bi048216r.
[10] K. E. Kadler, C. Baldock, J. Bella, and R. P. Boot-Handford, 'Collagens at a glance', *J. Cell Sci.*, vol. 120, no. 12, pp. 1955–1958, Jun. 2007, doi: 10.1242/jcs.03453.
[11] Y. M. Michelacci, 'Collagens and proteoglycans of the corneal extracellular matrix', *Braz. J. Med. Biol. Res.*, vol. 36, no. 8, pp. 1037–1046, Aug. 2003, doi: 10.1590/S0100-879X2003000800009.
[12] H. Johansson *et al.*, 'A Meta-Analysis of Reference Markers of Bone Turnover for Prediction of Fracture', *Calcif. Tissue Int.*, vol. 94, no. 5, pp. 560–567, May 2014, doi: 10.1007/s00223-014-9842-y.
[13] C. Rosenquist *et al.*, 'Serum CrossLaps One Step ELISA. First application of monoclonal antibodies for measurement in serum of bone-related degradation products from C-terminal telopeptides of type I collagen', *Clin. Chem.*, vol. 44, no. 11, pp. 2281–2289, Nov. 1998, doi: 10.1093/clinchem/44.11.2281.
[14] D. J. S. Hulmes, 'Building Collagen Molecules, Fibrils, and Suprafibrillar Structures', *J. Struct. Biol.*, vol. 137, no. 1–2, pp. 2–10, Jan. 2002, doi: 10.1006/jsbi.2002.4450.
[15] K. E. Kadler, D. F. Holmes, J. A. Trotter, and J. A. Chapman, 'Collagen fibril formation', *Biochem. J.*, vol. 316, no. 1, pp. 1–11, May 1996, doi: 10.1042/bj3160001.
[16] J. Zhu, C. L. Hoop, D. A. Case, and J. Baum, 'Cryptic binding sites become accessible through surface reconstruction of the type I collagen fibril', *Sci. Rep.*, vol. 8, no. 1, p. 16646, Dec. 2018, doi: 10.1038/s41598-018-34616-z.
[17] J. K. Mouw, G. Ou, and V. M. Weaver, 'Extracellular matrix assembly: a multiscale deconstruction', *Nat. Rev. Mol. Cell Biol.*, vol. 15, no. 12, pp. 771–785, Dec. 2014, doi: 10.1038/nrm3902.
[18] V. H. Rao *et al.*, 'Transcriptional regulation of MMP-9 expression in stromal cells of human giant cell tumor of bone by tumor necrosis factor-alpha.', *Int. J. Oncol.*, Feb. 1999, doi: 10.3892/ijo.14.2.291.

[19] R. Nigdelioglu *et al.*, 'Transforming Growth Factor (TGF)-β Promotes de Novo Serine Synthesis for Collagen Production', *J. Biol. Chem.*, vol. 291, no. 53, pp. 27239–27251, Dec. 2016, doi: 10.1074/jbc.M116.756247.
[20] C. Frantz, K. M. Stewart, and V. M. Weaver, 'The extracellular matrix at a glance', *J. Cell Sci.*, vol. 123, no. 24, pp. 4195–4200, Dec. 2010, doi: 10.1242/jcs.023820.
[21] S. N. Kehlet *et al.*, 'Age-related collagen turnover of the interstitial matrix and basement membrane: Implications of age- and sex-dependent remodeling of the extracellular matrix', *PLOS ONE*, vol. 13, no. 3, p. e0194458, Mar. 2018, doi: 10.1371/journal.pone.0194458.
[22] M. Egeblad, M. G. Rasch, and V. M. Weaver, 'Dynamic interplay between the collagen scaffold and tumor evolution', *Curr. Opin. Cell Biol.*, vol. 22, no. 5, pp. 697–706, Oct. 2010, doi: 10.1016/j.ceb.2010.08.015.
[23] L. Kass, J. T. Erler, M. Dembo, and V. M. Weaver, 'Mammary epithelial cell: Influence of extracellular matrix composition and organization during development and tumorigenesis', *Int. J. Biochem. Cell Biol.*, vol. 39, no. 11, pp. 1987–1994, 2007, doi: 10.1016/j.biocel.2007.06.025.
[24] J. Varani, P. Perone, S. E. G. Fligiel, G. J. Fisher, and J. J. Voorhees, 'Inhibition of Type I Procollagen Production in Photodamage: Correlation Between Presence of High Molecular Weight Collagen Fragments and Reduced Procollagen Synthesis', *J. Invest. Dermatol.*, vol. 119, no. 1, pp. 122–129, Jul. 2002, doi: 10.1046/j.1523-1747.2002.01810.x.
[25] J. D. Mott and Z. Werb, 'Regulation of matrix biology by matrix metalloproteinases', *Curr. Opin. Cell Biol.*, vol. 16, no. 5, pp. 558–564, Oct. 2004, doi: 10.1016/j.ceb.2004.07.010.
[26] A. R. Khan and M. N. G. James, 'Molecular mechanisms for the conversion of zymogens to active proteolytic enzymes: Zymogens activation', *Protein Sci.*, vol. 7, no. 4, pp. 815–836, Apr. 1998, doi: 10.1002/pro.5560070401.
[27] J. A. Martignetti *et al.*, 'Mutation of the matrix metalloproteinase 2 gene (MMP2) causes a multicentric osteolysis and arthritis syndrome', *Nat. Genet.*, vol. 28, no. 3, pp. 261–265, Jul. 2001, doi: 10.1038/90100.
[28] R. Chiusaroli *et al.*, 'Collagenase Cleavage of Type I Collagen Is Essential for Both Basal and Parathyroid Hormone (PTH)/PTH-Related Peptide Receptor-Induced Osteoclast Activation and Has Differential Effects on Discrete Bone Compartments', *Endocrinology*, vol. 144, no. 9, pp. 4106–4116, Sep. 2003, doi: 10.1210/en.2003-0254.
[29] A. H. M. Beare, S. O'Kane, M. W. J. Ferguson, and S. M. Krane, 'Severely Impaired Wound Healing in the Collagenase-Resistant Mouse', *J. Invest. Dermatol.*, vol. 120, no. 1, pp. 153–163, Jan. 2003, doi: 10.1046/j.1523-1747.2003.12019.x.
[30] M. L. Lindsey *et al.*, 'Effect of a Cleavage-Resistant Collagen Mutation on Left Ventricular Remodeling', *Circ. Res.*, vol. 93, no. 3, pp. 238–245, Aug. 2003, doi: 10.1161/01.RES.0000085580.45279.60.
[31] H. Nagase, R. Visse, and G. Murphy, 'Structure and function of matrix metalloproteinases and TIMPs', *Cardiovasc. Res.*, vol. 69, no. 3, pp. 562–573, Feb. 2006, doi: 10.1016/j.cardiores.2005.12.002.
[32] H. Laronha and J. Caldeira, 'Structure and Function of Human Matrix Metalloproteinases', *Cells*, vol. 9, no. 5, p. 1076, Apr. 2020, doi: 10.3390/cells9051076.
[33] T. Fischer, N. Senn, and R. Riedl, 'Design and Structural Evolution of Matrix Metalloproteinase Inhibitors', *Chem. – Eur. J.*, vol. 25, no. 34, pp. 7960–7980, Jun. 2019, doi: 10.1002/chem.201805361.
[34] D. R. Yager and B. C. Nwomeh, 'The proteolytic environment of chronic wounds', *Wound Repair Regen.*, vol. 7, no. 6, pp. 433–441, Nov. 1999, doi: 10.1046/j.1524-475X.1999.00433.x.
[35] C. López-Otín and L. M. Matrisian, 'Emerging roles of proteases in tumour suppression', *Nat. Rev. Cancer*, vol. 7, no. 10, pp. 800–808, Oct. 2007, doi: 10.1038/nrc2228.
[36] B. Breznik, H. Motaln, and T. Lah Turnšek, 'Proteases and cytokines as mediators of interactions between cancer and stromal cells in tumours', *Biol. Chem.*, vol. 398, no. 7, pp. 709–719, Jun. 2017, doi: 10.1515/hsz-2016-0283.

[37] L. Hedstrom, ‘Serine Protease Mechanism and Specificity’, *Chem. Rev.*, vol. 102, no. 12, pp. 4501–4524, Dec. 2002, doi: 10.1021/cr000033x.
[38] E. Di Cera, ‘Serine proteases’, *IUBMB Life*, vol. 61, no. 5, pp. 510–515, May 2009, doi: 10.1002/iub.186.
[39] S. Patel, ‘A critical review on serine protease: Key immune manipulator and pathology mediator’, *Allergol. Immunopathol. (Madr.)*, vol. 45, no. 6, pp. 579–591, Nov. 2017, doi: 10.1016/j.aller.2016.10.011.
[40] C. J. Farady and C. S. Craik, ‘Mechanisms of Macromolecular Protease Inhibitors’, *ChemBioChem*, vol. 11, no. 17, pp. 2341–2346, Nov. 2010, doi: 10.1002/cbic.201000442.
[41] W. Sanrattana, C. Maas, and S. de Maat, ‘SERPINs—From Trap to Treatment’, *Front. Med.*, vol. 6, p. 25, Feb. 2019, doi: 10.3389/fmed.2019.00025.
[42] F. Raynaud, B. Bauvois, P. Gerbaud, and D. Evain-Brion, ‘Characterization of specific proteases associated with the surface of human skin fibroblasts, and their modulation in pathology’, *J. Cell. Physiol.*, vol. 151, no. 2, pp. 378–385, May 1992, doi: 10.1002/jcp.1041510219.
[43] A. V. Rawlings and R. Voegeli, ‘Stratum corneum proteases and dry skin conditions’, *Cell Tissue Res.*, vol. 351, no. 2, pp. 217–235, Feb. 2013, doi: 10.1007/s00441-012-1501-x.
[44] R. Voegeli, A. V. Rawlings, M. Breternitz, S. Doppler, T. Schreier, and J. W. Fluhr, ‘Increased stratum corneum serine protease activity in acute eczematous atopic skin’, *Br. J. Dermatol.*, vol. 161, no. 1, pp. 70–77, Jul. 2009, doi: 10.1111/j.1365-2133.2009.09142.x.
[45] C. P. Wild, ‘Complementing the Genome with an “Exposome”: The Outstanding Challenge of Environmental Exposure Measurement in Molecular Epidemiology’, *Cancer Epidemiol. Biomarkers Prev.*, vol. 14, no. 8, pp. 1847–1850, Aug. 2005, doi: 10.1158/1055-9965.EPI-05-0456.
[46] C. P. Wild, ‘The exposome: from concept to utility’, *Int. J. Epidemiol.*, vol. 41, no. 1, pp. 24–32, Feb. 2012, doi: 10.1093/ije/dyr236.
[47] J. Varani *et al.*, ‘Decreased Collagen Production in Chronologically Aged Skin’, *Am. J. Pathol.*, vol. 168, no. 6, pp. 1861–1868, Jun. 2006, doi: 10.2353/ajpath.2006.051302.
[48] C. Marionnet, C. Tricaud, and F. Bernerd, ‘Exposure to Non-Extreme Solar UV Daylight: Spectral Characterization, Effects on Skin and Photoprotection’, *Int. J. Mol. Sci.*, vol. 16, no. 1, pp. 68–90, Dec. 2014, doi: 10.3390/ijms16010068.
[49] J. H. Chung *et al.*, ‘Modulation of Skin Collagen Metabolism in Aged and Photoaged Human Skin In Vivo’, *J. Invest. Dermatol.*, vol. 117, no. 5, pp. 1218–1224, Nov. 2001, doi: 10.1046/j.0022-202x.2001.01544.x.
[50] Y. R. Helfrich, D. L. Sachs, and J. J. Voorhees, ‘Overview of skin aging and photoaging’, *Dermatol. Nurs.*, vol. 20, no. 3, pp. 177–183; quiz 184, Jun. 2008.
[51] J. M. Denu and K. G. Tanner, ‘Specific and Reversible Inactivation of Protein Tyrosine Phosphatases by Hydrogen Peroxide: Evidence for a Sulfenic Acid Intermediate and Implications for Redox Regulation’, *Biochemistry*, vol. 37, no. 16, pp. 5633–5642, Apr. 1998, doi: 10.1021/bi973035t.
[52] R. Ganceviciene, A. I. Liakou, A. Theodoridis, E. Makrantonaki, and C. C. Zouboulis, ‘Skin anti-aging strategies’, *Dermatoendocrinol.*, vol. 4, no. 3, pp. 308–319, Jul. 2012, doi: 10.4161/derm.22804.
[53] G. J. Fisher *et al.*, ‘c-Jun–dependent inhibition of cutaneous procollagen transcription following ultraviolet irradiation is reversed by all-trans retinoic acid’, *J. Clin. Invest.*, vol. 106, no. 5, pp. 663–670, Sep. 2000, doi: 10.1172/JCI9362.
[54] M. Cavinato *et al.*, ‘UVB-Induced Senescence of Human Dermal Fibroblasts Involves Impairment of Proteasome and Enhanced Autophagic Activity’, *J. Gerontol. A. Biol. Sci. Med. Sci.*, p. glw150, Aug. 2016, doi: 10.1093/gerona/glw150.
[55] M. Cavinato and P. Jansen-Dürr, ‘Molecular mechanisms of UVB-induced senescence of dermal fibroblasts and its relevance for photoaging of the human skin’, *Exp. Gerontol.*, vol. 94, pp. 78–82, Aug. 2017, doi: 10.1016/j.exger.2017.01.009.
[56] B. G. Childs *et al.*, ‘Senescent cells: an emerging target for diseases of ageing’, *Nat. Rev.*

Drug Discov., vol. 16, no. 10, pp. 718–735, Oct. 2017, doi: 10.1038/nrd.2017.116.
[57] M. C. A. Issa, *Daily routine in cosmetic dermatology*. New York, NY: Springer Science+Business Media, 2017.
[58] A. M. Kligman, G. L. Grove, R. Hirose, and J. J. Leyden, 'Topical tretinoin for photoaged skin', *J. Am. Acad. Dermatol.*, vol. 15, no. 4, pp. 836–859, Oct. 1986, doi: 10.1016/S0190-9622(86)70242-9.
[59] D. Kligman, 'Cosmeceuticals', *Dermatol. Clin.*, vol. 18, no. 4, pp. 609–615, Oct. 2000, doi: 10.1016/S0733-8635(05)70211-4.
[60] C. M. Choi and D. S. Berson, 'Cosmeceuticals', *Semin. Cutan. Med. Surg.*, vol. 25, no. 3, pp. 163–168, Sep. 2006, doi: 10.1016/j.sder.2006.06.010.
[61] S. Manfredini and S. Vertuani, *Prodotti cosmetici a connotazione naturale e sostenibile*. Roma: ARACNE ed., 2022.
[62] Z. D. Draelos, 'The cosmeceutical realm', *Clin. Dermatol.*, vol. 26, no. 6, pp. 627–632, Nov. 2008, doi: 10.1016/j.clindermatol.2007.09.005.
[63] H. Dureja, D. Kaushik, M. Gupta, V. Kumar, and V. Lather, 'Cosmeceuticals: An emerging concept', *Indian J. Pharmacol.*, vol. 37, no. 3, p. 155, 2005, doi: 10.4103/0253-7613.16211.
[64] K. A. Walters and M. S. Roberts, Eds., *Dermatologic, Cosmeceutic, and Cosmetic Development*, 0 ed. CRC Press, 2007. doi: 10.3109/9780849375903.
[65] L. Pickart and M. M. Thaler, 'Tripeptide in human serum which prolongs survival of normal liver cells and stimulates growth in neoplastic liver', *Nature. New Biol.*, vol. 243, no. 124, pp. 85–87, May 1973.
[66] Z. D. Draelos, 'Cosmeceuticals', *Dermatol. Clin.*, vol. 32, no. 2, pp. 137–143, Apr. 2014, doi: 10.1016/j.det.2013.12.002.
[67] J. Juan, I. Marlen, and C. Luisa, 'Chemical and Physical Enhancers for Transdermal Drug Delivery', in *Pharmacology*, L. Gallelli, Ed. InTech, 2012. doi: 10.5772/33194.
[68] J. Juan Escobar-Chavez and V. Merino, Eds., *Current Technologies To Increase The Transdermal Delivery Of Drugs*. BENTHAM SCIENCE PUBLISHERS, 2012. doi: 10.2174/97816080519151100101.
[69] J. Renukuntla, A. D. Vadlapudi, A. Patel, S. H. S. Boddu, and A. K. Mitra, 'Approaches for enhancing oral bioavailability of peptides and proteins', *Int. J. Pharm.*, vol. 447, no. 1–2, pp. 75–93, Apr. 2013, doi: 10.1016/j.ijpharm.2013.02.030.
[70] B. Wang, N. Xie, and B. Li, 'Influence of peptide characteristics on their stability, intestinal transport, and in vitro bioavailability: A review', *J. Food Biochem.*, vol. 43, no. 1, p. e12571, Jan. 2019, doi: 10.1111/jfbc.12571.
[71] P. Ledwoń, F. Errante, A. M. Papini, P. Rovero, and R. Latajka, 'Peptides as Active Ingredients: A Challenge for Cosmeceutical Industry', *Chem. Biodivers.*, vol. 18, no. 2, Feb. 2021, doi: 10.1002/cbdv.202000833.
[72] F. Errante, P. Ledwoń, R. Latajka, P. Rovero, and A. M. Papini, 'Cosmeceutical Peptides in the Framework of Sustainable Wellness Economy', *Front. Chem.*, vol. 8, p. 572923, Oct. 2020, doi: 10.3389/fchem.2020.572923.
[73] T. Lima and Carla Pedriali Moraes, 'Bioactive Peptides: Applications and Relevance for Cosmeceuticals', *Cosmetics*, vol. 5, no. 1, p. 21, Mar. 2018, doi: 10.3390/cosmetics5010021.
[74] S. Schagen, 'Topical Peptide Treatments with Effective Anti-Aging Results', *Cosmetics*, vol. 4, no. 2, p. 16, May 2017, doi: 10.3390/cosmetics4020016.
[75] M. P. Lupo and A. L. Cole, 'Cosmeceutical peptides: Cosmeceutical peptides', *Dermatol. Ther.*, vol. 20, no. 5, pp. 343–349, Nov. 2007, doi: 10.1111/j.1529-8019.2007.00148.x.
[76] H. Husein el Hadmed and R. F. Castillo, 'Cosmeceuticals: peptides, proteins, and growth factors', *J. Cosmet. Dermatol.*, vol. 15, no. 4, pp. 514–519, Dec. 2016, doi: 10.1111/jocd.12229.
[77] C. Blanes-Mira *et al.*, 'A synthetic hexapeptide (Argireline) with antiwrinkle activity', *Int. J. Cosmet. Sci.*, vol. 24, no. 5, pp. 303–310, Oct. 2002, doi: 10.1046/j.1467-2494.2002.00153.x.
[78] Y. Yamaguchi, K. Hosokawa, Y. Nakatani, S. Sano, K. Yoshikawa, and S. Itami, 'Gastrin-

Releasing Peptide, a Bombesin-like Neuropeptide, Promotes Cutaneous Wound Healing', *Dermatol. Surg.*, vol. 28, no. 4, pp. 314–319, Apr. 2002, doi: 10.1046/j.1524-4725.2002.99279.x.
[79] S. Pascarella *et al.*, 'Serpin A1 C-Terminal Peptides as Collagen Turnover Modulators', *ChemMedChem*, vol. 11, no. 16, pp. 1850–1855, Aug. 2016, doi: 10.1002/cmdc.201500472.
[80] C. Cipriani *et al.*, 'Serpin A1 and the modulation of type I collagen turnover: Effect of the C-terminal peptide 409-418 (SA1-III) in human dermal fibroblasts: Serpin-A1 C-terminal modulates collagen levels', *Cell Biol. Int.*, vol. 42, no. 10, pp. 1340–1348, Sep. 2018, doi: 10.1002/cbin.11018.
[81] P. G. W. Gettins, 'Serpin Structure, Mechanism, and Function', *Chem. Rev.*, vol. 102, no. 12, pp. 4751–4804, Dec. 2002, doi: 10.1021/cr010170+.
[82] S. Chotirmall, M. Al-Alawi, T. McEnery, and N. G. McElvaney, 'Alpha-1 proteinase inhibitors for the treatment of alpha-1 antitrypsin deficiency: safety, tolerability, and patient outcomes', *Ther. Clin. Risk Manag.*, p. 143, Jan. 2015, doi: 10.2147/TCRM.S51474.
[83] W. C. Groutas, D. Dou, and K. R. Alliston, 'Neutrophil elastase inhibitors', *Expert Opin. Ther. Pat.*, vol. 21, no. 3, pp. 339–354, Mar. 2011, doi: 10.1517/13543776.2011.551115.
[84] L. F. Congote, 'The C-terminal 26-residue peptide of serpin A1 is an inhibitor of HIV-1', *Biochem. Biophys. Res. Commun.*, vol. 343, no. 2, pp. 617–622, May 2006, doi: 10.1016/j.bbrc.2006.02.190.
[85] L. F. Congote and N. Temmel, 'The C-terminal 26-residue peptide of serpin A1 stimulates proliferation of breast and liver cancer cells: role of protein kinase C and CD47', *FEBS Lett.*, vol. 576, no. 3, pp. 343–347, Oct. 2004, doi: 10.1016/j.febslet.2004.09.035.
[86] C. N. Rao, D. A. Ladin, K. Chilukuri, D. T. Woodley, Y. Y. Liu, and Z. Z. Hou, 'α1-Antitrypsin Is Degraded and Non-Functional in Chronic Wounds But Intact and Functional in Acute Wounds: The Inhibitor Protects Fibronectin from Degradation by Chronic Wound Fluid Enzymes', *J. Invest. Dermatol.*, vol. 105, no. 4, pp. 572–578, Oct. 1995, doi: 10.1111/1523-1747.ep12323503.
[87] T. Bjarnsholt *et al.*, 'Why chronic wounds will not heal: a novel hypothesis', *Wound Repair Regen.*, vol. 16, no. 1, pp. 2–10, Jan. 2008, doi: 10.1111/j.1524-475X.2007.00283.x.
[88] M. Fumakia and E. A. Ho, 'Nanoparticles Encapsulated with LL37 and Serpin A1 Promotes Wound Healing and Synergistically Enhances Antibacterial Activity', *Mol. Pharm.*, vol. 13, no. 7, pp. 2318–2331, Jul. 2016, doi: 10.1021/acs.molpharmaceut.6b00099.
[89] F. Grinnell and M. Zhu, 'Identification of Neutrophil Elastase as the Proteinase in Burn Wound Fluid Responsible for Degradation of Fibronectin', *J. Invest. Dermatol.*, vol. 103, no. 2, pp. 155–161, Aug. 1994, doi: 10.1111/1523-1747.ep12392625.
[90] L. F. Congote, N. Temmel, G. Sadvakassova, and M. C. Dobocan, 'Comparison of the effects of serpin A1, a recombinant serpin A1-IGF chimera and serpin A1 C-terminal peptide on wound healing', *Peptides*, vol. 29, no. 1, pp. 39–46, Jan. 2008, doi: 10.1016/j.peptides.2007.10.011.
[91] M. Cathomas, A. Schüller, D. Candinas, and R. Inglin, 'Severe postoperative wound healing disturbance in a patient with alpha-1-antitrypsin deficiency: the impact of augmentation therapy: Wound healing disturbance in a patient with alpha-1-antitrypsin deficiency', *Int. Wound J.*, vol. 12, no. 5, pp. 601–604, Oct. 2015, doi: 10.1111/iwj.12419.
[92] J. D. Bos and M. M. H. M. Meinardi, 'The 500 Dalton rule for the skin penetration of chemical compounds and drugs: The 500 Dalton rule for skin penetration of chemical compounds and drugs', *Exp. Dermatol.*, vol. 9, no. 3, pp. 165–169, Jun. 2000, doi: 10.1034/j.1600-0625.2000.009003165.x.
[93] G. Joslin, R. J. Fallon, J. Bullock, S. P. Adams, and D. H. Perlmutter, 'The SEC receptor recognizes a pentapeptide neodomain of alpha 1-antitrypsin-protease complexes', *J. Biol. Chem.*, vol. 266, no. 17, pp. 11282–11288, Jun. 1991.
[94] R. A. Ignotz, T. Endo, and J. Massagué, 'Regulation of fibronectin and type I collagen mRNA levels by transforming growth factor-beta.', *J. Biol. Chem.*, vol. 262, no. 14, pp. 6443–6446, May 1987, doi: 10.1016/S0021-9258(18)48258-0.
[95] B. L. Lyons and R. I. Schwarz, 'Ascorbate stimulation of PAT cells causes an increase in

transcription rates and a decrease in degradation rates of procollagen mRNA', *Nucleic Acids Res.*, vol. 12, no. 5, pp. 2569–2579, 1984, doi: 10.1093/nar/12.5.2569.
[96] J. K. Nguyen, N. Masub, and J. Jagdeo, 'Bioactive ingredients in Korean cosmeceuticals: Trends and research evidence', *J. Cosmet. Dermatol.*, p. jocd.13344, Feb. 2020, doi: 10.1111/jocd.13344.
[97] V. Pai, P. Bhandari, and P. Shukla, 'Topical peptides as cosmeceuticals', *Indian J. Dermatol. Venereol. Leprol.*, vol. 83, no. 1, p. 9, 2017, doi: 10.4103/0378-6323.186500.
[98] S. A. Nasrollahi, C. Taghibiglou, E. Azizi, and E. S. Farboud, 'Cell-penetrating Peptides as a Novel Transdermal Drug Delivery System: Transdermal Drug Targeting', *Chem. Biol. Drug Des.*, vol. 80, no. 5, pp. 639–646, Nov. 2012, doi: 10.1111/cbdd.12008.
[99] F. Errante, L. Giovannelli, A. M. Papini, and P. Rovero, 'Peptidi bioattivi e composizioni che li comprendono', 102019000008364
[100] F. Errante *et al.*, 'Susceptibility of cosmeceutical peptides to proteases activity: Development of dermal stability test by LC-MS/MS analysis', *J. Pharm. Biomed. Anal.*, vol. 194, p. 113775, Feb. 2021, doi: 10.1016/j.jpba.2020.113775.
[101] O. Fischer, 'Ueber Benz- und Napht-Imidazole', *Berichte Dtsch. Chem. Ges.*, vol. 34, no. 1, pp. 930–940, Jan. 1901, doi: 10.1002/cber.190103401159.
[102] M. Bergmann and L. Zervas, 'Über ein allgemeines Verfahren der Peptid-Synthese', *Berichte Dtsch. Chem. Ges. B Ser.*, vol. 65, no. 7, pp. 1192–1201, Jul. 1932, doi: 10.1002/cber.19320650722.
[103] V. du Vigneaud, C. Ressler, J. M. Swan, C. W. Roberts, and P. G. Katsoyannis, 'The Synthesis of Oxytocin 1', *J. Am. Chem. Soc.*, vol. 76, no. 12, pp. 3115–3121, Jun. 1954, doi: 10.1021/ja01641a004.
[104] A. D'Ercole *et al.*, 'An Optimized Safe Process from Bench to Pilot cGMP Production of API Eptifibatide Using a Multigram-Scale Microwave-Assisted Solid-Phase Peptide Synthesizer', *Org. Process Res. Dev.*, vol. 25, no. 12, pp. 2754–2771, Dec. 2021, doi: 10.1021/acs.oprd.1c00368.
[105] G. Sabatino *et al.*, 'An Optimized Scalable Fully Automated Solid-Phase Microwave-Assisted cGMP-Ready Process for the Preparation of Eptifibatide', *Org. Process Res. Dev.*, vol. 25, no. 3, pp. 552–563, Mar. 2021, doi: 10.1021/acs.oprd.0c00490.
[106] R. B. Merrifield, 'Solid Phase Peptide Synthesis. I. The Synthesis of a Tetrapeptide', *J. Am. Chem. Soc.*, vol. 85, no. 14, pp. 2149–2154, Jul. 1963, doi: 10.1021/ja00897a025.
[107] R. B. Merrifield, J. Morrow. Stewart, and Nils. Jernberg, 'Instrument for automated synthesis of peptides', *Anal. Chem.*, vol. 38, no. 13, pp. 1905–1914, Dec. 1966, doi: 10.1021/ac50155a057.
[108] R. B. Merrifield, 'New Approaches to the Chemical Synthesis of Peptides', in *Proceedings of the 1966 Laurentian Hormone Conference*, Elsevier, 1967, pp. 451–482. doi: 10.1016/B978-1-4831-9826-2.50013-1.
[109] S. Sakakibara, Y. Shimonishi, Y. Kishida, M. Okada, and H. Sugihara, 'Use of Anhydrous Hydrogen Fluoride in Peptide Synthesis. I. Behavior of Various Protective Groups in Anhydrous Hydrogen Fluoride', *Bull. Chem. Soc. Jpn.*, vol. 40, no. 9, pp. 2164–2167, Sep. 1967, doi: 10.1246/bcsj.40.2164.
[110] L. A. Carpino and G. Y. Han, '9-Fluorenylmethoxycarbonyl function, a new base-sensitive amino-protecting group', *J. Am. Chem. Soc.*, vol. 92, no. 19, pp. 5748–5749, Sep. 1970, doi: 10.1021/ja00722a043.
[111] Y. Yang, *Side Reactions in Peptide Synthesis*. Elsevier, 2016. doi: 10.1016/C2013-0-13700-2.
[112] H. M. Yu, S. T. Chen, and K. T. Wang, 'Enhanced coupling efficiency in solid-phase peptide synthesis by microwave irradiation', *J. Org. Chem.*, vol. 57, no. 18, pp. 4781–4784, Aug. 1992, doi: 10.1021/jo00044a001.
[113] F. Rizzolo, G. Sabatino, M. Chelli, P. Rovero, and A. M. Papini, 'A Convenient Microwave-Enhanced Solid-Phase Synthesis of Difficult Peptide Sequences: Case Study of

Gramicidin A and CSF114(Glc)', *Int. J. Pept. Res. Ther.*, vol. 13, no. 1–2, pp. 203–208, Jun. 2007, doi: 10.1007/s10989-006-9066-8.
[114] B. M. Dunn, Ed., *Peptide Chemistry and Drug Design*. Hoboken, NJ, USA: John Wiley & Sons, Inc, 2015. doi: 10.1002/9781118995303.
[115] J. C. Sheehan and G. P. Hess, 'A New Method of Forming Peptide Bonds', *J. Am. Chem. Soc.*, vol. 77, no. 4, pp. 1067–1068, Feb. 1955, doi: 10.1021/ja01609a099.
[116] F. Albeiicio, R. Chinchilla, D. J. Dodsworth, and C. Nájera, 'NEW TRENDS IN PEPTIDE COUPLING REAGENTS', *Org. Prep. Proced. Int.*, vol. 33, no. 3, pp. 203–303, Jun. 2001, doi: 10.1080/00304940109356592.
[117] R. Subirós-Funosas, R. Prohens, R. Barbas, A. El-Faham, and F. Albericio, 'Oxyma: An Efficient Additive for Peptide Synthesis to Replace the Benzotriazole-Based HOBt and HOAt with a Lower Risk of Explosion', *Chem. - Eur. J.*, vol. 15, no. 37, pp. 9394–9403, Sep. 2009, doi: 10.1002/chem.200900614.
[118] E. Atherton, J. L. Holder, M. Meldal, R. C. Sheppard, and R. M. Valerio, 'Peptide synthesis. Part 12. 3,4-Dihydro-4-oxo-1,2,3-benzotriazin-3-yl esters of fluorenylmethoxycarbonyl amino acids as self-indicating reagents for solid phase peptide synthesis', *J. Chem. Soc. Perkin 1*, no. 10, p. 2887, 1988, doi: 10.1039/p19880002887.
[119] G. B. Fields and R. L. Noble, 'Solid phase peptide synthesis utilizing 9-fluorenylmethoxycarbonyl amino acids', *Int. J. Pept. Protein Res.*, vol. 35, no. 3, pp. 161–214, Jan. 2009, doi: 10.1111/j.1399-3011.1990.tb00939.x.
[120] R. Frank and H. Overwln, 'SPOT Synthesis: Epitope Analysis with Arrays of Synthetic Peptides Prepared on Cellulose Membranes', in *Epitope Mapping Protocols*, vol. 66, New Jersey: Humana Press, 1996, pp. 149–170. doi: 10.1385/0-89603-375-9:149.
[121] L. Gentilucci, R. De Marco, and L. Cerisoli, 'Chemical Modifications Designed to Improve Peptide Stability: Incorporation of Non-Natural Amino Acids, Pseudo-Peptide Bonds, and Cyclization', *Curr. Pharm. Des.*, vol. 16, no. 28, pp. 3185–3203, Sep. 2010, doi: 10.2174/138161210793292555.
[122] N. Qvit, S. J. S. Rubin, T. J. Urban, D. Mochly-Rosen, and E. R. Gross, 'Peptidomimetic therapeutics: scientific approaches and opportunities', *Drug Discov. Today*, vol. 22, no. 2, pp. 454–462, Feb. 2017, doi: 10.1016/j.drudis.2016.11.003.
[123] C. Conato *et al.*, 'Copper complexes of glycyl-histidyl-lysine and two of its synthetic analogues: chemical behaviour and biological activity', *Biochim. Biophys. Acta BBA - Gen. Subj.*, vol. 1526, no. 2, pp. 199–210, May 2001, doi: 10.1016/S0304-4165(01)00127-1.
[124] M. Goodman and M. Chorev, 'On the concept of linear modified retro-peptide structures', *Acc. Chem. Res.*, vol. 12, no. 1, pp. 1–7, Jan. 1979, doi: 10.1021/ar50133a001.
[125] M. Chorev, 'The partial retro-inverso modification: A road traveled together', *Biopolymers*, vol. 80, no. 2–3, pp. 67–84, 2005, doi: 10.1002/bip.20219.
[126] A. Dalpozzo, K. Kanai, G. Kereszturi, and G. Calabrese, 'H-Gly-Hisψ(NHCO)Lys-OH, partially modified retro-inverso analogue of the growth factor glycyl-L-histidyl-L-lysine with enhanced enzymatic stability', *Int. J. Pept. Protein Res.*, vol. 41, no. 6, pp. 561–566, Jan. 2009, doi: 10.1111/j.1399-3011.1993.tb00478.x.
[127] C. Adessi and C. Soto, 'Converting a Peptide into a Drug: Strategies to Improve Stability and Bioavailability', *Curr. Med. Chem.*, vol. 9, no. 9, pp. 963–978, May 2002, doi: 10.2174/0929867024606731.
[128] S. Namjoshi and H. A. E. Benson, 'Cyclic peptides as potential therapeutic agents for skin disorders', *Biopolymers*, vol. 94, no. 5, pp. 673–680, May 2010, doi: 10.1002/bip.21476.
[129] H. Eagle, 'THE SPECIFIC AMINO ACID REQUIREMENTS OF A HUMAN CARCINOMA CELL (STRAIN HELA) IN TISSUE CULTURE', *J. Exp. Med.*, vol. 102, no. 1, pp. 37–48, Jul. 1955, doi: 10.1084/jem.102.1.37.
[130] R. I. Freshney, *Culture of animal cells: a manual of basic technique*. 2011.
[131] E. F. Hartree, 'Determination of protein: A modification of the lowry method that gives a

linear photometric response', *Anal. Biochem.*, vol. 48, no. 2, pp. 422–427, Aug. 1972, doi: 10.1016/0003-2697(72)90094-2.
[132] P.-C. Yang and T. Mahmood, 'Western blot: Technique, theory, and trouble shooting', *North Am. J. Med. Sci.*, vol. 4, no. 9, p. 429, 2012, doi: 10.4103/1947-2714.100998.
[133] C. Diehl, 'Peptides in cosmeceuticals', *Ukr. J. Dermatol. Venerol. Cosmetol.*, vol. 0, no. 1, pp. 28–35, Apr. 2019, doi: 10.30978/UJDVK2019-1-28.
[134] K. Rodan, K. Fields, and T. Falla, 'Bioactive Peptides', in *Cosmeceuticals and Cosmetic Practice*, P. K. Farris, Ed. Chichester, UK: John Wiley & Sons, Ltd, 2013, pp. 142–152. doi: 10.1002/9781118384824.ch14.
[135] S.-F. Ng, J. J. Rouse, F. D. Sanderson, V. Meidan, and G. M. Eccleston, 'Validation of a Static Franz Diffusion Cell System for In Vitro Permeation Studies', *AAPS PharmSciTech*, vol. 11, no. 3, pp. 1432–1441, Sep. 2010, doi: 10.1208/s12249-010-9522-9.
[136] A. Akbarzadeh *et al.*, 'Liposome: classification, preparation, and applications', *Nanoscale Res. Lett.*, vol. 8, no. 1, p. 102, Dec. 2013, doi: 10.1186/1556-276X-8-102.
[137] M. Coimbra *et al.*, 'Improving solubility and chemical stability of natural compounds for medicinal use by incorporation into liposomes', *Int. J. Pharm.*, vol. 416, no. 2, pp. 433–442, Sep. 2011, doi: 10.1016/j.ijpharm.2011.01.056.
[138] X. Ai, L. Zhong, H. Niu, and Z. He, 'Thin-film hydration preparation method and stability test of DOX-loaded disulfide-linked polyethylene glycol 5000-lysine-di-tocopherol succinate nanomicelles', *Asian J. Pharm. Sci.*, vol. 9, no. 5, pp. 244–250, Oct. 2014, doi: 10.1016/j.ajps.2014.06.006.
[139] H.-C. Chen, 'Boyden Chamber Assay', in *Cell Migration*, vol. 294, New Jersey: Humana Press, 2004, pp. 015–022. doi: 10.1385/1-59259-860-9:015.
[140] F. Tratar, G. Marc, M. Sollner, and D. Kikelj, 'Synthesis of the retro-inverso peptide analogues of N-acetylmuramyl-L-alanyl-D-isoglutamine (MDP)', *Arkivoc*, vol. 2001, no. 5, pp. 7–20, Aug. 2001, doi: 10.3998/ark.5550190.0002.502.
[141] N. Beglova, S. Maliartchouk, I. Ekiel, M. C. Zaccaro, H. U. Saragovi, and K. Gehring, 'Design and Solution Structure of Functional Peptide Mimetics of Nerve Growth Factor', *J. Med. Chem.*, vol. 43, no. 19, pp. 3530–3540, Sep. 2000, doi: 10.1021/jm990441x.
[142] F. J. Warner, P. Mack, A. Comis, R. C. Miller, and E. Burcher, 'Structure–activity relationships of neurokinin A (4–10) at the human tachykinin NK2 receptor: the role of natural residues and their chirality', *Biochem. Pharmacol.*, vol. 61, no. 1, pp. 55–60, Jan. 2001, doi: 10.1016/S0006-2952(00)00516-5.
[143] J. G. Pérez-Silva, Y. Español, G. Velasco, and V. Quesada, 'The Degradome database: expanding roles of mammalian proteases in life and disease', *Nucleic Acids Res.*, vol. 44, no. D1, pp. D351–D355, Jan. 2016, doi: 10.1093/nar/gkv1201.
[144] Y. L. Choi, E. J. Park, E. Kim, D. H. Na, and Y.-H. Shin, 'Dermal Stability and In Vitro Skin Permeation of Collagen Pentapeptides (KTTKS and palmitoyl-KTTKS)', *Biomol. Ther.*, vol. 22, no. 4, pp. 321–327, Jul. 2014, doi: 10.4062/biomolther.2014.053.
[145] S. Li, C. Schöneich, and R. T. Borchardt, 'Chemical instability of protein pharmaceuticals: Mechanisms of oxidation and strategies for stabilization', *Biotechnol. Bioeng.*, vol. 48, no. 5, pp. 490–500, Dec. 1995, doi: 10.1002/bit.260480511.
[146] J. S. Zigler, J. L. Lepe-Zuniga, B. Vistica, and I. Gery, 'Analysis of the cytotoxic effects of light-exposed hepes-containing culture medium', *In Vitro Cell. Dev. Biol.*, vol. 21, no. 5, pp. 282–287, May 1985, doi: 10.1007/BF02620943.
[147] T. Yoneyama, S. Ohtsuki, M. Tachikawa, Y. Uchida, and T. Terasaki, 'Scrambled Internal Standard Method for High-Throughput Protein Quantification by Matrix-Assisted Laser Desorption Ionization Tandem Mass Spectrometry', *J. Proteome Res.*, vol. 16, no. 4, pp. 1556–1565, Apr. 2017, doi: 10.1021/acs.jproteome.6b00941.
[148] A. Kluczyk *et al.*, 'Argireline: Needle-Free Botox as Analytical Challenge', *Chem. Biodivers.*, vol. 18, no. 3, Mar. 2021, doi: 10.1002/cbdv.202000992.

[149] A. Kluczyk *et al.*, 'Chemical and biological properties of anti-wrinkle peptide Argireline', *Aesthetic Cosmetol. Med.*, vol. 10, no. 3, pp. 125–133, Jun. 2021, doi: 10.52336/acm.2021.10.3.05.
[150] L. Risaliti *et al.*, 'Liposomes loaded with Salvia triloba and Rosmarinus officinalis essential oils: In vitro assessment of antioxidant, antiinflammatory and antibacterial activities', *J. Drug Deliv. Sci. Technol.*, vol. 51, pp. 493–498, Jun. 2019, doi: 10.1016/j.jddst.2019.03.034.
[151] M. Asprea, I. Leto, M. C. Bergonzi, and A. R. Bilia, 'Thyme essential oil loaded in nanocochleates: Encapsulation efficiency, in vitro release study and antioxidant activity', *LWT*, vol. 77, pp. 497–502, Apr. 2017, doi: 10.1016/j.lwt.2016.12.006.
[152] H. Zelová and J. Hošek, 'TNF-α signalling and inflammation: interactions between old acquaintances', *Inflamm. Res.*, vol. 62, no. 7, pp. 641–651, Jul. 2013, doi: 10.1007/s00011-013-0633-0.
[153] M. Duncan, 'Influence of surfactants upon protein/peptide adsorption to glass and polypropylene', *Int. J. Pharm.*, vol. 120, no. 2, pp. 179–188, Jun. 1995, doi: 10.1016/0378-5173(94)00402-Q.
[154] G. Vanti *et al.*, 'Development and optimisation of biopharmaceutical properties of a new microemulgel of cannabidiol for locally-acting dermatological delivery', *Int. J. Pharm.*, vol. 607, p. 121036, Sep. 2021, doi: 10.1016/j.ijpharm.2021.121036.
[155] M. Amer and M. Maged, 'Cosmeceuticals versus pharmaceuticals', *Clin. Dermatol.*, vol. 27, no. 5, pp. 428–430, Sep. 2009, doi: 10.1016/j.clindermatol.2009.05.004.
[156] V. Arul, D. Gopinath, K. Gomathi, and R. Jayakumar, 'Biotinylated GHK peptide incorporated collagenous matrix: A novel biomaterial for dermal wound healing in rats', *J. Biomed. Mater. Res. B Appl. Biomater.*, vol. 73B, no. 2, pp. 383–391, May 2005, doi: 10.1002/jbm.b.30246.
[157] L. R. Robinson, N. C. Fitzgerald, D. G. Doughty, N. C. Dawes, C. A. Berge, and D. L. Bissett, 'Topical palmitoyl pentapeptide provides improvement in photoaged human facial skin1', *Int. J. Cosmet. Sci.*, vol. 27, no. 3, pp. 155–160, Jun. 2005, doi: 10.1111/j.1467-2494.2005.00261.x.
[158] W. Johnson *et al.*, 'Safety Assessment of Tripeptide-1, Hexapeptide-12, Their Metal Salts and Fatty Acyl Derivatives, and Palmitoyl Tetrapeptide-7 as Used in Cosmetics', *Int. J. Toxicol.*, vol. 37, no. 3_suppl, pp. 90S-102S, Nov. 2018, doi: 10.1177/1091581818807863.
[159] M. A. Niemann, A. J. Narkates, and E. J. Miller, 'Isolation and Serine Protease Inhibitory Activity of the 44-Residue, C-Terminal Fragment of αl -Antitrypsin from Human Placenta', *Matrix*, vol. 12, no. 3, pp. 233–241, Jun. 1992, doi: 10.1016/S0934-8832(11)80066-1.
[160] M. A. Niemann, J. E. Baggott, and E. J. Miller, 'Binding of SPAAT, the 44-residue C-terminal peptide of alpha 1-antitrypsin, to proteins of the extracellular matrix', *J. Cell. Biochem.*, vol. 66, no. 3, pp. 346–357, Sep. 1997.
[161] S. Modrow, D. Falke, U. Truyen, and H. Schätzl, 'Viruses: Definition, Structure, Classification', in *Molecular Virology*, Berlin, Heidelberg: Springer Berlin Heidelberg, 2013, pp. 17–30. doi: 10.1007/978-3-642-20718-1_2.
[162] C. J. Burrell, C. R. Howard, and F. A. Murphy, 'Coronaviruses', in *Fenner and White's Medical Virology*, Elsevier, 2017, pp. 437–446. doi: 10.1016/B978-0-12-375156-0.00031-X.
[163] S. Su *et al.*, 'Epidemiology, Genetic Recombination, and Pathogenesis of Coronaviruses', *Trends Microbiol.*, vol. 24, no. 6, pp. 490–502, Jun. 2016, doi: 10.1016/j.tim.2016.03.003.
[164] J. Cui, F. Li, and Z.-L. Shi, 'Origin and evolution of pathogenic coronaviruses', *Nat. Rev. Microbiol.*, vol. 17, no. 3, pp. 181–192, Mar. 2019, doi: 10.1038/s41579-018-0118-9.
[165] J. F.-W. Chan *et al.*, 'A familial cluster of pneumonia associated with the 2019 novel coronavirus indicating person-to-person transmission: a study of a family cluster', *The Lancet*, vol. 395, no. 10223, pp. 514–523, Feb. 2020, doi: 10.1016/S0140-6736(20)30154-9.
[166] C. Huang *et al.*, 'Clinical features of patients infected with 2019 novel coronavirus in Wuhan, China', *The Lancet*, vol. 395, no. 10223, pp. 497–506, Feb. 2020, doi: 10.1016/S0140-6736(20)30183-5.
[167] R. Lu *et al.*, 'Genomic characterisation and epidemiology of 2019 novel coronavirus: implications for virus origins and receptor binding', *The Lancet*, vol. 395, no. 10224, pp. 565–574,

Feb. 2020, doi: 10.1016/S0140-6736(20)30251-8.
[168] A. Grifoni, J. Sidney, Y. Zhang, R. H. Scheuermann, B. Peters, and A. Sette, 'A Sequence Homology and Bioinformatic Approach Can Predict Candidate Targets for Immune Responses to SARS-CoV-2', *Cell Host Microbe*, vol. 27, no. 4, pp. 671-680.e2, Apr. 2020, doi: 10.1016/j.chom.2020.03.002.
[169] K. Dhama *et al.*, 'SARS-CoV-2 jumping the species barrier: Zoonotic lessons from SARS, MERS and recent advances to combat this pandemic virus', *Travel Med. Infect. Dis.*, vol. 37, p. 101830, Sep. 2020, doi: 10.1016/j.tmaid.2020.101830.
[170] S. S. Shaikh, A. P. Jose, D. A. Nerkar, M. Vijaykumar KV, and S. K. Shaikh, 'COVID-19 pandemic crisis—a complete outline of SARS-CoV-2', *Future J. Pharm. Sci.*, vol. 6, no. 1, p. 116, Dec. 2020, doi: 10.1186/s43094-020-00133-y.
[171] A. Popa *et al.*, 'Genomic epidemiology of superspreading events in Austria reveals mutational dynamics and transmission properties of SARS-CoV-2', *Sci. Transl. Med.*, vol. 12, no. 573, p. eabe2555, Dec. 2020, doi: 10.1126/scitranslmed.abe2555.
[172] B. J. Bosch, R. van der Zee, C. A. M. de Haan, and P. J. M. Rottier, 'The Coronavirus Spike Protein Is a Class I Virus Fusion Protein: Structural and Functional Characterization of the Fusion Core Complex', *J. Virol.*, vol. 77, no. 16, pp. 8801–8811, Aug. 2003, doi: 10.1128/JVI.77.16.8801-8811.2003.
[173] D. Wrapp *et al.*, 'Cryo-EM structure of the 2019-nCoV spike in the prefusion conformation', *Science*, vol. 367, no. 6483, pp. 1260–1263, Mar. 2020, doi: 10.1126/science.abb2507.
[174] R. Yan, Y. Zhang, Y. Li, L. Xia, Y. Guo, and Q. Zhou, 'Structural basis for the recognition of SARS-CoV-2 by full-length human ACE2', *Science*, vol. 367, no. 6485, pp. 1444–1448, Mar. 2020, doi: 10.1126/science.abb2762.
[175] E. Hartenian, D. Nandakumar, A. Lari, M. Ly, J. M. Tucker, and B. A. Glaunsinger, 'The molecular virology of coronaviruses', *J. Biol. Chem.*, vol. 295, no. 37, pp. 12910–12934, Sep. 2020, doi: 10.1074/jbc.REV120.013930.
[176] A. J. Turner and N. M. Hooper, 'Angiotensin-Converting Enzyme-2 (ACE2)', in *xPharm: The Comprehensive Pharmacology Reference*, Elsevier, 2007, pp. 1–4. doi: 10.1016/B978-008055232-3.62913-7.
[177] N. Zamorano Cuervo and N. Grandvaux, 'ACE2: Evidence of role as entry receptor for SARS-CoV-2 and implications in comorbidities', *eLife*, vol. 9, p. e61390, Nov. 2020, doi: 10.7554/eLife.61390.
[178] D. D. Chaplin, 'Overview of the immune response', *J. Allergy Clin. Immunol.*, vol. 125, no. 2, pp. S3–S23, Feb. 2010, doi: 10.1016/j.jaci.2009.12.980.
[179] D. S. Goodsell, 'The Molecular Perspective: Antibodies', *The Oncologist*, vol. 6, no. 6, pp. 547–548, Dec. 2001, doi: 10.1634/theoncologist.6-6-547.
[180] B. Alberts, Ed., *Molecular biology of the cell*, 4th ed. New York: Garland Science, 2002.
[181] J. L. Sanchez-Trincado, M. Gomez-Perosanz, and P. A. Reche, 'Fundamentals and Methods for T- and B-Cell Epitope Prediction', *J. Immunol. Res.*, vol. 2017, pp. 1–14, 2017, doi: 10.1155/2017/2680160.
[182] N. Kirtipal, S. Bharadwaj, and S. G. Kang, 'From SARS to SARS-CoV-2, insights on structure, pathogenicity and immunity aspects of pandemic human coronaviruses', *Infect. Genet. Evol.*, vol. 85, p. 104502, Nov. 2020, doi: 10.1016/j.meegid.2020.104502.
[183] L. Guo *et al.*, 'Profiling Early Humoral Response to Diagnose Novel Coronavirus Disease (COVID-19)', *Clin. Infect. Dis.*, vol. 71, no. 15, pp. 778–785, Jul. 2020, doi: 10.1093/cid/ciaa310.
[184] K. Duan *et al.*, 'Effectiveness of convalescent plasma therapy in severe COVID-19 patients', *Proc. Natl. Acad. Sci.*, vol. 117, no. 17, pp. 9490–9496, Apr. 2020, doi: 10.1073/pnas.2004168117.
[185] Y. Cao *et al.*, 'Potent Neutralizing Antibodies against SARS-CoV-2 Identified by High-Throughput Single-Cell Sequencing of Convalescent Patients' B Cells', *Cell*, vol. 182, no. 1, pp.

73-84.e16, Jul. 2020, doi: 10.1016/j.cell.2020.05.025.
[186] E. Andreano *et al.*, 'Identification of neutralizing human monoclonal antibodies from Italian Covid-19 convalescent patients', Immunology, preprint, May 2020. doi: 10.1101/2020.05.05.078154.
[187] D. Pinto *et al.*, 'Cross-neutralization of SARS-CoV-2 by a human monoclonal SARS-CoV antibody', *Nature*, vol. 583, no. 7815, pp. 290–295, Jul. 2020, doi: 10.1038/s41586-020-2349-y.
[188] A. Grifoni *et al.*, 'Targets of T Cell Responses to SARS-CoV-2 Coronavirus in Humans with COVID-19 Disease and Unexposed Individuals', *Cell*, vol. 181, no. 7, pp. 1489-1501.e15, Jun. 2020, doi: 10.1016/j.cell.2020.05.015.
[189] T. Li *et al.*, 'Significant Changes of Peripheral T Lymphocyte Subsets in Patients with Severe Acute Respiratory Syndrome', *J. Infect. Dis.*, vol. 189, no. 4, pp. 648–651, Feb. 2004, doi: 10.1086/381535.
[190] K. G. Beavis *et al.*, 'Evaluation of the EUROIMMUN Anti-SARS-CoV-2 ELISA Assay for detection of IgA and IgG antibodies', *J. Clin. Virol.*, vol. 129, p. 104468, Aug. 2020, doi: 10.1016/j.jcv.2020.104468.
[191] C. M. Poh *et al.*, 'Two linear epitopes on the SARS-CoV-2 spike protein that elicit neutralising antibodies in COVID-19 patients', *Nat. Commun.*, vol. 11, no. 1, p. 2806, Dec. 2020, doi: 10.1038/s41467-020-16638-2.
[192] P. J. M. Brouwer *et al.*, 'Potent neutralizing antibodies from COVID-19 patients define multiple targets of vulnerability', *Science*, vol. 369, no. 6504, pp. 643–650, Aug. 2020, doi: 10.1126/science.abc5902.
[193] D. F. Robbiani *et al.*, 'Convergent antibody responses to SARS-CoV-2 in convalescent individuals', *Nature*, vol. 584, no. 7821, pp. 437–442, Aug. 2020, doi: 10.1038/s41586-020-2456-9.
[194] C. Yi *et al.*, 'Key residues of the receptor binding motif in the spike protein of SARS-CoV-2 that interact with ACE2 and neutralizing antibodies', *Cell. Mol. Immunol.*, vol. 17, no. 6, pp. 621–630, Jun. 2020, doi: 10.1038/s41423-020-0458-z.
[195] M. Yarmarkovich, J. M. Warrington, A. Farrel, and J. M. Maris, 'Identification of SARS-CoV-2 Vaccine Epitopes Predicted to Induce Long-Term Population-Scale Immunity', *Cell Rep. Med.*, vol. 1, no. 3, p. 100036, Jun. 2020, doi: 10.1016/j.xcrm.2020.100036.
[196] J. Lan *et al.*, 'Structure of the SARS-CoV-2 spike receptor-binding domain bound to the ACE2 receptor', *Nature*, vol. 581, no. 7807, pp. 215–220, May 2020, doi: 10.1038/s41586-020-2180-5.
[197] E. Shrock *et al.*, 'Viral epitope profiling of COVID-19 patients reveals cross-reactivity and correlates of severity', *Science*, vol. 370, no. 6520, p. eabd4250, Nov. 2020, doi: 10.1126/science.abd4250.
[198] B. Ju *et al.*, 'Human neutralizing antibodies elicited by SARS-CoV-2 infection', *Nature*, vol. 584, no. 7819, pp. 115–119, Aug. 2020, doi: 10.1038/s41586-020-2380-z.
[199] J. Nilvebrant and J. Rockberg, 'An Introduction to Epitope Mapping', in *Epitope Mapping Protocols*, vol. 1785, J. Rockberg and J. Nilvebrant, Eds. New York, NY: Springer New York, 2018, pp. 1–10. doi: 10.1007/978-1-4939-7841-0_1.
[200] M. Z. Atassi, 'Antigenic structures of proteins. Their determination has revealed important aspects of immune recognition and generated strategies for synthetic mimicking of protein binding sites', *Eur. J. Biochem.*, vol. 145, no. 1, pp. 1–20, Nov. 1984, doi: 10.1111/j.1432-1033.1984.tb08516.x.
[201] M. H. V. Van Regenmortel, 'Mapping Epitope Structure and Activity: From One-Dimensional Prediction to Four-Dimensional Description of Antigenic Specificity', *Methods*, vol. 9, no. 3, pp. 465–472, Jun. 1996, doi: 10.1006/meth.1996.0054.
[202] R.-H. Hua *et al.*, 'Comprehensive mapping of a novel NS1 epitope conserved in flaviviruses within the Japanese encephalitis virus serocomplex', *Virus Res.*, vol. 185, pp. 103–109, Jun. 2014, doi: 10.1016/j.virusres.2014.03.001.
[203] K. Li *et al.*, 'Antisera preparation and epitope mapping of a recombinant protein comprising

three peptide fragments of the cystic fibrosis transmembrane conductance regulator', *Protein Expr. Purif.*, vol. 114, pp. 23–29, Oct. 2015, doi: 10.1016/j.pep.2015.06.005.
[204] C.-W. Chen, M.-S. Wu, Y.-J. Huang, C.-A. Cheng, and C.-Y. Chang, 'Recognition of Linear B-Cell Epitope of Betanodavirus Coat Protein by RG-M18 Neutralizing mAB Inhibits Giant Grouper Nervous Necrosis Virus (GGNNV) Infection', *PLOS ONE*, vol. 10, no. 5, p. e0126121, May 2015, doi: 10.1371/journal.pone.0126121.
[205] D. Torres and A. M. Espino, 'Mapping of B-Cell Epitopes on a Novel 11.5-Kilodalton *Fasciola hepatica-Schistosoma mansoni* Cross-Reactive Antigen Belonging to a Member of the *F. hepatica* Saposin-Like Protein Family', *Infect. Immun.*, vol. 74, no. 8, pp. 4932–4938, Aug. 2006, doi: 10.1128/IAI.00442-06.
[206] A. M. Papini, 'The use of post-translationally modified peptides for detection of biomarkers of immune-mediated diseases', *J. Pept. Sci.*, vol. 15, no. 10, pp. 621–628, Sep. 2009, doi: 10.1002/psc.1166.
[207] H. M. Geysen, S. J. Rodda, and T. J. Mason, 'A priori delineation of a peptide which mimics a discontinuous antigenic determinant', *Mol. Immunol.*, vol. 23, no. 7, pp. 709–715, Jul. 1986, doi: 10.1016/0161-5890(86)90081-7.
[208] L. Whitmore and B. A. Wallace, 'DICHROWEB, an online server for protein secondary structure analyses from circular dichroism spectroscopic data', *Nucleic Acids Res.*, vol. 32, no. Web Server, pp. W668–W673, Jul. 2004, doi: 10.1093/nar/gkh371.
[209] A. C. Walls, Y.-J. Park, M. A. Tortorici, A. Wall, A. T. McGuire, and D. Veesler, 'Structure, Function, and Antigenicity of the SARS-CoV-2 Spike Glycoprotein', *Cell*, vol. 181, no. 2, pp. 281-292.e6, Apr. 2020, doi: 10.1016/j.cell.2020.02.058.
[210] T. Zhou *et al.*, 'Cryo-EM Structures of SARS-CoV-2 Spike without and with ACE2 Reveal a pH-Dependent Switch to Mediate Endosomal Positioning of Receptor-Binding Domains', *Cell Host Microbe*, vol. 28, no. 6, pp. 867-879.e5, Dec. 2020, doi: 10.1016/j.chom.2020.11.004.
[211] M. A. Tortorici *et al.*, 'Ultrapotent human antibodies protect against SARS-CoV-2 challenge via multiple mechanisms', *Science*, vol. 370, no. 6519, pp. 950–957, Nov. 2020, doi: 10.1126/science.abe3354.
[212] P. Pino *et al.*, 'Trimeric SARS-CoV-2 Spike Proteins Produced from CHO Cells in Bioreactors Are High-Quality Antigens', *Processes*, vol. 8, no. 12, p. 1539, Nov. 2020, doi: 10.3390/pr8121539.
[213] N. Sreerama and R. W. Woody, 'Estimation of Protein Secondary Structure from Circular Dichroism Spectra: Comparison of CONTIN, SELCON, and CDSSTR Methods with an Expanded Reference Set', *Anal. Biochem.*, vol. 287, no. 2, pp. 252–260, Dec. 2000, doi: 10.1006/abio.2000.4880.
[214] Y. Cai *et al.*, 'Distinct conformational states of SARS-CoV-2 spike protein', *Science*, vol. 369, no. 6511, pp. 1586–1592, Sep. 2020, doi: 10.1126/science.abd4251.
[215] J. Shang *et al.*, 'Structural basis of receptor recognition by SARS-CoV-2', *Nature*, vol. 581, no. 7807, pp. 221–224, May 2020, doi: 10.1038/s41586-020-2179-y.
[216] Y. Yuan *et al.*, 'A bivalent nanoparticle vaccine exhibits potent cross-protection against the variants of SARS-CoV-2', *Cell Rep.*, vol. 38, no. 3, p. 110256, Jan. 2022, doi: 10.1016/j.celrep.2021.110256.
[217] X. Pan *et al.*, 'RBD-homodimer, a COVID-19 subunit vaccine candidate, elicits immunogenicity and protection in rodents and nonhuman primates', *Cell Discov.*, vol. 7, no. 1, p. 82, Dec. 2021, doi: 10.1038/s41421-021-00320-y.
[218] N. C. Kyriakidis, A. López-Cortés, E. V. González, A. B. Grimaldos, and E. O. Prado, 'SARS-CoV-2 vaccines strategies: a comprehensive review of phase 3 candidates', *Npj Vaccines*, vol. 6, no. 1, p. 28, Dec. 2021, doi: 10.1038/s41541-021-00292-w.
[219] F. Amanat and F. Krammer, 'SARS-CoV-2 Vaccines: Status Report', *Immunity*, vol. 52, no. 4, pp. 583–589, Apr. 2020, doi: 10.1016/j.immuni.2020.03.007.

PUBLISHED PAPERS: ABSTRACTS

AUTHOR= Errante Fosca, Ledwoń Patrycja, Latajka Rafal, Rovero Paolo, Papini Anna Maria

TITLE= Cosmeceutical Peptides in the Framework of Sustainable Wellness Economy

JOURNAL= Frontiers in Chemistry

VOLUME= 8

YEAR= 2020

URL= https://www.frontiersin.org/article/10.3389/fchem.2020.572923

DOI= 10.3389/fchem.2020.572923

ISSN= 2296-2646

ABSTRACT= Among the many aspects that contribute to the wellness of each individual, healthy and younger-looking skin play a relevant role, as clearly shown by the important growth of the skin-care products market observed in recent years. In this scenario, the field of cosmeceuticals appears particularly promising, being based on cosmetic products containing active ingredients. Among these, several peptides were proposed for cosmeceutical applications, thanks to their specific interaction with biological targets. In this mini-review, we report some of the most investigated and used peptides for cosmetic formulations, taking into account that cosmeceutical peptides are basically divided into three main categories (i.e., neurotransmitter inhibitors, carriers, and signal peptides). Special attention was paid to the scientific studies supporting the claimed biological activity of these peptides, as a fundamental aspect that should underpin the growth of this field in the framework of a sustainable wellness economy.

AUTHOR= Ledwoń Patrycja, Fosca Errante, Anna Maria Papini, Paolo Rovero, Rafal Latajka

TITLE= Peptides as Active Ingredients: A Challenge for Cosmeceutical Industry

JOURNAL= Chemistry & Biodiversity

VOLUME= 18

YEAR= 2021

URL= https://onlinelibrary.wiley.com/doi/10.1002/cbdv.202000833

DOI= 10.1002/cbdv.202000833

ISSN= e2000833

ABSTRACT= Cosmeceutical field, which merges cosmetics and pharmaceuticals, is nowadays a highly investigated research area, because a scientific demonstration of the claimed bioactivity of new cosmeceutical ingredients is increasingly requested. In fact, an aspect differentiating traditional cosmetics from cosmeceuticals is the identification and characterization of the active ingredients and demonstrating its efficacy in the claimed activity. An interesting group of bioactive cosmeceutical ingredients are peptides, which due to their particular properties, meets most of the requirements presented by the cosmeceutical industry when composing new formulas. In this context, beside bioactivity, two additional aspects have been recently considered, when dealing with peptides as cosmeceutical ingredients: bioavailability and stability. We describe herein novel methods applied in order to enhance peptides skin-penetration and stability, reviewing both scientific articles and patents, issued in the cosmeceutical arena.

AUTHOR= Fosca Errante, Marta Menicatti, Marco Pallecchi, Lisa Giovannelli, Anna Maria Papini, Paolo Rovero, Gianluca Bartolucci

TITLE= Susceptibility of Cosmeceutical Peptides to Proteases Activity: Development of Dermal Stability Test by LC-MS/MS Analysis

JOURNAL= Journal of Pharmaceutical and Biomedical Analysis

VOLUME= 194

YEAR= 2021

URL= https://www.sciencedirect.com/science/article/pii/S0731708520316617

DOI= 10.1016/j.jpba.2020.113775

ISSN= 0731-7085

ABSTRACT= Recently, several peptides are used as active ingredients in topical cosmetic formulations, few information are available on their dermal stability against proteases. In this study, it was developed a simple and reliable assay to evaluate the stability of cosmeceutical peptides in skin homogenates. The quantification of studied peptides was performed by liquid chromatography coupled with a triple quadrupole mass spectrometer operating in tandem mass spectrometry mode (LC–MS/MS) and the conditions were tuned through energy resolved MS/MS (ERMS) experiments. The sample preparation procedure was carried out on rat skin homogenates by employing pal-KTTKS (reference peptide and the parameters that may affect the assay results were evaluated, including substrate concentration, dilution of skin homogenate, protein concentration and batch-to-batch variation of the homogenate. The optimized conditions were applied to check the degradation profile of pal-KTTKS in human skin samples and the obtained results were compared. Finally, the degradation profiles of SA1-III and pamSA1-III, recently described as cosmeceutical peptides, in human skin homogenate were evaluated. The results showed that proposed peptides are stable toward proteases for up to 8 h of incubation. Thanks to this characteristic, these peptides can be considered very interesting candidates as active ingredients for creams intended for a daily application.

AUTHOR= Traoré Abdouramane, Guindo Merepen A., Konaté Drissa, Traoré Bourama, Diakité Seidina A., Kanté Salimata, Dembélé Assitan, Cissé Abdourhamane, Incandela Nathan C., Kodio Mamoudou, Coulibaly Yaya I., Faye Ousmane, Kajava Andrey V., Pratesi Federico, Migliorini Paola, Papini Anna Maria, Pacini Lorenzo, Rovero Paolo, Errante Fosca, Diakité Mahamadou, Arevalo-Herrera Myriam, Herrera Socrates, Corradin Giampietro, Balam Saidou

TITLE= Seroreactivity of the Severe Acute Respiratory Syndrome Coronavirus 2 Recombinant S Protein, Receptor-Binding Domain, and Its Receptor-Binding Motif in COVID-19 Patients and Their Cross-Reactivity with Pre-COVID-19 Samples From Malaria-Endemic Areas

JOURNAL= Frontiers in Immunology

VOLUME= 13

YEAR= 2022

URL= https://www.frontiersin.org/article/10.3389/fimmu.2022.856033

DOI= 10.3389/fimmu.2022.856033

ISSN= 1664-3224

ABSTRACT= Despite the global interest and the unprecedented number of scientific studies triggered by the COVID-19 pandemic, few data are available from developing and low-income countries. In these regions, communities live under the threat of various transmissible diseases aside from COVID-19, including malaria. This study aims to determine the severe acute respiratory syndrome coronavirus 2 (SARS-CoV-2) seroreactivity of antibodies from COVID-19 and pre-COVID-19 samples of individuals in Mali (West Africa). Blood samples from COVID-19 patients (n = 266) at Bamako Dermatology Hospital (HDB) and pre-COVID-19 donors (n = 283) from a previous malaria survey conducted in Dangassa village were tested by ELISA to assess IgG antibodies specific to the full-length spike (S) protein, the receptor-binding domain (RBD), and the receptor-binding motif ($RBM_{436–507}$). Study participants were categorized by age, gender, treatment duration for COVID-19, and comorbidities. In addition, the cross-seroreactivity of samples from pre-COVID-19, malaria-positive patients against the three antigens was assessed. Recognition of the SARS-CoV-2 proteins by sera from COVID-19 patients was 80.5% for S, 71.1% for RBD, and 31.9% for RBM ($p < 0.001$). While antibody responses to S and RBD tended to be age-dependent, responses to RBM were not. Responses were not gender-dependent for any of the antigens. Higher antibody levels to S, RBD, and RBM at hospital entry were associated with shorter treatment durations, particularly for RBD ($p < 0.01$). In contrast, higher body weights negatively influenced the anti-S antibody response, and asthma and diabetes weakened the anti-RBM antibody responses. Although lower, a significant cross-reactive antibody response to S (21.9%), RBD (6.7%), and RBM (8.8%) was detected in the pre-COVID-19 and malaria samples. Cross-reactive antibody responses to RBM were mostly associated ($p < 0.01$) with the absence of current Plasmodium falciparum infection, warranting further study.

AUTHOR= Federico Pratesi, Fosca Errante, Lorenzo Pacini, Irina Charlot Peña-Moreno, Sebastian Quiceno, Alfonso Carotenuto, Saidou BALAM, Drissa Konaté, Mahamadou DIAKITE, Myriam Arevalo-Herrera, Andrey V Kajava, Paolo Rovero, Giampietro Corradin, Paola Migliorini, Anna Maria Maria Papini, Socrates Herrera Valencia

TITLE= A SARS-CoV-2 Spike Receptor Binding Motif peptide induces anti-spike antibodies in mice and is recognized by COVID-19 patients

JOURNAL= Frontiers in Immunology

VOLUME= 13

YEAR= 2022

URL= https://www.frontiersin.org/article/10.3389/fimmu.2022.856033

DOI= 10.3389/fimmu.2022.879946

ISSN= 1664-3224

ABSTRACT= The currently devastating pandemic of severe acute respiratory syndrome known as coronavirus disease 2019 or COVID-19 is caused by the coronavirus SARS-CoV-2. Both the virus and the disease have been extensively studied worldwide. A trimeric spike (S) protein expressed on the virus outer bilayer leaflet has been identified as a ligand that allows the virus to penetrate human host cells and cause infection. Its receptor-binding domain (RBD) interacts with the angiotensin-converting enzyme 2 (ACE2), the host-cell viral receptor, and is, therefore, the subject of intense research for the development of virus control means, particularly vaccines. In this work, we search for smaller fragments of the S protein able to elicit virus-neutralizing antibodies, suitable for production by peptide synthesis technology. Based on the analysis of available data, we selected a 72 aa long receptor binding motif ($RBM_{436-507}$) of RBD. We used ELISA to study the antibody response to each of the three antigens (S protein, its RBD domain and the $RBM_{436-507}$ synthetic peptide) in humans exposed to the infection and in immunized mice. The seroreactivity analysis showed that anti-RBM antibodies are produced in COVID-19 patients and immunized mice and may exert neutralizing function, although with a frequency lower than anti-S and -RBD. These results provide a basis for further studies towards the development of vaccines or treatments focused on specific regions of the S virus protein, which can benefit from the absence of folding problems, conformational constraints and other advantages of the peptide synthesis production.